FUNDAMENTAL AND APPLICATION OF SURFACE -INITIATED ATOM TRANSFER RADICAL POLYMERIZATION FOR SURFACE MODIFICATION OF SHEETS AND NANOPARTICLES

By

RENXU CHEN, B.Sc.

A Thesis

Submitted to the School of Graduate Studies

In Partial Fulfillment of the Requirements

For the Degree of

Doctor of Philosophy

McMaster University

DOCTOR OF PHILOSOPHY(2009)	McMaster University
(Chemical Engineering)	Hamilton, Ontario

TITLE:	Fundamental and Application of Surface-initiated Atom Transfer Radical Polymerization For Surface Modification of Sheets and Nanoparticles
AUTHOR:	Renxu Chen B.Sc. (Peking University)
SUPERVISOR:	Professor Shiping Zhu
NUMBER OF PAGES:	xxx, 191

ABSTRACT

A recently developed surface grafting technique, surface-initiated atom transfer radical polymerization (ATRP), has the ability to directly graft polymer chains with controllable chain lengths, densities and functionalities from various kinds of surfaces. This thesis has two main focuses. First is to study the use of this technique in grafting monomers with special structures and functionalities. The other is to apply this technique to the modification of reactive metal surfaces.

Both of fluorinated polymers and polyhedral oligomeric silsesquioxane (POSS)-containing polymers have very interesting properties. In this thesis, for the first time, a highly fluorinated monomer, 2,2,2-trifluoroethyl methacrylate (TFEMA) and a POSS-containing monomer, POSS-MA were successfully polymerized from silicon wafers by surface-initiated ATRP. This is also the first work to use this technique to graft polymers with bulky, rigid side groups.

To achieve very high grafting density is a big challenge for surface-initiated ATRP. We designed a novel surface-attachable difunctional initiator, 11-(2,2-bis(2-bromo-2-methylpropionyloxy methyl)propionyloxy) undecyltrichlorosilane. With its

help, the grafting density of PTFEMA was almost doubled, from 0.48 to 0.86chains/nm^2. This is so far the most effective method to increase the grafting density.

Unlike other kinds of materials, the surfaces of metals are active in electrochemical and acid/base reactions and this reactivity complicates ATRP reactions. With the help of triethoxysilane-based initiator and mild Fe(II)/Fe(III) catalyst system, various acrylic polymers were successfully grafted from flat nickel and copper surfaces by surface-initiated ATRP. This work provided a convenient method to prepare functional polymer coatings with very stable adhesions to the metal surfaces. The same strategy can be extended to the surface modification of a shape-memory-alloy, nitinol.

Metal nanoparticles were also modified by this technique. Polymer shells were grafted from nickel nanoparticles surfaces. After the polymer grafting, both of the dispersibility and dispersion stability of nickel nanoparticles in appropriate solvents were greatly improved.

ACKNOWLEDGEMENT

First, I would like to express my deep gratitude to my academic supervisor Professor Shiping Zhu, Canada Research Chair in Advanced Polymerization Technology, who has brought me to the frontier of polymer engineering science research. His creative ideas and inspiring discussions have been very helpful for the progress of my research project. His enthusiasm, insight, patience and attention greatly impressed me.

I would like to thank the members of my supervisory committee, Professor Gianluigi Botton, Canada Research Chair in Microscopy of Nanoscale Materials, Professor Raja Ghosh, Canada Research Chair in Bioseparations Engineering, for their valuable advices and help during the project.

I would like to thank Dr. Beng S. Ong and Dr.Yiliang Wu for their generous support during my work period in Xerox, and I would like to thank Dr. Yuning Li and Ms. Ping Liu for valuable discussions.

I would like to thank Dr. Shane Maclaughlin for his continuous guidance, generous support and valuable discussions with my research project. I really benefit a lot

from his expertise of surface chemistry and metal materials.

I am grateful to my group members, Dr. Zhibin Ye, Dr. Aileen Ruiling Wang, Dr. Santiago Faucher, Dr. Wei Feng, Dr. Hormoz Eslami, Dr. Hualong Pan, Dr. Junwei Zhang, Ni Zhao, Phil Whitney, Jen Mahon, Xiang Gao, Yixin Gong, Zhilin Jin, Hongyan Gu, Mark Machado, Mohammad Haj Abed, Sarah Alibeik, Jason Doggart, Tom Kowpak for their support, encouragement and understanding. I also would like to thank Dr. Yang Chen, Dr. Zhilin Peng, Dr. Xiaonong Chen and many others for their friendship, tremendous help, and useful discussions.

Finally, to my parents who taught me how to love the beautiful life and my wife, Ya, for her unconditional love, patience, understanding and firm support. I really owe her a lot.

PUBLICATIONS

This Ph.D. thesis is organized in a sandwich style based on the following published/submitted papers:

1. **Renxu Chen,** Shane Maclaughlin, Gianluigi Botton, Shiping Zhu, "Preparation of Ni-*g*-Polymer Core-Shell Nanoparticles by Surface-initiated Atom Transfer Radical Polymerization" submitted to *Polymer* on May 21, 2009

2. **Renxu Chen,** Shane Maclaughlin, Shiping Zhu, "Grafting Acrylic Polymers from Flat Nickel and Copper Surfaces by Surface-initiated Atom Transfer Radical Polymerization" *Langmuir*, **2008**, *24*, 6889.

3. **Renxu Chen,** Wei Feng, Shiping Zhu, Gianluigi Botton, Beng S. Ong, Yiliang Wu, "Surface-initiated Atom Transfer Radical Polymerization of Polyhedral Oligomeric Silsesquioxane (POSS) Methacrylate from Flat Silicon Wafer" *Polymer,* **2006**, *47*, 1119.

4. **Renxu Chen,** Wei Feng, Shiping Zhu, Gianluigi Botton, Beng S. Ong, Yiliang Wu, "Surface-initiated Atom Transfer Radical Polymerization Grafting of

Poly(2,2,2-trifluoroethyl Methacrylate) from Flat Silicon Wafer Surfaces" *Journal of Polymer Science Part A: Polymer Chemistry,* **2006**, *44*, 1252.

TABLE OF CONTENTS

LIST OF FIGURES

LIST OF TABLES

LIST OF SCHEMES

LIST OF ABBREVIATIONS

AA	acrylic acid
AAO	anodic aluminium oxide
AFM	atomic force microscopy
ATRP	atom transfer radical polymerization
BA	*n*-butyl acrylate
BE	binding energy
BIEA	2-(2-bromoisobutytyloxy)ethyl acrylate
bpy	2,2' -bipyridine
BSA	bovine serum albumin
CFRP	conventional free radical polymerization
cPEA	2-chloropropionate ethyl acrylate
CLRP	controlled/living radical polymerization
CV	cyclic voltammetry
DI	deionized
DMAEMA	*N,N'*-dimethylaminoethyl methacrylate
DMF	*N,N*-dimethylformamide

dNnbpy	4,4’-dinonyl-2,2’-dipyridyl
EBIB (EBiB)	ethyl 2-bromoisobutyrate
EG	ethylene glycol
EIS	electrochemical impedance spectroscopy
GPC	gel permeation chromatography
FT-IR	fourier transform infrared spectroscopy
HDA	hexadecylamine
HEA	2-hydroethyl acrylate
HEMA	2-hydroethyl methacrylate
HMTETA	1,1,4,7,10,10-hexamethyltriethylenetetramine
HPLC	high-performance liquid chromatography
ICP-MS	inductively coupled plasma–mass spectroscopy
LB	Langmuir-Blodgett
LCST	Lower critical solution temperature
MA	methyl acrylate
MAPL	molecular assembly patterning by lift-off
MBAA	*N,N’*-methylenebisacrylamide
METAC	[2-(methacryloyloxy)ethyl]trimethylammonium chloride
MMA	methyl methacrylate

MMT	montmorillonite
M_n	number average molecular weight
MPC	2-methacryloyloxyethyl phosphorylcholine
MRI	magnetic resonance imaging
MWD	molecular weight distribution
MWNTs	multi-walled carbon nanotubes
NaMA	sodium methacrylate
NaSS	sodium 4-styrenesulfonate
NIPAM	*n*- isopropylacrylamide
NIR	near-infrared red
NMP	nitroxide-mediated radical polymerization
NMR	nuclear magnetic resonance
OEGMA	oligo(ethylene glycol) methyl ether methacrylate
OTS	octadecyltrichlorosilane
PDI	polydispersity index
PEG	polyethylene glycol
PEGMA	poly(ethylene glycol) methyl ether methacrylate
PEO	polyethylene oxide
PEOMA	poly(ethylene oxide) methacrylate

PFS	2,3,4,5,6-pentafluorostyrene
POSS	polyhedral oligomeric silsesquioxane
POSS-MA	3-(3,5,7,9,11,13,15-heptacyclopentylpentacyclo-[9.5.1.1.^{3,9} 1.^{5,15}1^{7,13}]-octa- siloxane-1-yl) propyl methacrylate
PTFE	polytetrafluoroethylene
PVDF	poly(vinylidene fluoride)
RAFT	reversible addition-fragmentation chain transfer polymerization
RI	refractive index
RMS	root-mean square
ROMP	ring-opening metathesis polymerization
SAM	self-assembled monolayer
SAv	streptavidin
SEC	size exclusion chromatography
SEM	scanning electron microscopy
SEMQ	scanning electron microscopy, quantometer
SFRP	stable free radical polymerization
SQUID	superconducting quantum interface device
St	styrene

SWNTs	single-walled carbon nanotubes
TBAEMA	2-(*tert*-butylamino)-ethyl methacrylate
TEM	transmission electron microscopy
TEMPO	2,2,6,6-tetramethyl-1-piperidinoxyl
TFEMA	2,2,2-trifluoroethyl methacrylate
TGA	thermogravimetric analysis
TPP	triphenylphosphine
TPPO	trioctylphosphine oxide
THF	tetrahydrofuran
UHP	ultrahigh-purity
XPS	x-ray photoelectron spectroscopy

CHAPTER 1

Introduction and Literature Review

1.1 Surface grafting techniques

Polymers have been considered as excellent candidates for all purposes of surface modifications. Thin polymer films may improve wetting property and biocompatibility of biomaterials, reduce corrosion rate of metals and serve as conductive layers or insulators in modern microelectronics industry. The major challenge here is to develop proper techniques to achieve uniform and robust polymer thin films on different kinds of surfaces.

Coating is the most commonly use method for preparing polymer thin films. This method is fast and simple, appropriate solvents are selected to dissolve polymers and to supply good wettability over targeted substrates; then the polymer solutions are coated onto the substrates by different kinds of techniques, such as casting, spin-coating, dip-coating, and printing techniques which cause lots of interest recently. However, no matter which technique is used here, polymer chains are just absorbed to the surfaces by very weak physical interactions such as Van der Walls forces and hydrogen bonding. These coated polymer films are thus lack of robustness; they can be easily rinsed off by solvents, or peeled off by physical forces. In order to improve robustness, polymers should be covalently bonded to surfaces.

In recent years, polymer brushes prepared by surface grafting technique have gained great interests. The initial use of the surface grafting technique is to help stabilize colloidal particles through modification of surface chemistry and morphology. By this technique, polymer chains are covalently bound to a variety of surfaces, such as flat silicon wafers, nanoparticles, carbon nanotubes and polymer films. Because of steric congestion, polymer chains are forced to stretch out from surface in an entropically unfavourable conformation. These stretched polymer chains are termed as polymer brushes. Polymer brushes have been proved to have many applications in different areas, for example, stabilizer of colloids, bioactive coatings, and barriers for corrosion resistance, etc.

For surface grafting technique, two parameters are of special importance. One is grafting density and the other is polymer chain length. Grafting density is defined as the number of polymer chains grafted per unit area of surface, and it can be calculated using the following equation:

$$\sigma = \frac{d \times N_A \times \rho}{M_n} \tag{1.1}$$

Where d is the thickness of polymer film, ρ is the density of bulk polymer, N_A is the Avogadro constant, M_n is the number-average molecular weight of polymer chain on surface.

There are two general strategies to prepare polymer brushes by surface grafting technique; one is “grafting to”[1] and the other is “grafting from”.[2,3] In “grafting to” approach, both polymer chain ends (or side chains) and surfaces are functionalized. Polymer chains are then covalently bound to surfaces via condensation type of reactions. The advantage of this method is that the polymer chains are made in advance, so that it is easy to design and characterize their structures prior to grafting. However, grafting densities (chains/nm^2) and film thickness achieved by this method are just comparable to those obtained by physical absorption method. Grafting densities and film thicknesses are in the order of 0.1chains/nm^2 and a few nanometers, respectively.[4,5,6] That is because once some polymer chains are attached to surface; these chains form a diffusion barrier and prevent other polymer chains from approaching the surface. In this case, the grafting densities decrease as polymer molecular weight increases,[5] which limits the available polymer molecular weight to 10^3 to 10^4Da.[4,5,6] As a result of the low grafting densities, polymer chains on surface have lots of free space, so that they adopt a “mushroom-like” configuration on the surface. Generally speaking, “grafting to” method is not a good choice for preparing high-density thick polymer films.

The drawbacks of “grafting to” methods can be avoided by surface-initiated polymerization (“grafting from” method). This method is newly developed and has drawn great attention in the recent years. In this method, initiators are first immobilized onto surface. Many immobilization methods can be used, for instance, treating surface with plasma or forming an initiator-containing self-assembled monolayer (SAM) using “solution” or “gas” methods. After that, polymer brushes are grafted from the immobilized initiators on the surface by *in-situ* polymerization. Because monomer molecules are very small in size, they can easily diffuse to the propagating sites on the surface, which results in high grafting densities (0.3-0.7chain/nm^2) and high molecular weight (10^4-10^5Da). The high grafting densities force polymer chains to strand up from the surface to satisfy their volume requirements; so that, the polymer chains have “brush-like” configurations (see Scheme 1.1). The most important advantage of the “grafting from” method is that it allows the preparation of very dense and thick polymer films (10nm to 1μm) which improve surface coverage and therefore performance. [7-10] However, because the polymer brushes are directly grafted from the surface, their characterization remains to be a big problem.

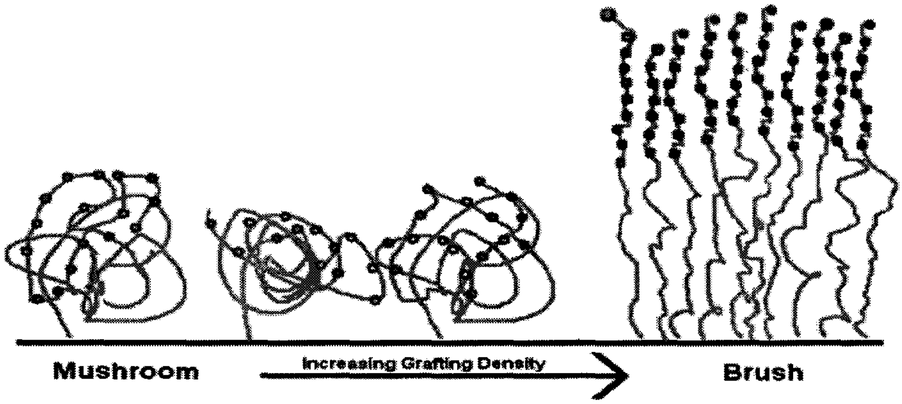

Scheme 1.1 Transition of polymer chains from "mushroom" to "brush"

1.2 Surface-initiated polymerization

1.2.1 Overview of surface-initiated polymerization techniques

A number of polymerization methods have been used to graft polymers from surfaces; including cationic polymerization,[11] anionic polymerization,[11] ring-opening polymerization,[12] ring-opening metathesis polymerization (ROMP),[13,14] conventional free radical polymerizations (CFRP) and controlled/living radical polymerizations (CLRP). Both of living anionic and cationic polymerizations are able to produce nearly monodisperse polymers. However, the two polymerization techniques require very stringent reaction conditions, and are very sensitive to moisture and impurities (i.e. at very low temperatures and very pure systems). The main limitations of ring-opening polymerization and ring-opening metathesis polymerization are the lack of control and the limited monomer types. In this case, free radical polymerization becomes the most widely used method for grafting of polymer from surface. Rühe et al.[14] was the first to use conventional free radical polymerization for surface modification purposes. In their study, silica gel surfaces were modified with self-assembled monolayer of azo initiators; polystyrene was then grafted from these initiators. However, they found that a precise control of grafted polymer layer thickness was very difficult. The thickness always increased very fast at the beginning and then leveled off. This is because in conventional radical polymerization, polymer chains have very short life. From initiation to termination, it takes only seconds or subseconds for an individual chain to propagate thousands of repeat units. The early grown polymer chains cover large surface areas and thus prevent further grafting of polymer chains at their vicinities. Another drawback of conventional free radical polymerization is the high polydispersity of polymer molecular weight distribution. The polydispersity keeps on increasing during the whole stage of reaction, from 1.50 at the beginning to around 2.0 at the end. The high polydispersity indicates that grafted polymers have very different chain lengths from each other. The uniformity of grafted polymer layer was therefore very poor.

In order to overcome these drawbacks of conventional free radical polymerization, varieties of controlled/living radical polymerization (CLRP) techniques have been used. CLRP techniques have ability to grow polymer chains without or with very limited chain termination or chain transfer, which results in well-controlled molecular weight and very narrow polydispersity index (PDI) of the final polymer product. Another very unique characteristic of the CLRP techniques is "living" polymer chain ends, which are benefited from no or limited radical termination. The "living" polymer chain ends can easily initiate growth of a second polymer block with an addition of another monomer. In recent years, these aforementioned advantages or features of CLRP techniques, plus versatility of monomer types, tolerance of impurities, mild reaction conditions have gained themselves great interests (see Scheme 1.2).

The CLRP techniques include nitroxide-mediated radical polymerization (NMP),[15] atom transfer radical polymerization (ATRP),[16-20] and reversible addition-fragmentation chain transfer polymerization (RAFT).[21] CLRP techniques allow preparation of uniform polymer films with well controlled thickness. In addition, as living chains are less susceptible to early termination, the CLRP methods can offer higher grafting densities than CFRP methods. Among these CLRP techniques, ATRP, independently developed by Matyjaszewski and Sawamoto, has been so far the most widely applied method for surface grafting. ATRP uses metal halide/nitrogen-based ligand systems as catalysts.[6]

It can be operated under both homogeneous and heterogeneous conditions. Reaction temperatures can be varied from room temperature to over 100□. Versatile types of solvents such as organic solvents, water, supercritical carbon dioxide, and ionic liquids or in bulk can be used for ATRP.

Compared to NMP and RAFT, ATRP has its own advantages. Typical ATRP initiators are commercially available α-haloesters or benzyl halides. In contrast, NMP uses alkoxyamines as initiator and RAFT uses dithioesters as chain transfer agent. Both have more complicated structures and always require multi-step synthesis. Also, the cleavage of alkoxyamine initiators for NMP requires high temperature (>100□), so that NMP can only use solvents that have very high boiling points. Compared to the versatile monomer types for ATRP, NMP is only good for quite limited types of monomers, such as styrene and its derivatives, MMA, 1,3-butadiene, 2-methyl-1,3-butadiene. RAFT has all of ATRP's advantages, and it can produce polymers with very high molecular weights. However, so far, surface-initiated RAFT can only graft very thin polymer films (<30nm). That is believed to be attributable to RAFT's propensity to become diffusion controlled within the polymer film growing at the surface.

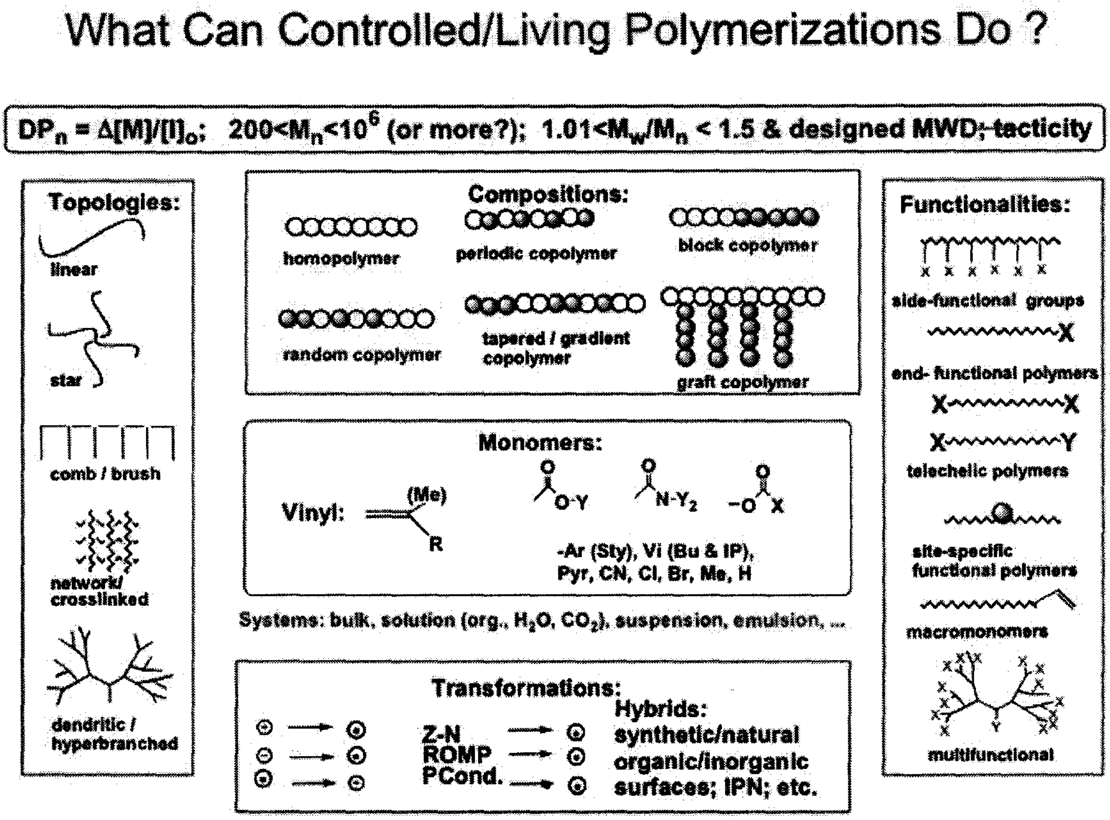

Scheme 1.2 Examples of the architectures produced by CRP/LRP technique.[2]

1.2.2 Introduction of surface-initiated atom transfer radical polymerization

In order to immobilize ATRP initiators onto surfaces, surface-attachable initiators bearing silane or thiol reactive groups are synthesized. These initiators then react with surface functional groups to form monolayer of initiators. Polymer brushes with different compositions can then be easily grafted simultaneously from these immobilized initiators. ATRP is controlled by a fast equilibrium between activation and deactivation which was shown in Scheme 1.3. Because the rate constant of deactivation k_{deact} is usually many orders of magnitude higher than that of activation k_{act}, the concentration of propagating species remains at a very low level and thus radical termination was efficiently avoided. Based on the mechanism, a high concentration of deactivating species (Cu(II) complex) is indispensable in order to get control of ATRP. For solution ATRP, the red-ox reaction of free initiator with Cu(I) can provide enough Cu(II) complex. However, when it comes to surface- initiated ATRP, there are very limited numbers of initiators on the surface and thus the red-ox reaction can only produce a low concentration of Cu(II) complex. As a result, the system cannot achieve good control.

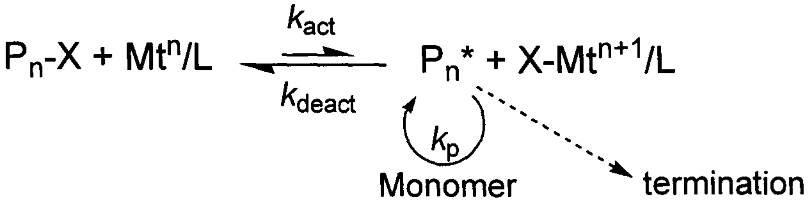

Scheme 1.3 General scheme of ATRP

There are generally two approaches to solve this control problem in surface-initiated ATRP. One is to add some free initiator at the beginning of reaction, so that ATRP occurs simultaneously in solution and from surface. The free initiators in solution are responsible for providing proper amount of deactivator (Cu(II) complex). In this approach, "free" polymer is formed in the solution. The "free" polymer molecular weight is confirmed to be almost the same as that of the "grafted" polymer chains. In this case, the grafting density can be estimated from the equation (1.1). However, this approach has one disadvantage. Most monomer molecules are consumed by "free" initiators in solution. Moreover, the "free" polymer chains formed in solution may absorb onto surface. These absorbed polymer chains act as barriers for growth of surface polymer chains. As a result, thick polymer layers cannot be achieved by this method. Also in order to clean these absorbed polymer chains, it may require an intense effort. The other approach was proposed by Matyjaszewski et al.[16] A predetermined amount of extra Cu(II) halide (10-30mol% of Cu(I)) is directly added into the system at the beginning. It can assure a sufficient amount of deactivating species. Because all monomer molecules are used to graft polymer brushes and there is no "free" polymer chain problem, this approach is very useful for preparing thick polymer films. The problem of this approach is that it cannot give the grafting density because of difficulty to obtain molecular weight data of the "grafted" polymers. Although the polymer chains can be cleaved from surfaces by HF acid, however, the limited number of polymer chains on the surface makes it very difficult to characterize the tiny amount sample.

1.2.3 Surface-initiated ATRP from planar surfaces

Recently, considerable attentions have been paid to dense polymer brushes immobilized on flat surfaces for their potential applications as corrosion barriers, biomaterials and microelectronic devices, etc. Surface-initiated ATRP is a very effective and convenient method to graft polymer brushes from flat surfaces. Due to the well-controlled nature of ATRP, it is easy to control thickness, functionality and other properties of the grafted polymer brushes. In addition, polymer brushes with complicated structures such as hyperbranched and crosslinked networks can be easily achieved by the use of inimers and divinyl monomers.

The first work of surface-initiated ATRP was reported by Fukuda and coworkers in 1998.[22] They used Langmuir-Blodgett (LB) technique to form a monolayer of ATRP initiators on silicon surfaces. Poly(methyl methacrylate) (PMMA) was then grafted from the immobilized ATRP initiators with added free initiator. The "free" polymer formed in solution was found to have very narrow polydispersities. In addition, a linear relationship between "free" polymer molecular weight and monomer conversion was also found, which indicated that the ATRP initiated from silicon surface was well controlled. More than 80nm thick PMMA film was achieved after 12 hours of reaction. The PMMA film thickness was dependant on the free initiator concentration. The lower the concentration was, the thicker the film was.

Surface-initiated ATRP with added deactivator was first reported by Matyjaszewski and coworkers in 1999.[16] Although it was not easy to characterize the grafted polymer chains, a linear increase in polymer film thickness with reaction time confirmed that the grafting polymerization was well controlled. A control experiment of solution ATRP was carried out under identical experimental conditions, and with the same reaction time. The length of grafted polymer chains was found to be only 1/6 of the calculated extended length of free polymer chains in solution. Due to the geometric constraint caused by high grafting density, polymer chains on surface cannot grow as freely as those in solution. Moreover, the high grafting density also enhanced the chance of radical termination reactions. These two reasons can explain the much shorter length of grafted polymer chains compared to free polymer chains in solution.

Nowadays, ATRP in aqueous media is of great interest because it is particularly useful in preparation of water soluble polymers and polyelectrolytes, which have very important applications in biomedical science. Moreover, water was found to have an ability to greatly accelerate the ATRP process. Surface-initiated ATRP in aqueous media allows for preparation of polymer brushes under room temperature, which not only facilitates the use of temperature-sensitive substrates, for example, thiol SAMs on gold, but also prevents spontaneous thermal polymerization and other unfavourable side reactions such as elimination reactions, thermal cross-linking and transesterification. By use of this technique, many water-soluble polymers, such as poly(2-hydroxyethyl methacrylate) (PHEMA), poly(oligo(ethylene glycol) methyl ether methacrylate) (POEGMA) and polyelectrolytes have been prepared with greatly enhanced reaction rates. In 2002,[18] Huang et al. reported the preparation of more than 700nm thick of PHEMA film from gold in only 12 hours. They did a control experiment of surface-initiated ATRP of HEMA in the absence of water. After 12 hours of reaction, the PHEMA film was only 6nm thick. The dramatic difference in PHEMA film thickness proved the effectiveness of water to accelerate surface-initiated ATRP. Even for non-water-soluble polymers, water can also enhance the polymerization rate. For example, Huck reported the preparation of PMMA brushes in aqueous media in 2001[23] and the thickness reached 30nm in only 35min. Compared to the previously reported reaction time of up to 12 hours to achieve the same thickness, the polymerization rate was enhanced by more than ten times.

Polyelectrolyte brushes, both cationic and anionic, have been prepared by Huck and coworkers[24] using aqueous ATRP. Charged monomers, such as [2-(methacryloyloxy)ethyl]trimethylammonium chloride (METAC) and sodium methacrylate (NaMA) were grafted from gold surfaces. Different from the conventional post-polymerization charge introduction method, the direct grafting of polyelectrolyte brushes ensured that every repeat unit carry a charge.

Because of the “living” nature of polymer chain ends prepared by ATRP, it is possible to graft block copolymer brushes by this technique. Brittain and Cheng[25] have grafted polystyrene (PSt)-*b*-PMMA diblock and PSt-*b*-PMMA-*b*-PSt triblock copolymer brushes with various compositions from silicon wafers, and studied the response of these copolymer brushes to selected solvents, such as dichloromethane or dichloromethane-cyclohexane mixtures (see Scheme 1.4). They found that these block copolymer brushes had the ability to self-assemble into different conformations by treatment with different solvents, and the transformation was totally reversible. This work has demonstrated that stimulus-responsive or “smart” polymer brushes can be achieved by the synthesis of diblock or triblock copolymers which have segments with distinct stimuli triggers. Change in environment causes change in conformation of these grafted brushes, and then affect both morphologies and properties of the polymer films.

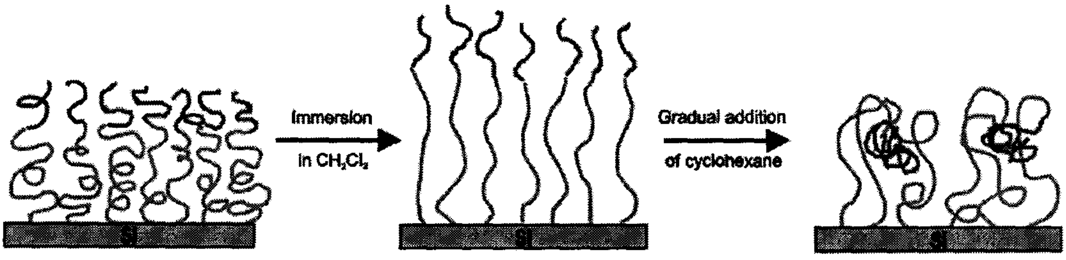

Scheme 1.4 Surface morphology changes of PSt-*b*-PMMA diblock copolymer brushes

upon treatment with different solvents.[25]

Patterned polymer films have very promising prospects in biotechnology and microelectronics. Many techniques including photolithography, micro-contact and nano-contact printing can be employed to localize ATRP initiators on surface, followed by growth of patterned polymer brushes from these immobilized initiators. Hawker and coworkers[26] reported the first trial to prepare patterned polymer brushes by surface-initiated ATRP. Patterned ATRP initiators were first immobilized on gold surface by micro-contact printing, and then PMMA, PHEMA and other polymer brushes were grafted from these initiators (see Scheme 1.5). To achieve the similar goal, Zhou et al.[27] prepared PMMA and PHEMA films by surface-initiated ATRP and then exposed them to ultraviolet irradiation through a transmission electron microscopy (TEM) grid. All polymer brushes in the irradiated region were removed to give a well-patterned film.

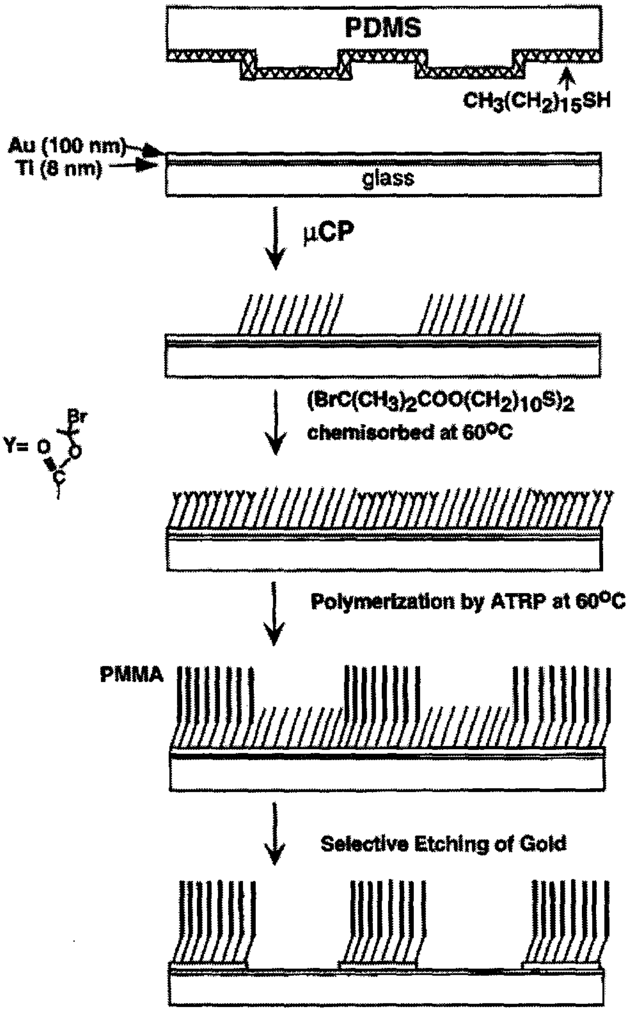

Scheme 1.5 Preparation of patterned polymer films by surface-initiated ATRP.[26]

1.2.4 Surface-initiated ATRP from non-planar surfaces

Surface-initiated ATRP technique is especially useful in preparation of uniform polymer films on non-planar surfaces, which cannot be achieved by traditional coating methods. Many non-planar surfaces have been used as substrate, such as silica, gold, latex, magnetite particles and carbon nanotubes. For surface-initiated ATRP, controlled polymerization simultaneously occurs across entire surfaces, which allows for growth of well-defined polymer brushes from non-planar surfaces. These dense polymer brushes intensively affect interactions between the modified surface and surrounding environment at the molecular level. For example, the dispersibility and dispersion stability of nanoparticles and nanotubes in appropriate solvents can be greatly enhanced and the separation selectivity of chromatographic supports can be effectively improved.

Silica particles are the mostly used non-planar substrate for surface-initiated ATRP. The first work was reported by Patten et al.[28,29] They successfully grafted PSt and PMMA from silica particles with an average diameter of 75 or 300nm(see Scheme 1.6). By the use of sol-gel chemistry, Matyjaszewski et al.[30] synthesized ATRP initiator-functionalized silica particles with an average diameter of about 20nm, and then homopolymer and block copolymers were grafted from these silica particles.

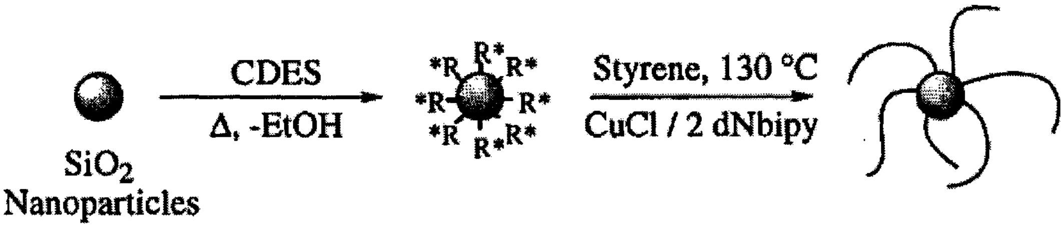

Scheme 1.6 Surface-initiated from SiO_2 nanoparticles.[28]

This strategy can be easily extended to other inorganic nanoparticles, for example, gold, CdS quantum dots, and magnetite, etc. The first work of surface-initiated ATRP from gold nanoparticles was reported by Walt et al. in 2002.[31] Gold nanoparticles were prepared in the presence of 11-mercaptoundecanol and subsequently esterified with 2-bromoisobutyryl bromide. PMMA brushes were then grafted from these initiator-functionalized gold nanoparticles to produce gold-core, polymer-shell nanoparticles.

Other than these inorganic particles, surface-initiated ATRP can also be applied to modification of polymer particles. Zheng and Stöver[32] grafted poly(methyl acrylate) (PMA), poly(*N,N'*-dimethylaminoethyl methacrylate) (PDMAEMA), PMMA, PHEMA, and block copolymer brushes from functionalized divinylbenzene/hydroxyethyl methacrylate copolymer microspheres at room temperature. Guerrini et al.[33] used cross-linked poly[styrene-*co*-2-(2-bromopropionyloxy)] latex particles as the core, the ATRP of 2-hydroxyethyl acrylate (HEA) and METAC from these latex particles formed a hydrophilic shell around the hydrophobic core.

Single-walled (SWNTs) and multi-walled carbon nanotubes (MWNTs) are of great interest for their extraordinary mechanical and electrical properties. However, the poor dispersibility of carbon nanotubes in most solvents greatly hinders their processability. Chemical modifications of nanotubes can help to improve their dispersibility, but at the same time, the structure and properties of the nanotubes may also be destroyed because a large number (at least one of ten) of sidewall carbons must be modified to achieve desirable dispersibility. Surface-initiated ATRP was proved to be a much more suitable method. Polymer chains were grown from only 1 of 250 sidewall carbons, which can achieve good dispersibility without destroying the nanotube structure. Recently, numerous investigations of surface-initiated ATRP from both SWNTs and MWNTs have been reported. Qin et al.[34] grafted polystyrene from SWNTs (see Scheme 1.7). The dispersibility of these nanotubes in common organic solvents was greatly improved after the polymer grafting. The grafted polymer chains also had the ability to force the starting carbon nanotube bundles to separate into smaller bundles or ever individual tubes. Kong et al.[35] used the same method to graft a PMMA layer on MWNTs and then grew a second block of PHEMA atop the PMMA layer, thus yielded a nanotube surrounded by a non-polar PMMA layer which itself was surrounded by a more polar PHEMA layer. The resulting block copolymer modified nanotubes exhibited very good solubility in good solvent for PHEMA, the outer layer.

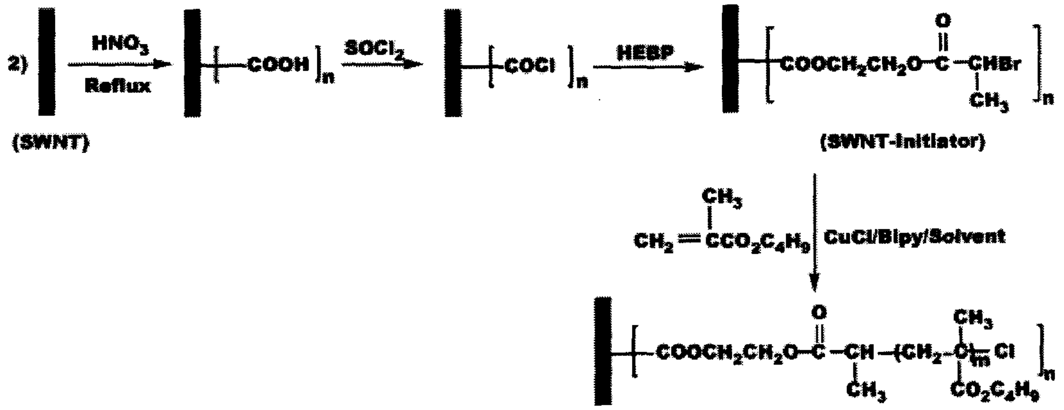

Scheme 1.7 Modification of SWNTs by surface-initiated ATRP.[34]

1.2.5 Surface-initiated ATRP from other substrates

As discussed above, surface-initiated ATRP is a very powerful technique to prepare well-defined polymer brushes from surfaces. Its applications were not limited to aforementioned planar and non-planar substrates; many other special materials were also successfully used as substrates for it. In 2005,[36] Maynard et al. reported the first work of surface-initiated ATRP from protein. Streptavidin (SAv) was chosen as the protein to demonstrate the technique. The general procedure of ATRP from SAv is outlined in Scheme 1.8. A biotinylated ATRP initiator was prepared and reacted with streptavidin to be liked to the protein. The prepared protein macroinitiator was then used to initiate the polymerization of *n*-isopropylacrylamide (NIPAM) and poly(ethylene glycol) methyl ether methacrylate (PEGMA). The successful grafting of polymers was confirmed by

SDS-PAGE and size exclusion chromatography (SEC) measurements.

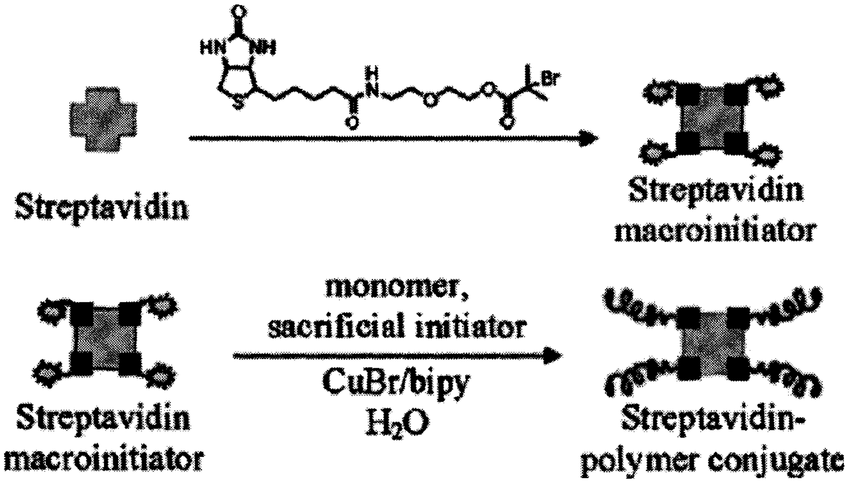

Scheme 1.8 Preparation of streptavidin-polymer conjugates.[36]

Surface-initiated ATRP has been used as a very useful tool to modify the pores of membranes, either inorganic or polymeric, to improve the separation efficiency or incorporate special separating ability for certain molecules. In 2004, Kang et al.[37] carried out grafting copolymerization of an intiator-containing monomer, 2-(2-bromoisobutytyloxy) ethyl acrylate (BIEA) from ozone-pretreated poly(vinylidene fluoride) (PVDF) to achieve PVDF-*g*-PBIEA copolymer. The copolymer solution was used to fabricate porous membranes by phase inversion. As shown in Scheme 1.9, ATRP of PEGMA and sodium 4-styrenesulfonate (NaSS) can be initiated from the BIEA side chains. By this method, the inner surfaces of membrane pores were modified by PPEGMA or PNaSS polymer chains, which generated antifouling membrane and electrolyte-responsive membrane, respectively.

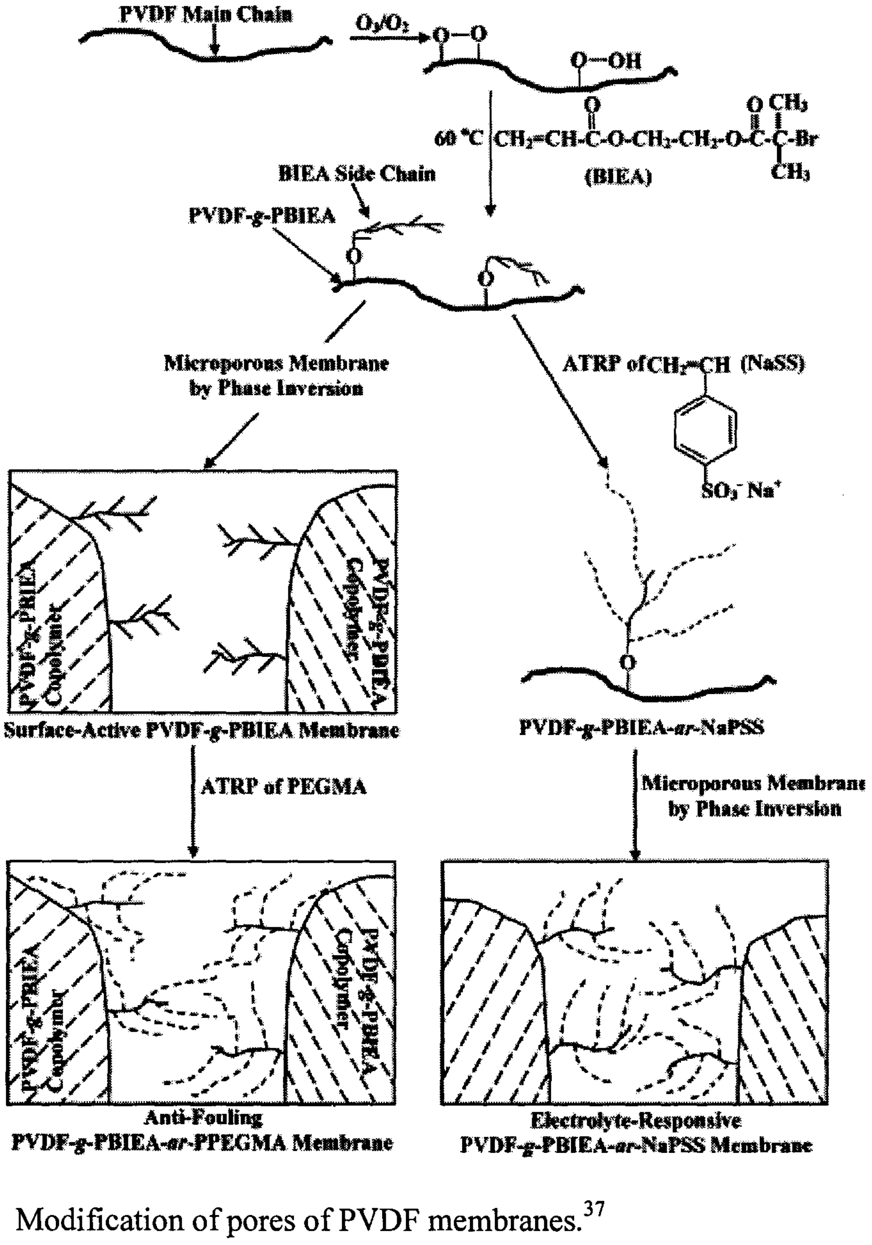

Scheme 1.9 Modification of pores of PVDF membranes.[37]

The pores of inorganic membranes can also act as a template for the preparation of polymer nanotubes. In 2005, Li et al.[38] immobilized silane-based ATRP initiators on the pore walls of porous anodic aluminium oxide (AAO) membrane and then a crosslinked copolymer of NIPAM and *N,N'*-methylene-bisacrylamide (PNIPAM-*co*-MBAA) was grafted from the pore inner walls. The AAO membranes were then dissolved in NaOH solution and PNIPAM-*co*-MBAA nanotubes with well defined length, outer diameter, wall thickness were achieved. The prepared polymeric nanotubes had very high flexibility and they also exhibited a reversible thermo-responsive behaviour. The process is outlined in Scheme 1.10.

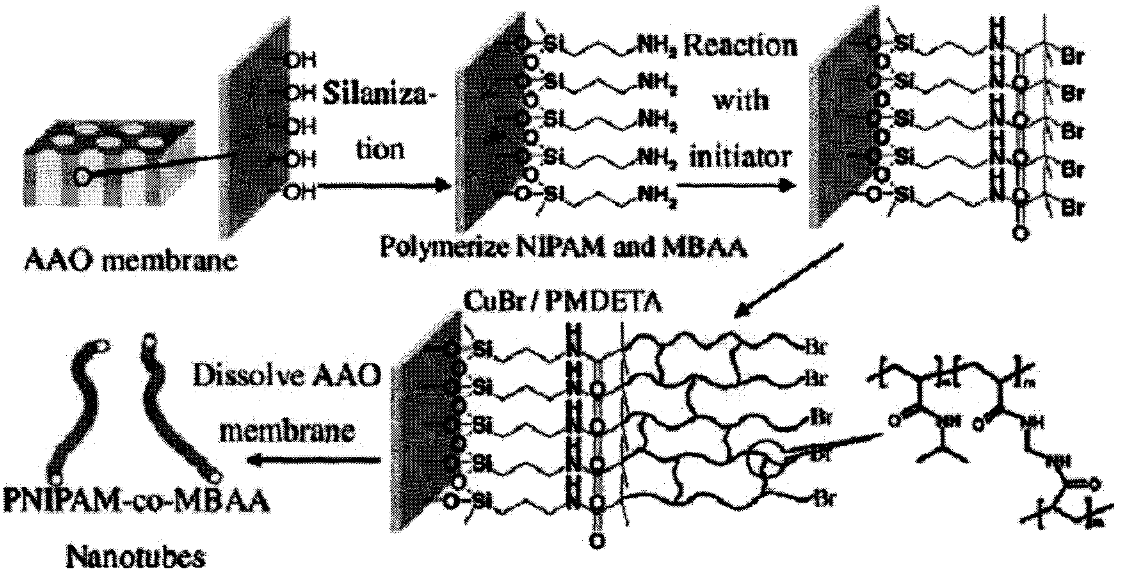

Scheme 1.10 Fabrication of PNIPAM nanotubes in a porous AAO membrane.[38]

Clay-polymer nanocomposite materials combine the mechanical strength of clay and the flexibility of polymer, which have drawn great interests. The surface-initiated ATRP technique also finds its uses in preparation of clay-polymer nanocomposite materials. In Shipp et. al.'s work,[39] an ATRP initiator consisting of a quaternary ammonium salt moiety and a 2-bromoisobutyrate moiety was intercalated into the interlayer spacing of montmorillonite (MMT). Subsequent ATRP of styrene, MMA, or *n*-butyl acrylate (BA) from these immobilized initiators significantly helped the exfoliation of MMT platelets (as shown in Scheme 1.11).

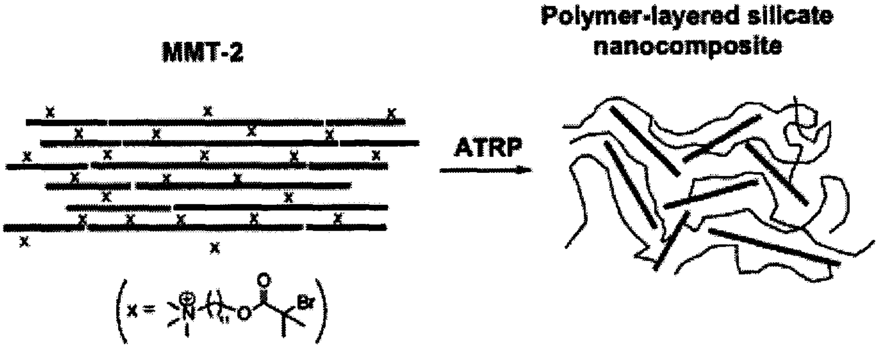

Scheme 1.11 Preparation of polymer-MMT nanocomposite materials.[39]

1.3 Grafting of polymers from metal surface

1.3.1 Introduction of metals

Because of their high mechanical strength, superior electrical and thermal conductivities and other important physical properties, metals and alloys are probably the most widely used and most useful materials in our daily life. We can easily find numerous metal-made objects around us, such as car bodies, building materials, and varieties of tools.

Iron is the most commonly used metal today, accounting for 95% of worldwide metal production. Its low cost and high strength makes it a very important component of many different industries, for example, construction, automobile manufacturing and machinery fabrication. As it is well known, the major disadvantage of iron and steel is that they can be easily corroded in wet atmosphere and their mechanical strength suffers badly from rust. In order to solve corrosion problem, stainless steels were developed. Stainless steels are a group of iron alloys which contain at least 10wt.% of chromium. The function of chromium is to help build a passivation film on the surface which has recovering ability after mechanical abrasion. For some applications, molybdenum was also added into stainless steel to further improve its corrosion resistance. The resulting materials can withstand pitting and crevice corrosion at the presence of chlorine.

Aluminium is a soft, durable, lightweight and malleable metal. It is the second most produced metal in today's market, only after iron. Due to a very thin, but very dense layer of aluminium oxide, the corrosion resistance of aluminium is very good. The excellent corrosion resistance, combined with the light weight makes aluminium alloys a very useful group of materials for space engineering. They are widely used to form vital components of aircraft and rockets. Aluminium is also a very good electrical and thermal conductor, so it is also widely used as household wiring material.

Copper and nickel are the two metals which have important applications in our day life. Copper has played a very important role in the history of mankind, especially before the discovery of iron. Copper has excellent electrical and thermal conductivity, good malleability and ductility; also it has a very unique property to kill bacteria. It is widely used as electrical wires, computer heat sinks, building materials, and doorknobs in hospitals. The use of nickel can be tracked back as far as 3500 BC. Nickel is persistent to oxidation, so that it is an important component of stainless steels. Nickel can be used as magnets for it is one of five ferromagnetic elements. Nickel is also a good catalyst for hydrogenation in the laboratory. Other than these applications listed above, copper and nickel are also key components of many useful alloys, such as brass (copper and zinc), cupronickel (copper and nickel) and all kinds of superalloys.

1.3.2 Surface-initiated ATRP from metal surfaces

In sprite of wide spread uses of the surface-initiated ATRP technique to various substrates, little effort has been made to metals and alloys. Different from other materials used in surface-initiated ATRP, metals have very high reactivity and their surface chemical compositions are very complicated.

Jérôme's group was the first to succeed in applying this technique to steel surface.[40] In 2003, they synthesized a dual monomer, 2-chloropropionate ethyl acryalate (cPEA), which had acrylate structure and an activated chloride able to initiate ATRP. The functional monomer was electro-grafted from steel surface to form a dense layer of ATRP macroinitiators. PSt then was grafted from these macroinitiators by surface-initiated ATRP (See Scheme 1.12). Because copper catalysts were found to corrode steel surface, the authors used Grubbs catalyst and nickel catalyst instead. However, these catalysts cannot provide good control over the polymerization. The grafted PSt had very high polydispersity. The polymer film surfaces were very rough. Using this "macroinitiator" strategy, this group successfully grafted many other monomers from steel surfaces. In 2006, they grafted 2-(*tert*-butylamino)-ethyl methacrylate (TBAEMA) from stainless steel surfaces.[41] They also succeeded in the copolymerization of TBAEMA with either monomethyl ether of poly(ethylene oxide) methacrylate (PEOMA) or acrylic acid (AA) or styrene. Peeling tests revealed that the polymer films had very strong adherence to the stainless steel surface. The surface roughness was found to decrease after the grafting of polymer films. Poly(TBAEMA) brushes copolymerized with either negatively charged carboxylate groups or flexible hydrophilic PEO chains were very effective in preventing protein absorption as well as in reducing the adhesion of bacteria *S. aureus*. The antibacterial stainless steel can be made into biomedical implants which are very important in orthopaedic applications.

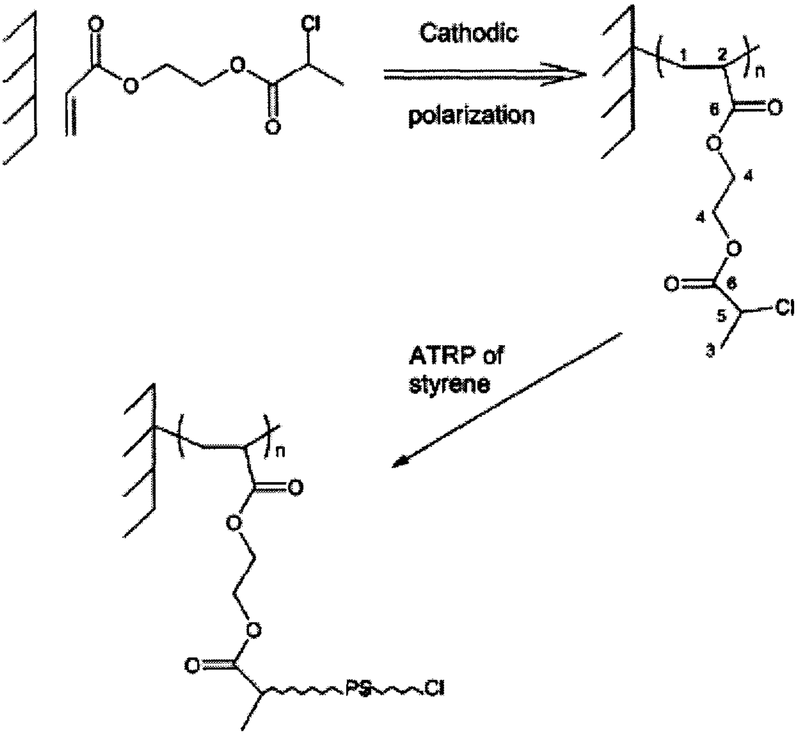

Scheme 1.12 Two step process for the grafting of polystyrene from steel surfaces. [40]

In 2005, Matrab et al. reported a novel approach for surface-initiated ATRP from steel surface (see Scheme 1.13).[42] A brominated aryl diazonium salt $BF_4^-, {}^+N_2\text{-}C_6H_4\text{-}CH(CH_3)\text{-}Br$ was grafted onto steel surfaces by electrochemical reduction. ATRP of MMA, BA and styrene was initiated from the $-C_6H_4\text{-}CH(CH_3)\text{-}Br$ species on surface. The grafted polymer films were found to have very compact structures by AFM studies. However, the surface was still very rough after the polymerization.

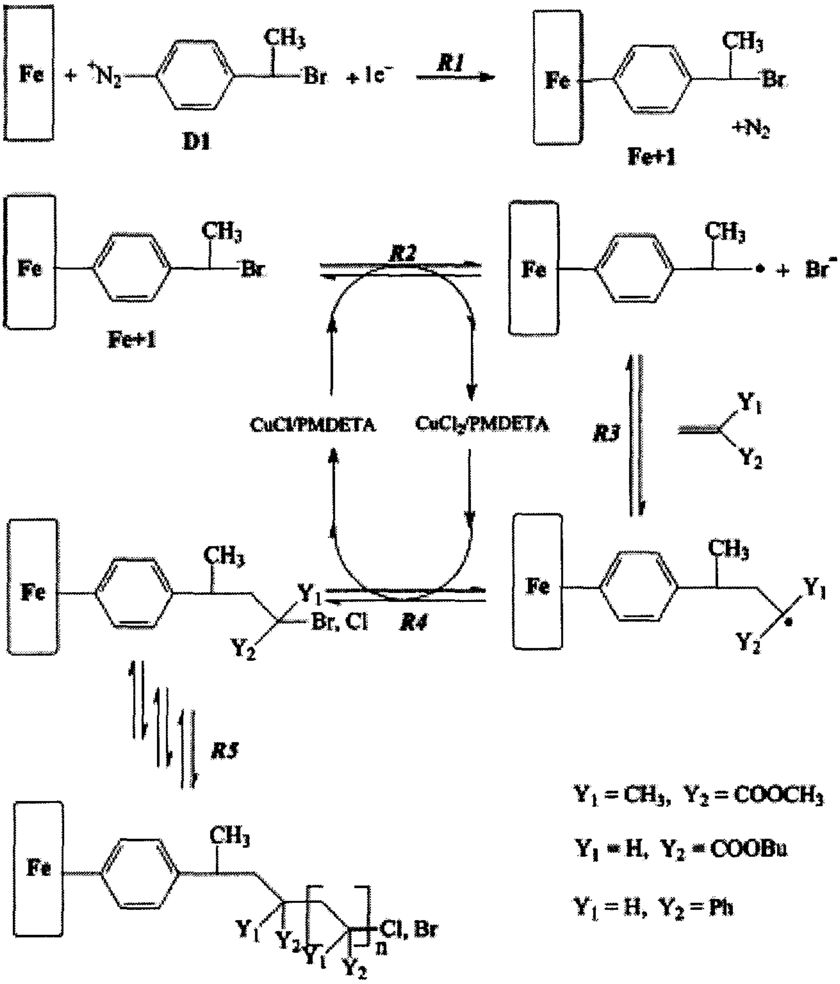

Scheme 1.13 Surface-initiated ATRP using electro-grafted initiators based on aryl diazonium salts.[42]

In a recent paper,[43] Fan et al. prepared a biomimetic anchor – a catecholic ATRP initiator. This catecholic initiator can readily absorb to titanium and 316L stainless steel surfaces. ATRP of OEGMA was then initiated from these immobilized biomimetic initiators to prepare antifouling polymer coatings on the metal surfaces (see Scheme 1.14). More than 100nm thick of POEGMA films were achieved by this method. By combining molecular assembly patterning by lift-off (MAPL) with surface-initiated ATRP, they also succeeded in preparing micropatterned polymer coatings on titanium surfaces for potential uses as cell arrays. In 2006, they reported a further study on the effect of ethylene glycol side chain length on the cell fouling resistance properties. OEGMA monomers containing side chains of 4, 9 and 23 ethylene glycol (EG) units were used for surface-initiated ATRP from a titanium substrate. The polymer films have the same short term (three weeks) antifouling properties. However, in the long-term experiments, the polymer films with shorter EG side chain length succumbed to cell fouling more rapidly than those with longer EG side chains.

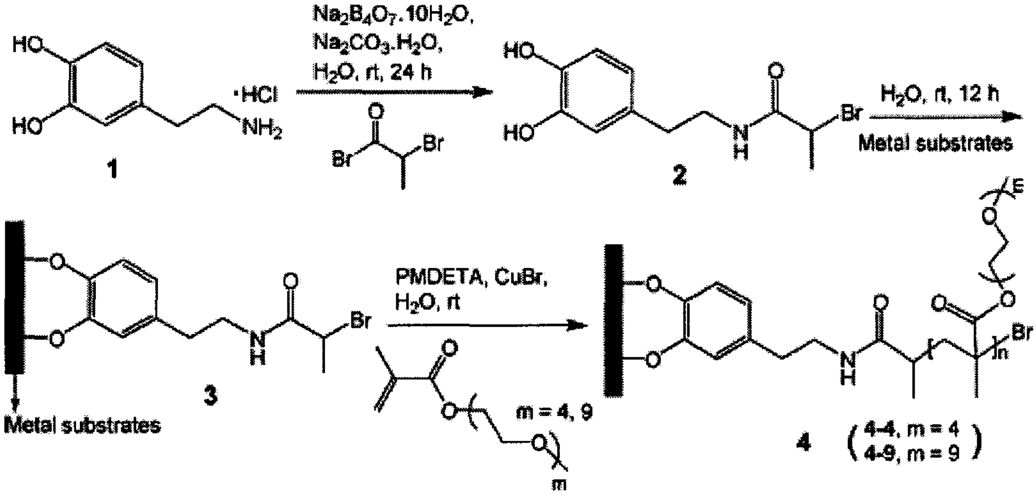

Scheme 1.14 Synthesis and anchoring of the DOPA mimetic initiator and subsequent

Si-ATRP.[43]

Kang's group investigated the surface-initiated ATRP from silicon and polymer surfaces. They succeeded in applying the surface-initiated ATRP to titanium surfaces (see Scheme 1.15).[44] A typical trichlorosilane type surface-attachable ATRP initiators was immobilized onto titanium foil surfaces by reacting with the hydroxyl groups. Well defined polymer brushes of PPEGMA, PDMAEMA, and Poly(2,3,4,5,6-pentafluorostyrene) (PFS) were successfully grafted from these initiators. Because ATRP is well known as a powerful tool for preparing block copolymers, they also tried to graft diblock copolymer brushes consisting of PEGMA and DMAEMA blocks from the titanium surface.

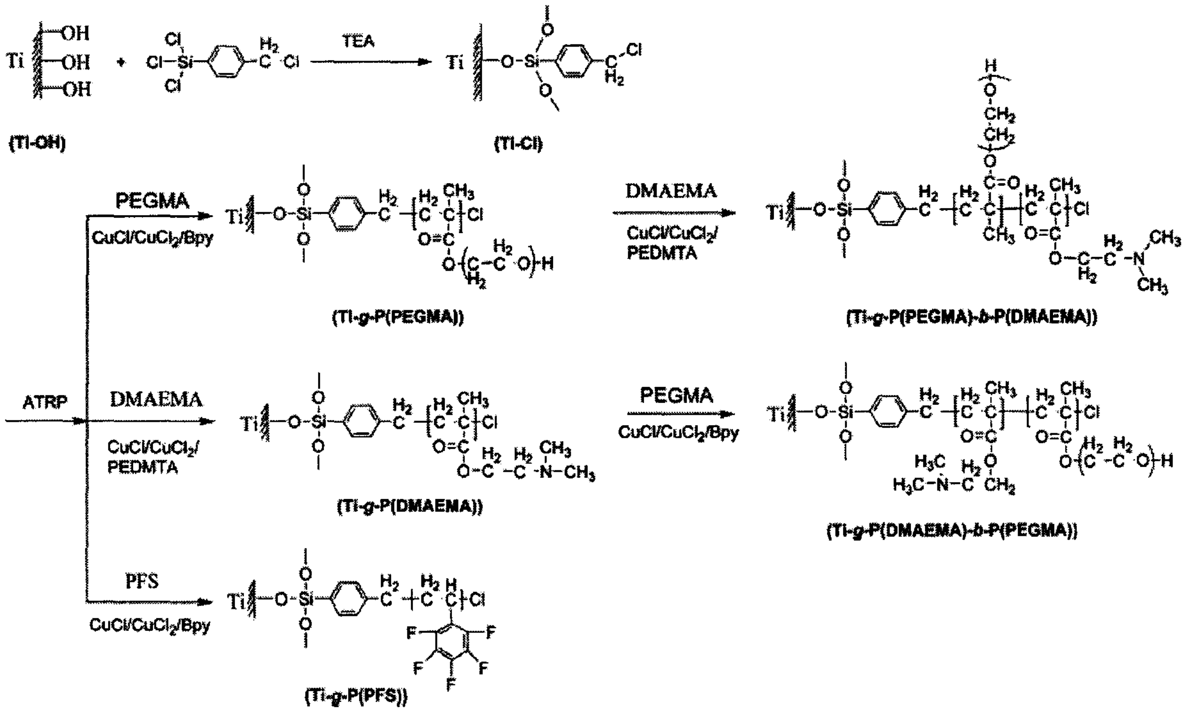

Scheme 1.15 Surface-initiated ATRP from titanium surfaces using trichlorosilane initiator.[44]

All the works by far about the surface-initiated ATRP from metal surfaces are listed above. Interestingly, all the efforts focused on a few kinds of metals, like steel, stainless steel and titanium. Most works used the surface-initiated ATRP to functionalize the metal surface for antifouling or antibacterial applications. However, besides steel and titanium, there are many other important metals which are also of great use in our life, such as copper, aluminium, nickel and zinc etc. Other than pure metals, grafting of polymers from alloys also requires much attention.

1.4 References

(1) Mansky, P.; Liu, Y.; Huang, E.; Russell, T. P.; Hawker, C. *Science* **1997**, *275*, 1458.

(2) Pyun, J.; Kowalewski, T.; Matyjaszewski, K. *Macromol. Rapid. Commun.* **2003**, *23*, 1043.

(3) Zhao, B.; Brittain, W. J. *Prog. Polym. Sci.* **2000**, *25*, 677.

(4) Bridger, K.; Vincent, B. *Eur. Polym. J.* **1980,** *16*, 1017.

(5) Tusbokawa, N.; Hosoya, M.; Yanadori, K.; Sone, Y. *J. Macromol. Sci.-Chem.* **1990,** *A27(4)*, 445.

(6) Ouada, H.B.; Hommel, H.; Legrand, A.P.; Balard, H.; Papirer, E. *J. Chem. Soc. Faraday Trans.* **1988,** *122*, 441.

(7) Baum, M.; Brittain, W. J. *Macromolecules* **2002,** 35, 610.

(8) Tsujii, Y.; Ejaz, M.; Sato, K.; Goto, A.; Fukuda, T. *Macromolecules* **2001,** *34*, 8872.

(9) Feng, W.; Brash, J.; Zhu, S. P. *J. Polym. Sci. Part A: Polym. Chem.* **2004,** *42*, 2931.

(10) Edmondson, S.; Osborne, V. L.; Huck, W. T. S. *Chem. Soc. Rev.* **2004,** *33*, 14.

(11) Advincula, R. *Adv. Polym. Sci.* **2006,** *197*, 107.

(12) Joubert, M.; Delaite, C.; Bourgeat-Lami, E.; Dumas, P. *Macromol. Rapid. Commum.* **2005,** *26*, 602.

(13) Feng, J. X.; Stoddart, S. S.; Weerakoon, K. A.; Kanchana, A.; Chen, W. *Langmuir* **2007,** *23*, 1004.

(14) Prucker, O.; Rühe, J. *Macromolecules* **1998,** *31*, 592.

(15) Husseman, M.; Malmstrom, E. E.; McNamara, M.; Mate, M.; Mecerreyes, D.; Benoit, D. G.; Hedrick, J. L.; Mansky, P.; Huang, E.; Russell, T. P.; Hawker, C. J. *Macromolecules* **1999,** *32*, 1424.

(16) Matyjaszewski, K. ; Miller, P. J. ; Shukla, N. ; Immaraporn, B. ; Gelman, A. ; Luokala, B. ; Siclovan, T. M. ; Kickelbick, G. ; Vallant, T. ; Hoffmann, H. ; Pakula, T. *Macromolecules* **1999**, *32*, 8716.

(17) Prucker, O.; Rühe, J. *Langmuir* **1998**, *14*, 6893.

(18) Huang, W. X.; Kim, J. B.; Bruening, M. L.; Baker, G. L. *Macromolecules* **2002**, *35*, 1175.

(19) Yu, W. H.; Kang, E. T.; Negh, K. G.; Zhu, S. P. *J. Phy. Chem. B* **2003**, *107*, 10198.

(20) Xu, F. J.; Zhong, S. P.; Yung, L. Y. L.; Kang, E. T.; Neoh, K. G. *Biomacromolecules* **2004**, *5*, 2392.

(21) Baum, M.; Brittain, W. J. *Macromolecules* **2002**, *35*, 610.

(22) Ejaz, M.; Yamamoto, S.; Ohno, K.; Tsujii, Y.; Fudaka, T. *Macromolecules* **1998**, *31*, 5934.

(23) Edmondson, S.; Huck, W. T. S. *J. Mater. Chem.* **2004**, *14*, 730.

(24) Osborne, V. L.; Jones, D. M.; Huck, W. T. S. *Chem. Commun.* **2002**, 1838.

(25) Zhao, B.; Brittain, W. J.; Zhou, W.; Cheng, S. Z. D. *J. Am. Chem. Soc.* **2000**, *122*, 2407.

(26) Husemann, M.; Mecerreyes, D.; Hawker, C. J. *Angew. Chem. Int. Ed.* **1999**, *38*, 647.

(27) Zhou, F.; Liu, W. M.; Hao, J. C.; Xu, T.; Chen, M.; Xue, Q. J. *Adv. Funct. Mater.* **2003**, *13*, 938.

(28) von Werne, T.; Patten, T. E. *J. Am. Chem. Soc.* **1999**, *121*, 7409.

(29) von Werne, T.; Patten, T. E. *J. Am. Chem. Soc.* **2001**, *123*, 7497.

(30) Pyun, J.; Matyjaszewski, K. *J. Am. Chem. Soc.* **2001**, *123*, 9445.

(31) Mandal, T. K.; Fleming, M. S; Walt, D. R. *Nano. Lett.* **2002**, *2*, 3.

(32) Zheng, G.; Stöver, H. D. H. *Macromolecules* **2002**, *35*, 7612.

(33) Guerrini, M. M.; Charleux, B.; Vairon, J. P. *Macromol. Rapid. Commun.* **2000**, *21*, 669.

(34) Qin, S. H.; Qin, D. Q. ; Ford, W. T. ; Resasco, D. E.; Herrera, J. E. *Macromolecules* **2004**, *37*, 752.

(35) Kong, H.; Gao, C.; Yan, D. Y. *J. Am. Chem. Soc.* **2004**, *126*, 412.

(36) Bontempo, D.; Maynard, H. D. *J. Am. Chem. Soc.* **2005**, *127*, 6508.

(37) Zhai, G. Q.; Kang, E. -T.; Neoh, K. -G. *Macromolecules* **2004**, *37*, 7240.

(38) Cui, Y.; Chen, T.; Zheng, S. P.; He, Q.; Ai, S. F.; Li, J. B. *Macromol. Rapid. Commun.* **2005**, *26,* 1552..

(39) Zhao, H. Y.; Argoti, S. D.; Farrell, B. P.; Shipp, D. A. *J. Polym. Sci., Part A: Polym. Chem.* **2003**, *41*, 916.

(40) Claes, M ; Voccia, S.; Detrembleur, C.; Jérôme, C.; Gilbert, B.; Leclère, P.; Geskin, V. M.; Gouttebaron, R.; Hecq, M.; Lazzaroni, R.; Jérôme, R. *Macromolecules* **2003**, *36*, 5926.

(41) Ignatova, M.; Voccia, S.; Gilbert, B.; Markova, N.; Cossement, D.; Gouttebaron, R.; Jérôme, R.; Jérôme, C. *Langmuir* **2006**, *22*, 255.

(42) Matrab, T.; Chehimi, M.M.; Perruchot, C.; Adenier, A.; Guillez, A.; Save, M.; Charleux, B.; Cabet-Deliry, E.; Pinson, J. *Langmuir* **2005**, *21*, 4686.

(43) Fan, X.W.; Li, L.J.; Dalsin, J.L.; Messersmith, P.B. *J. Am. Chem. Soc.* **2005**, *127*, 15843.

(44) Zhang, F; Xu, F. J.; Kang, E. T.; Neog, K. G *Ind. Eng. Chem. Res.* **2006**, *45*, 3067.

CHAPTER 2

Research Objectives, Thesis Outline and Contributions to Articles

2.1 Research objectives

Surface-initiated ATRP is an effective method for preparation of polymer coatings covalently bonded to surface, which can provide high adhesion strength and well-defined polymer functionalities.

The objectives of this research are:

i. To study applications of the surface-initiated ATRP in preparation of polymer brushes with special functionalities, such as fluorinated polymers and polymers with bulky POSS side groups.

ii. To develop novel methods to increase grafting density for the surface-initiated ATRP.

iii. To investigate fundamentals of the surface-initiated ATRP from reactive metal surfaces.

2.2 Thesis outline

This thesis consists of seven chapters. Chapter 1 gives an introduction and literature review of the surface-initiated polymerization techniques. Chapter 2 states the research objectives of this thesis. Chapter 7 concludes the significant contributions of this study and provides recommendations for future work. Chapter 3-6 are based on four papers that have been published or submitted to peer-referred journals. This is a sandwich type thesis that follows McMaster's guideline for thesis writing.

Chapter 3 consists of an investigation of the surface-initiated ATRP of a partially fluorinated polymer, poly(2,2,2-trifluoroethyl methacrylate) (PTFEMA) from flat silicon wafer surfaces. The main objective of this chapter is to study the applicability of the surface-initiated ATRP in preparation of fluorinated polymer films. The ATRP grafting kinetics of PTFEMA is described in details based on two methods used to control the polymerization, i.e., adding free initiator and adding excess deactivator to the reaction system. More than 100nm thick PTFEMA layers were obtained and the PTFEMA chains ends were "living", allowed for the extension of a second block of PMMA.

Another important objective of this chapter is to investigate the effect of a novel surface-attachable difunctional initiator, 11-(2,2-bis(2- bromo-2-methyl propionyloxy methyl)propionyloxy) undecyltrichlorosilane on the grafting density. The grafting density was found to be almost doubled using this difunctional initiator, from 0.48 to 0.86chains/nm^2.

Chapter 4 studies the surface-initiated ATRP of a novel Polyhedral Oligomeric Silsesquioxane(POSS)-containing methacrylate monomer, 3-(3,5,7,9,11,13,15-heptacyclo pentyl-pentacyclo[9.5.1.1.^{3,9}1.^{5,15}1^{7,13}]-octa-siloxane-1-yl) propyl methacrylate (POSS-MA) from flat silicon wafers. The objective of this chapter is to investigate the applicability of the surface-initiated ATRP in preparation of polymer brushes with very large and rigid pendant groups. The ATRP grafting kinetics of Poly(POSS-MA) is also described in details based on the two general methods to control polymerization.

Chapter 5 studied the surface-initiated ATRP of acrylic polymers from flat metal (Ni and Cu) surfaces. The metal surfaces were thoroughly cleaned and precisely polished to facilitate initiator immobilization and characterizations. A mild sillane-based initiator, 3-(2-bromo-2-methyl)amino propyl triethoxysilane was immobilized onto the metal surfaces without any corrosion. Various acrylic polymers including PMMA, PTFEMA, PDMAEMA and PHEMA were grafted from the flat Ni and Cu surfaces. The kinetic study of the surface-initiated ATRP on metal surfaces was investigated in details using both "adding free initiator" and "adding deactivator" methods. The potential of this surface-initiated ATRP technique in alloy surface modification was also studied. PDMAEMA and POEGMA were grafted from the surface of a shape-memory-alloy, nitinol.

Chapter 6 is an extension of the work of Chapter 5. The same technique was employed to graft polymer brushes from metal nanoparticles. The similar siloxane-based ATRP initiators were covalently bonded onto the surface of Ni nanoparticles by combination of ligand exchange and condensation reactions. PMMA, PSt, PNIPAM and PDMAEMA were successfully grafted from the Ni nanoparticle surface. The grafted polymer outer shells can effectively help facilitate and stabilize the dispersion of Ni nanoparticles in appropriate solvents. Moreover, by tuning polymer shell thickness through varying polymerization time, the saturation magnetization of Ni nanoparticles can be easily tuned to desired values.

2.3 Contributions to articles

Four articles are embodied in this thesis (Chapters 3-6). Professor Shiping Zhu provided guidance with the initial research direction and idea generation. Most experimental works were designed and carried out by myself. Professor Gianluigi Botton provided guidance and help on the electron microscopy setup and data analysis. Dr. Beng S. Ong and Dr. Yiliang Wu provided guidance on organic synthesis. Dr. Shane Maclaughlin provided guidance on the metal surface treatment and modification. I prepared the first drafts of all these papers and the initial responses to the comments of the journal reviewers. I worked with Professor Shiping Zhu on the subsequent drafts until they are accepted. I was the first author for all four papers.

CHAPTER 3

Surface-initiated ATRP Grafting of Poly(2,2,2-trifluoroethyl methacrylate) from Flat Silicon Wafer

This chapter is organized based on the published article: Chen R, Feng W, Zhu SP, Botton G, Ong BS, Wu YL. *J Polym Sci Part A: Polym Chem* **2006**, *44*, 1252-1262.

3.1 Abstract

Poly(2,2,2-trifluoroethyl methacrylate) (PTFEMA), a partially fluorinated polymer, was directly grafted from silicon wafer surfaces by a surface-initiated atom transfer radical polymerization (ATRP). The polymer layer thickness increased linearly with monomer conversion and molecular weight of free polymers in solution. The thickness was mainly determined by the experimental conditions such as activator/deactivator ratio, monomer/catalyst ratio, and monomer concentration. PTFEMA layers of more than 100nm thick were obtained. The grafted PTFEMA chains were "living" and allowed the extension of a second block of PMMA. An X-ray photoelectron spectroscopy study showed that the chemical compositions at the surfaces agreed well with their theoretical values. A novel surface-attachable difunctional

initiator was also synthesized and applied to the grafting of PTFEMA. The grafting density was doubled using this difunctional initiator, from 0.48 to 0.86chains/nm^2.

3.2 Introduction

Recently, considerable attentions have been paid to the organic/inorganic hybrid structures that are composed of dense polymer brushes immobilized on solid substrate surfaces, including flat substrates,[1-6] silica or gold nanoparticles,[7-10] carbon nanotubes,[11] and fullerenes[12] for their potential applications as biomaterials,[13] sensors,[14] microelectronic devices,[15] and so forth. There are two general ways to prepare the hybrid structures, one is "grafting to"[16] and the other is "grafting from".[17] In the "grafting to" approach, polymer chains are covalently bound to surfaces via reactions between reactive chain ends or side chains with coreactive surface moieties. The polymer chains are prepared in advance, and therefore it is easy to control and characterize their chain structure. However, there is a limitation to this approach. Once some chains are attached to the surface, these early chains form a diffusion barrier and prevent later chains from approaching the surface. As a result, this approach is not good for preparing high grafting density polymer brushes.

In the "grating from" approach, polymerization initiators are immobilized to surface. Successive *in situ* surface-initiated polymerization grows polymer chains from the surface. There are many methods to introduce initiator moieties, for example, treating surface with plasma or forming initiator-containing self-assembly monolayer (SAM).[17] The most important advantage of the "grafting from" method is that it allows preparation of high grafting density polymer brushes. However, the characterization of grafted polymer chains is challenging.

Polymer grafting via conventional free-radical polymerization mechanisms was first employed by Prucker and Rühe[18] to graft polystyrene from azo initiators immobilized on silicon gel particles. The thickness can be controlled by using the half-life of the azo initiator and the known chain transfer constant for the monomer used in the polymerization. However, because of the nature of conventional radical polymerization, the grafted polymer chains were not "living", and had broad molecular weight distributions.

To overcome the drawbacks of conventional radical polymerization grafting, various controlled/"living" polymerization techniques have been applied to grafting polymer brushes, for example, "living" anionic polymerization,[19] nitroxide-mediated radical polymerization (NMP),[2] reversible addition-fragmentation chain-transfer polymerization (RAFT),[6] and atom transfer radical polymerization (ATRP).[2,3,5] The transition metal mediated ATRP received great attention in the recent years because of its versatility of monomer types, tolerance of impurities, mild reaction conditions, and excellent control over molecular weight and polydispersity.[20] A variety of monomer have been successfully grafted from various substrate surface by ATRP such as styrene,[2,3] methyl methacrylate (MMA),[1-3] 2-hydroxyethyl methacrylate (HEMA)[5] and 2-methacryloxyloxyethyl phosphorylcholine (MPC).[21]

It is well known that fluorinated polymers have such special properties as high thermal and chemical stability, low refractive index, low surface energy, and high hydrophobicity.[22] Fluorinated polymers have been extensively exploited, and their applications include novel biomaterials, optical devices and high-quality coatings.[22-24] In recent years, a lot of work has been done on the preparation of fluorinated polymer brushes by surface-initiated "living" polymerization. Brantley and Jennings[25] used surface-initiated ATRP to graft poly(HEMA) films from gold surface, and the polymer films were fluorinated by the reaction between hydroxyl groups and fluorinated acid chlorides. The same method was employed by Baker and coworkers[26,27] to prepare porous alumina membranes coated with fluorinated poly(HEMA) films. Fluorinated monomers were also directly grafted from surfaces. Ober and coworkers,[28] synthesized styrene-based homopolymer and copolymer brushes bearing semifluorinated alkyl side groups by surface-initiated NMP. Brittain and coworkers[29] used surface-initiated ATRP to graft stimuli-responsive diblock copolymer brushes, consisting of poly(methyl acrylate) and poly(semifluorinated acrylates).

2,2,2-trifluoroethyl methacrylate (TFEMA), is a monomer with low fluorine content (34%), which can be easily synthesized by the reaction of 2,2,2-trifluoroethanol and methacryloyl chloride. Recently, TFEMA-containing homopolymers and copolymers have found applications in various areas, such as cladding materials in optical fibers,[23] protectives or consolidants for marble statues.[24] TFEMA has been polymerized via free radical mechanisms;[30] however, there is no report on grafting PTFEMA from substrate surfaces. In this work, we report the grafting of PTFEMA from silicon wafer surfaces by surface-initiated ATRP. The effects of different approaches and experimental conditions on the grafting polymerization are systematically investigated.

The grafting density is defined as the number of grafted polymer chains per unit of surface area. It is an important parameter in surface-initiated polymerization that determines surface properties of the materials in their applications. A higher grafting density results in a more uniform and dense brush layer. We aim to synthesize polymer brushes of high grafting density and well-control molecular weights. There were some investigations reported in the literature on surface-initiated ATRP systems with initiator SAM techniques.[2,3] The obtained grafting densities ranged from 0.1 to 0.60chains/nm^2. In this work, we also synthesize a novel surface-attachable difunctional initiator and demonstrate its effectiveness in increasing the grafting density of PTFEMA from 0.48 to 0.86chains/nm^2.

3.3 Experimental

3.3.1 Materials

Trichlorosilane (99%), 2-bromoisobutyryl bromide (98%), 10-undecen-1-ol (98%), 4,4'-dinonyl-2,2'-dipyridyl (dNnbpy) (97%), ethyl 2-bromoisobutyrate (EBIB) (98%), hydrogen hexachloroplatinate (IV) hydrate (H_2PtCl_6, 99.9%), 2,2-bis(hydroxyethyl) propionic acid (98%), PCl_5 (95%), CuCl (99.999%), $CuBr_2$ (99.999%) were purchased from Aldrich and were used as received. 2,2,2-Trifluoroethyl methacrylate (TFEMA) (98%; Aldrich), methyl methacrylate (MMA) (99%; Aldrich) and α,α,α-trifluorotoluene (anhydrous, +99%; Aldrich) were distilled over CaH_2 under vacuum and was stored at

-15°C before use. Toluene and tetrahydrofuran (both HPLC grade) were obtained from Caledon Laboratories Ltd. Toluene was distilled. Double-sided polished silicon wafers (P-doped, (100)-oriented, 10–20Ω·cm resistivity, 0.56mm thickness) were purchased from University Wafer Company (Boston, MA) and cut into 5×5mm pieces using a Micro Ace Series 3 dicer (Loadpoint Ltd., England). Deionized water with a resistivity of 18MΩ·cm was prepared from a Millipore Milli-Q filtration system. Ultra-high-purity-grade argon was used in this study.

3.3.2 Monofunctional initiator synthesis

The surface-attachable monofunctional initiator 11-(2-bromo-2-methyl) propionyloxy undecyltrichlorosilane was synthesized from 10-undecen-1-ol according to the published procedure.[2] ^{1}H NMR($CDCl_3$, 200MHz): δ 4.16 (t, 2H, $OC\boldsymbol{H}_2$, J = 8.8Hz), 1.90 (s, 6H, CBr-$C\boldsymbol{H}_3$), 1.27-1.74 (m, 20H, $CH_2C\boldsymbol{H}_2$).

3.3.3 Difunctional initiator synthesis

The synthetic route for the surface-attachable difunctional initiator 11-(2,2-bis(2-bromo-2-methyl propionyloxy methyl)propionyloxy) undecyltrichlorosilane is shown in

Scheme 1. The branching agent **4** was first prepared following the method of Gnanou et al.[31] In synthesizing the ester **5**, to a solution of 4.257g (25mmol) of 10-undecen-1-ol in 20ml of dry THF was added 2.10ml of pyridine (26.5mmol). A solution of 11.29g (25mmol) of **4** in 10ml of dry tetrahydrofuran was then dropwisely added over a period of 5min. The mixture was stirred overnight at room temperature and then diluted with hexane (50ml) and washed with 2N HCl once and water twice. The organic phase was dried over sodium sulphate and filtered. The solvent was removed from the filtrate under a reduced pressure. The colourless oily residue was purified by a column chromatography (hexane/ethyl acetate 5/1 v/v) to yield 11.64g (80%) of the ester **5** as colourless oil. The method of Hawker et al.[2] was employed for the hydrosilation of the ester **5**. Finally, a solution of the difunctional initiator **6** in toluene (about 0.5mol/l) was obtained and then used without further purification. ^{1}H NMR($CDCl_3$, 200MHz) δ 4.36 (dd, 4H, COC-C$\boldsymbol{H}_2$, J = 11.2 Hz, 6.0 Hz), 4.13 (t, 2H, OC$\boldsymbol{H}_2$, J = 6.6 Hz), 1.90 (s, 12H, CBr-C$\boldsymbol{H}_3$), 1.27-1.63 (m, 23H, CH_2C$\boldsymbol{H}_2$, COC-C$\boldsymbol{H}_3$)

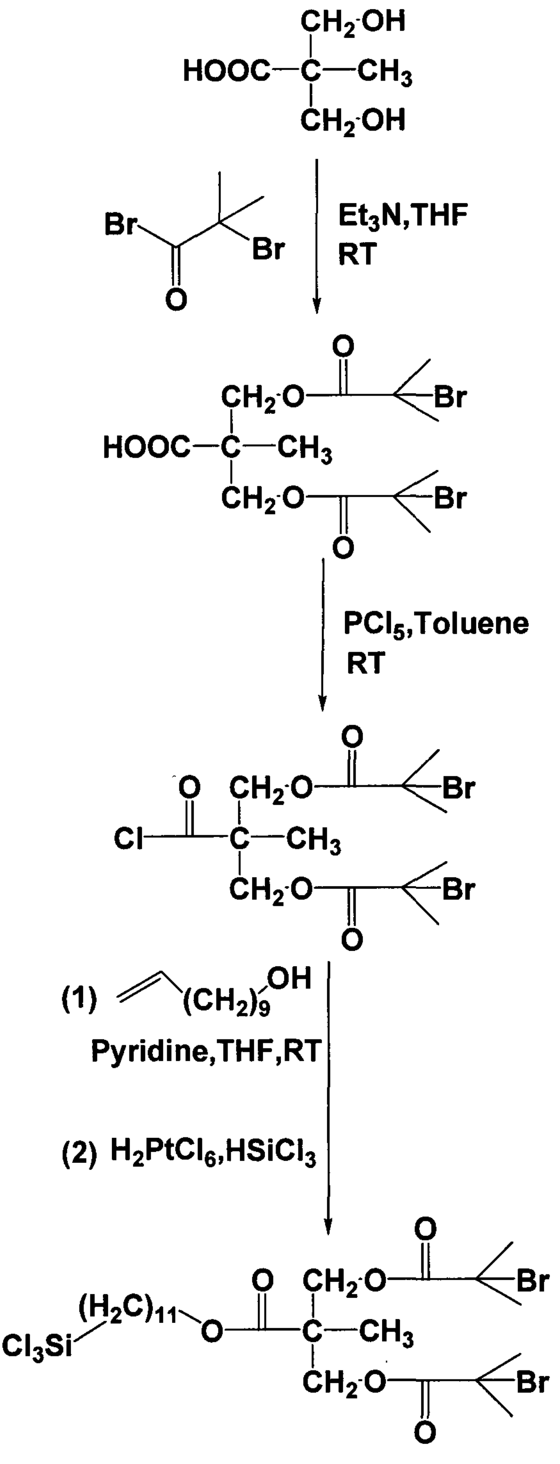

Scheme 3.1 Synthesis of surface-attachable difunctional initiator.

3.3.4 Preparation of initiator-functionalized silicon wafer

Si(100) wafers were first washed with the "piranha" solution (a mixture of 70vol% concentrated sulphuric acid and 30vol% of hydrogen peroxide) to remove the organic residue. The wafers were rinsed with copious amount of deionized water, dried in argon flow. After that, these wafers were immersed in HF solution to remove the native oxide film and then placed into UV-ozone cleaner for 3min to grow a uniform oxide film. The clean wafers were placed in a crystallizing dish to that a solution of initiator (15μl) in dry toluene (15ml) was added. 25μl of triethylamine was also added. The dish was covered and left at room temperature for 18h. The wafers was then rinsed with toluene, acetone and methanol and dried in an argon stream.

3.3.5 ATRP of TFEMA from initiator-functionalized silicon wafer

A representative ATRP grafting run with an added amount of free initiator is as follows: Initiator-functionalized silicon wafers were placed into glass tubes separately. These tubes, capped with rubber septum, were deoxygenated with argon for 10min. 8.7mg (0. 088mmol) of CuCl, 41.8mg (0.176mmol) of dNnbpy were placed into a 10-ml flask that contains a magnetic stir bar. The flask was fitted with a rubber septum and purged with argon. 3.28ml of α,α,α-trifluorotoluene and 2.00ml (14.0mmol) of TFEMA were added to the flask via syringe (both were bubbled for 1h with argon before use). The mixture was stirred and degassed with argon until a homogeneous brown solution formed (about 10min). The flask was kept at room temperature and 12.7μl (0.088mmol) of EBIB initiator was added into the mixture via syringe. The reaction mixture was homogenized by intense agitation and quickly transferred into the prepared glass tubes that contain initiator-functionalized silicon wafers via a cannula. These tubes were placed into an oil bath of 90□. After desired periods of time of polymerization, the tubes were sampled and unsealed. The silicon wafers were taken out from solution, rinsed with THF, cleaned ultrasonically for 30min in THF, rinsed again with THF and then dried in a nitrogen stream.

In a representative ATRP grafting run with an added excess amount of deactivator, 8.0mg (0.08 mmol) of CuCl, 2.0mg (0.0081mmol) of $CuBr_2$ and 71.4mg (0.178mmol) of dNnbpy were placed into a 10-ml flask containing a magnetic stir bar. The flask was deoxygenated through several evacuation/backfilling cycles of argon. Argon bubbled 3.28ml of α,α,α-trifluorotoluene and 2.00ml (14.0mmol) of TFEMA were then added to the flask via syringe. The mixture was stirred intensively, degassed with argon for another 10min, and then transferred to the glass tubes that contain initiator-functionalized silicon wafers via a cannula. The silicon wafers were taken out from the glass tubes after the desired time periods and cleaned by the same procedure as in the added free initiator case.

3.3.6 Preparation of P(TFEMA-*b*-MMA) brushes on silicon wafers

PTFEMA-grafted silicon wafers were placed into glass tubes and degassed. 9.3mg (0.094mmol) of CuCl, 2.2mg (0.0094mmol) of $CuBr_2$ and 82.9mg (0.207mmol) of dNnbpy were placed into a deoxygenated flask. 2.00ml (18.7mmol) of degassed MMA and 2.00ml of degassed toluene were then added via syringe. The mixture was stirred and degassed with argon for 5min, and then transferred via a cannula into the glass tubes than contain PTFEMA-grafted silicon wafers. The glass tubes were heated for 12h in an oil bath of 70°C. The silicon wafers were removed and cleaned.

3.3.7 Instruments

The initiator and polymer layer thickness on silicon wafers was determined by an Exacta 2000 ellipsometer (Waterloo Digital Electronics, Waterloo, ON, Canada) equipped with a He-Ne laser (632.8nm) at a 70° incident angle. The optical constants (refractive index, extinction coefficient) of Si (n=3.865, k =0.020) and SiO_2 (n =1.465, k =0) were used to determine the thickness of the SiO_2 layer of the freshly cleaned silicon surfaces. The values of n=1.5000 and k=0 were used to calculate the thickness of the initiator-covered silicon wafers and n=1.437 and k=0 for the polymer-covered substrates. The data were collected at three spots on each wafer sample. X-ray Photoelectron Spectroscopy (XPS) was recorded on a Leybold Max 200 XPS with an aluminum anode non-monochromatic source. Survey scans (0–1000eV) were performed to identify constitutive elements. Low-resolution scans of the peaks corresponding to these elements provided their atomic concentrations. These scans were measured with a takeoff angle of 90°. Immediately prior to the measurement, the samples were rinsed with 1,1,2-trichlorotrifluoroethane to remove contaminants. Water contact angles were measured using a Ramé-Hart NRL goniometer (Mountain Lakes, NJ). Silicon wafers were rinsed in methanol and dried in a nitrogen stream immediately prior to the measurement. Advancing and receding contact angles were measured using the sessile drop method.

The molecular weights of PTFEMA were determined by a gel permeation chromatography (GPC). A Waters710 sample autoinjector, three linear columns in series (Waters Styragel HR 5E, 2_Shodex KF-804L), a Waters 600 pump system and a

410 RI detector were used for the assays. The eluent (THF + 2vol% triethylamine) was pumped through the system at a fixed flow rate of 1ml/min. The columns and detector were heated to 35°C and 40°C, respectively. Narrow polystyrene samples were used as standards to generate the calibration curve. Data were recorded and manipulated using the Waters Millennium software package. The nuclear magnetic resonance (NMR) data was measured using a Bruker AC-P200 NMR spectrometer (200MHz) in *d*-chloroform. The monomer conversion in ATRP grafting in the added free initiator case was calculated by the equation below:

$$x = 1 - (I_{\delta=6.25(CH2=CCH3)} + I_{\delta=5.71(CH2=CCH3)})/(I_{\delta=4.30\sim4.65\ (CH2CF3)}).$$

3.4 Results and discussion

3.4.1 Synthesis and characterization of initiators on silicon surface

In this work, highly dense initiator monolayers were formed on the silicon wafers by the reaction of the initiator's trichlorosilane moieties with the surface hydroxyl groups. The thickness of the monolayer was 2.5 ± 0.2nm measured by ellipsometry, which was very close to the reported thickness for an octadecyltrichlorosilane (OTS) monolayer (2.6nm).[32] For each sample, the deviation of the thicknesses at three different spots was smaller than 0.2nm. The monolayer was very uniform, with no clusters/domains observed. The chemical compositions of the initiator-functionalized silicon wafers were examined by XPS (please see appendix). The presence of the Br_{3d} core-level spectrum at the BE (Binding Energy) of ~70.5eV and the reappearance of the O=C-O peak component in the C_{1s} core-level spectrum indicated that the 2-bromoisobutyrate species was successfully immobilized on the silicon surfaces. The advancing and receding water contact angles of the wafers were 78.2° and 67.4, respectively. These contact angles were much higher than the value of < 10° for the hydrophilic silicon wafer.

3.4.2 Surface-initiated ATRP of TFEMA from functionalized silicon wafer

ATRP is controlled by the fast equilibrium of radical activation and deactivation, as shown in Scheme 3.2. Since the deactivation rate constant k_{deact} is usually many orders of magnitude higher than the activation k_{act}, the radical concentration is very low, so that the termination can be effectively minimized. To have a good control over polymer molecular weight development, a high concentration of deactivating species (i.e., Cu(II)/ligand complex) is indispensable. In a solution ATRP, the red-ox reaction of initiator with Cu(I) and successive termination of the primary radicals provide a sufficient level of Cu(II). In the surface-initiated ATRP, the number of initiator moieties on the surface is inadequate to generate enough Cu(II) species for the ATRP system. There are normally two approaches to tackle this problem: one is to add some free initiator to solution,[1,2] and the other is to add Cu(II) directly at the very beginning of polymerization.[3] In the former approach, "free" polymer chains are formed in solution. If the molecular weight of the free chains is assumed to be the same as that of "grafted" chains, one can readily estimate the polymer grafting density at the surface. However, the surface samples prepared using this approach requires an intense cleaning process to remove adsorbed chains. The latter approach is often used to yield thicker polymer layers.

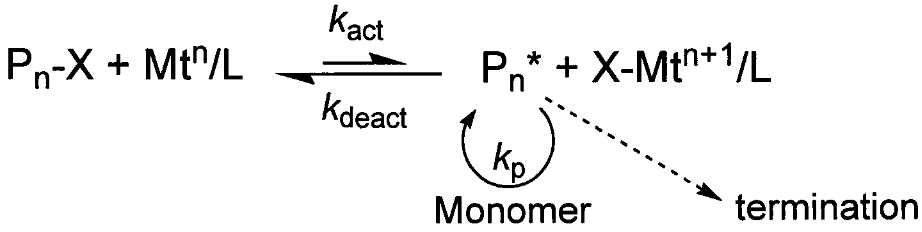

Scheme 3.2 General scheme of ATRP.

As a preliminary experiment, a solution ATRP of TFEMA was carried out. Haddleton et al.[33] were the first who reported a solution ATRP of TFEMA with pyridine imine as ligand and toluene as solvent. However, the kinetic plot of monomer conversion showed a significant level of irreversible termination at the late stage of the polymerization. The initiator efficiencies were low and the polydispersities were high at about 1.30. To improve the control, we made some modifications to the recipe. A fluoric solvent, α,α,α-trifluorotoluene, was used to replace toluene and the ligand was changed from pyridine imine to dNnbpy. Figure 3.1 shows the conversion and molecular weight profiles. A linear ln([M]$_0$/[M]) versus time was obtained. The experimental molecular weights were very close to their theoretic values with polydispersities <1.15.

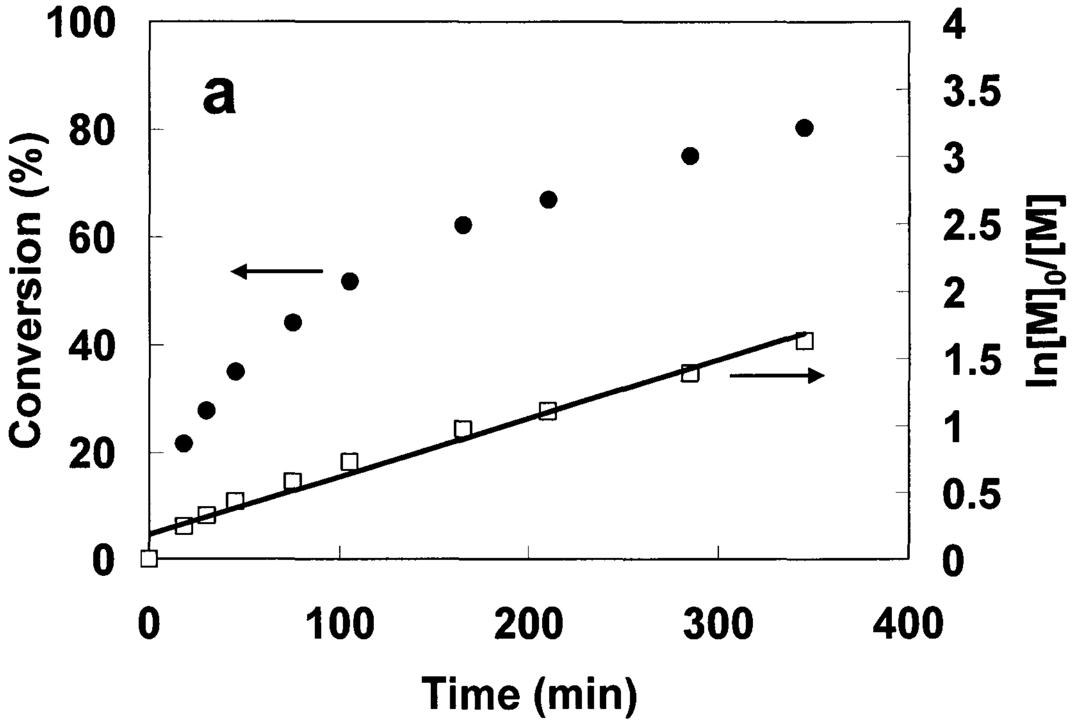

Figure 3.1 (a) First-order kinetic plot and (b) evolution of molecular weight for the polymerization of 2,2,2-trifluoroethyl methacrylate at 90°C initiated by ethyl 2-bromoisobutyrate. [TFEMA]/[CuCl]/[EBiB]/[dNnbpy] = 107/1/1/2, [TFEMA] = 2.66M, Solvent: *α,α,α*-trifluorotoluene.

3.4.3 ATRP grafting of TFEMA with added free initiator

Scheme 3.3 illustrates the ATRP "grafting from" approach. In the ATRP grafting of TFEMA from silicon wafers with the added free initiator, the same recipe as that of the solution ATRP was used. The monomer concentration remained unchanged while the free initiator concentration varied targeting for different degrees of polymerization (DP). As shown in Figure 3.2(a), the thickness of the grafted PTFEMA layer increased linearly with monomer conversion for both of the targeted DPs. A linear relationship between the thickness of the grafted PTFEMA layer and the molecular weight of the "free" polymer formed in solution was also observed, as shown in Figure 3.2(b). These results demonstrated a good control in the ATRP grafting of TFEMA from silicon surfaces.

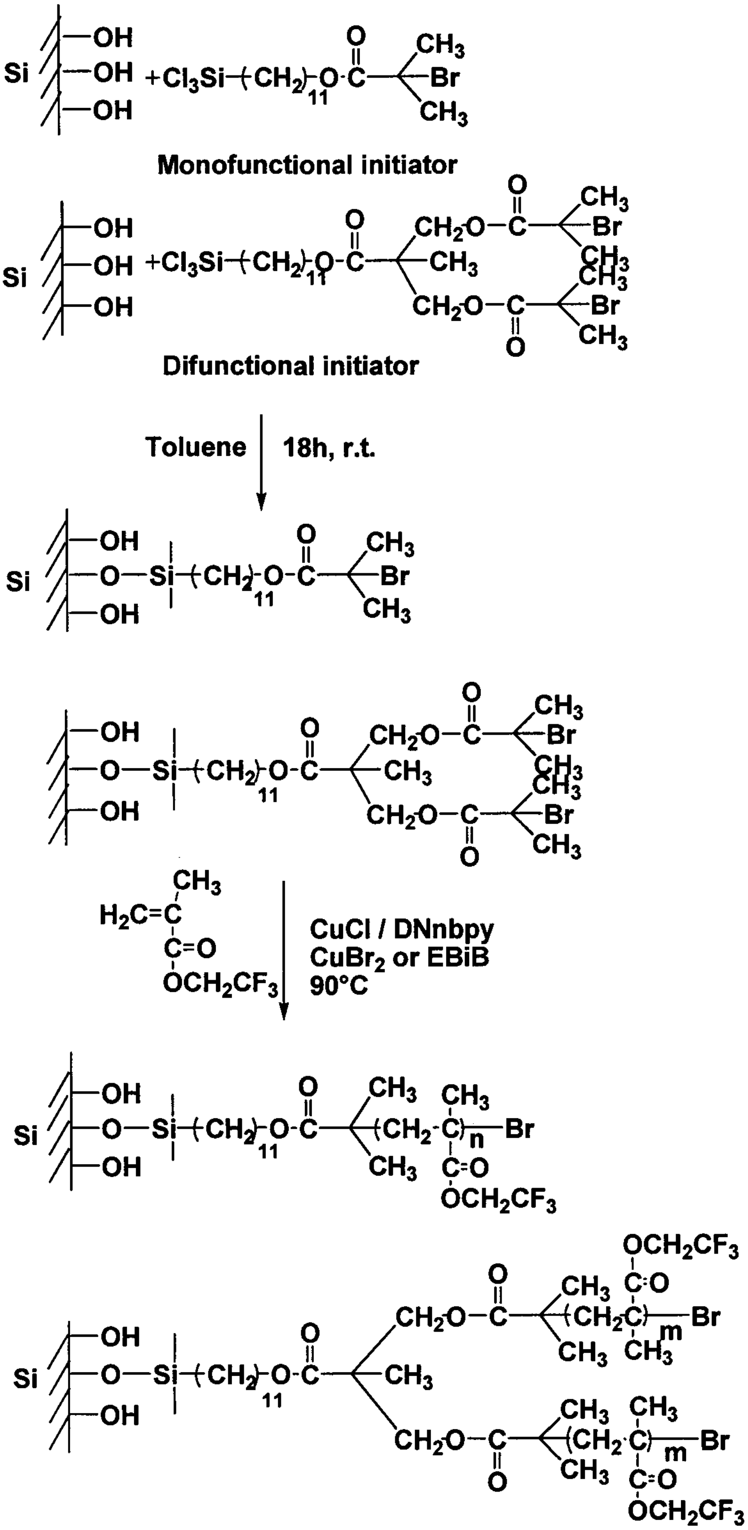

Scheme 3.3 Surface-initiated ATRP.

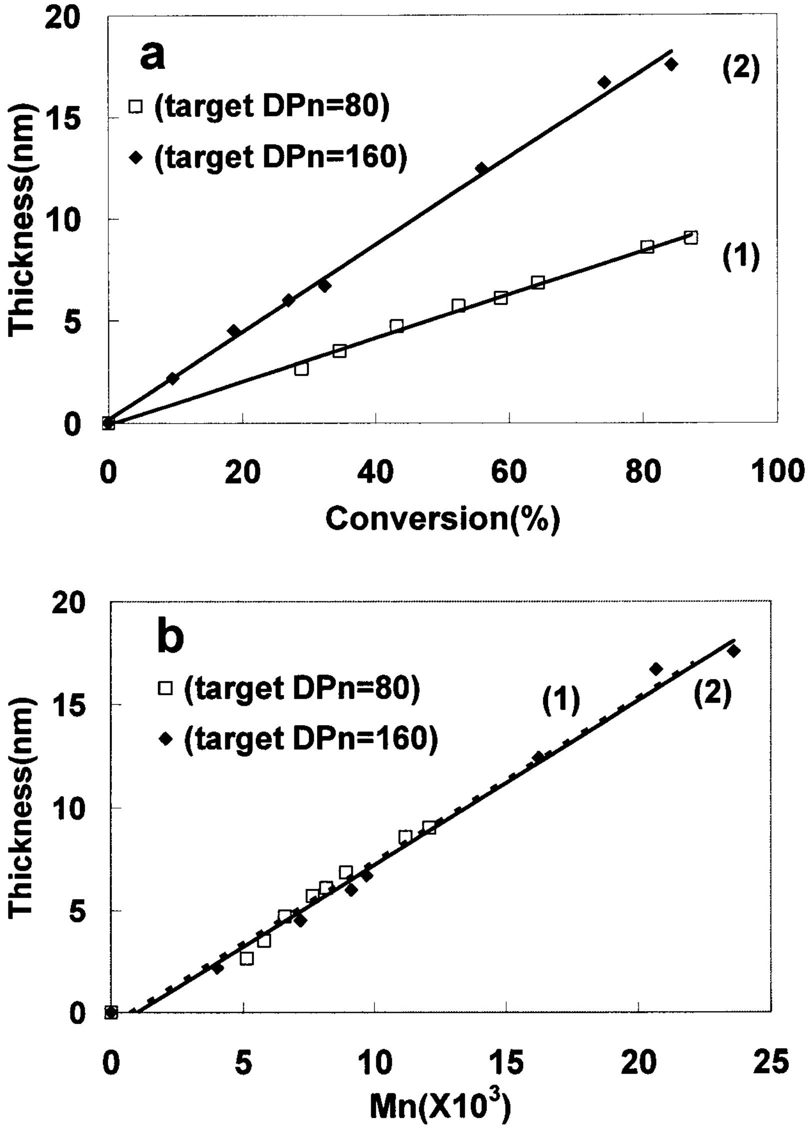

Figure 3.2 Thickness of the PTFEMA layer versus (a) monomer conversion and (b) molecular weight of "free" polymer with added free initiator. (1) [TFEMA]/[CuCl]/[EBiB]/ [dNnbpy] = 160/1/1/2, (2) [TFEMA]/[CuCl]/[EBiB]/ [dNnbpy] = 80/1/1/2. [TFEMA] = 2.66M. Solvent: α,α,α- trifluorotoluene.

The PTFEMA grafting densities can be estimated from the equation: $\Gamma = d\rho/M_n$,[34] where d is the thickness (nm) of the grafted polymer layer, ρ is the bulk density of the polymer (1.181g/cm^3 used for PTFEMA), and M_n is the number-average molecular weight of the polymer grafted from the surface. Although the exact molecular weight of the grafted polymer is unknown, we can just use the molecular weight of the polymer formed in solution for estimation. In this way, the grafting densities were calculated to be 0.49chains/nm^2 and 0.50 hains/nm^2, respectively, for the targeted DP = 160 and DP = 80. However, from Figure 3.2(b), we can find that the initiation of polymerization on surface was slower than that in solution, so the molecular weight of the grafted polymer was lower than that of polymer in solution. In this case, the actual grafting density was larger than the estimated value.

3.4.4 ATRP grafting of TFEMA with added deactivator

With the free initiator addition approach, the surface-initiated ATRP was well controlled. However, this approach could not yield thick polymer layers. To overcome this drawback, the deactivator addition approach was examined. The recipe was similar to the one used in the previous experiments. The only difference was that $CuBr_2$, instead of free initiator, was added at the beginning of polymerization. We kept the

TFEMA and CuCl concentrations constant and varied the $CuBr_2$ and dNnbpy concentrations to have different $CuBr_2$/CuCl molar ratios from zero to 50%. Figure 3.3 shows the data. Without $CuBr_2$ added, the PTFEMA layer thickness increased at the early stage and levelled off rapidly. This suggested that the radicals were not adequately deactivated and therefore terminated because of a lack of the deactivator species. When the $CuBr_2$/CuCl molar ratio was increased to 10%, the initial increase in thickness slowed down because of a reduced radical concentration. However, the thickness kept increasing for a long period of time. Increasing the ratio to 20% further reduced the thickness growth rate. When the ratio of 50% was used, the thickness increased linearly with the reaction time, i.e., at a constant but low growth rate. In order to achieve a compromise between the control with the rate, we selected the ratio of 10 mol% to further examine the effects of concentration and catalyst concentrations on the grafting.

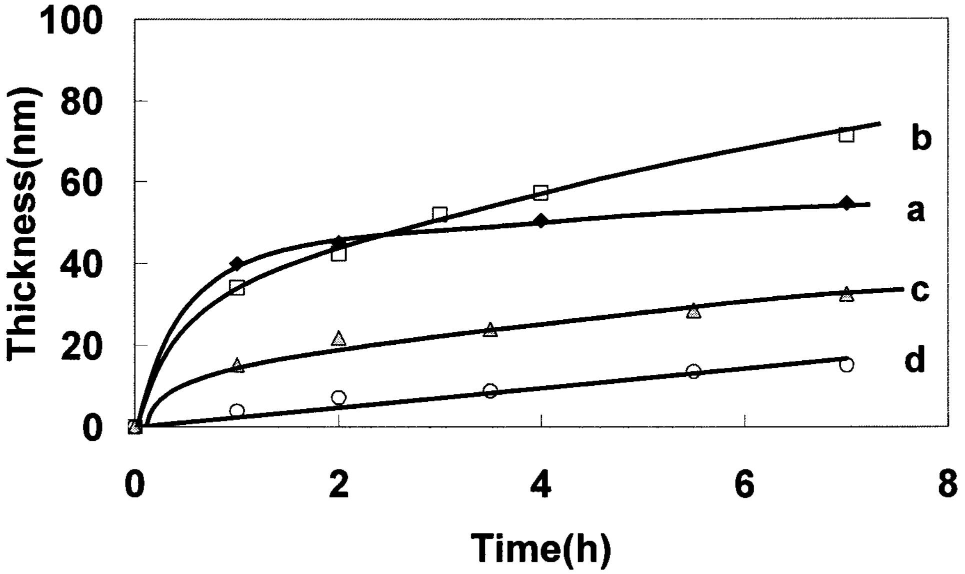

Figure 3.3 PTFEMA thickness versus polymerization time for different [CuCl]/[$CuBr_2$] ratios at [TFEMA] = 2.66M with added excess deactivator. (a) [TFEMA]/[CuCl]/[$CuBr_2$]/[dNnbpy] = 173/1/0/2; (b) [TFEMA]/[CuCl]/[$CuBr_2$]/[dNnbpy] = 173/1/0.1/2.2; (c) [TFEMA]/[CuCl]/[$CuBr_2$]/[dNnbpy] = 173/1/0.2/2.4; and (d) [TFEMA]/[CuCl]/[$CuBr_2$]/[dNnbpy] = 173/1/0.5/3.0. Solvent: *α,α,α*-trifluorotoluene.

Figure 3.4 shows the effect of monomer concentration on the grafting polymerization. The TFEMA concentration was 2.66M and 6.0M, respectively, and the TFEMA/CuCl molar ratio was 173/1 in both cases. For a given reaction time, a much thicker PTFEMA layer was achieved with a higher TFEMA concentration. With [TFEMA] = 6.0M, the PTFEMA layer reached thicknesses greater than >110nm only after 3 hours of reaction.

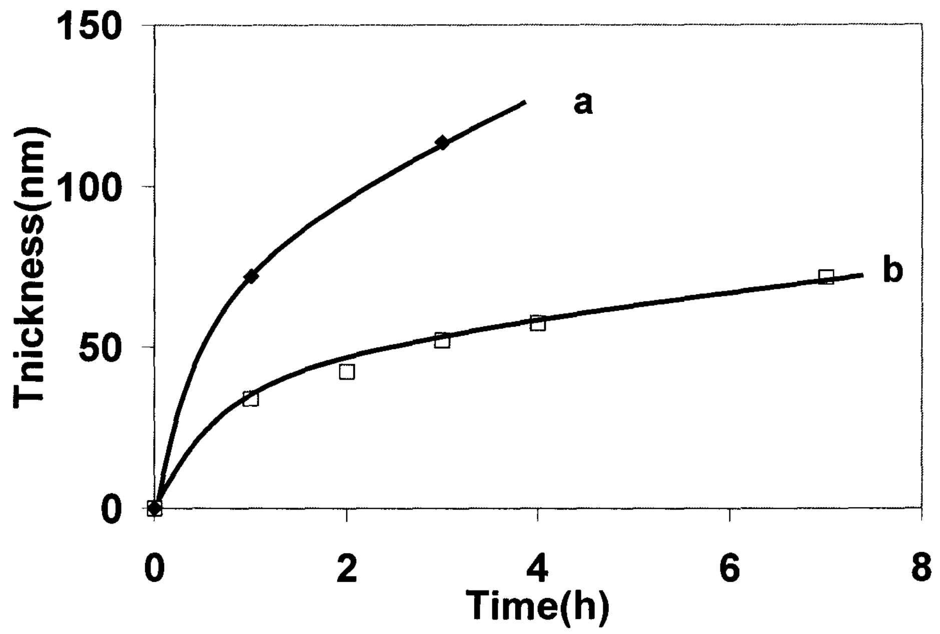

Figure 3.4 PTFEMA thickness versus polymerization time for different monomer concentrations with added excess deactivator. (a) [TFEMA] = 6.0M and (b) [TFEMA] = 2.66M. [TFEMA]/[CuCl]/[$CuBr_2$]/[dNnbpy] = 173/1/0.1/2.2. Solvent: *α,α,α*-trifluorotoluene.

Figure 3.5 shows that for a given reaction time, the PTFEMA layer was thicker at a lower catalyst concentration. The growth of polymer chains was determined by both propagation and termination reactions. Decreasing the catalyst concentration reduced the radical concentration and thus suppressed the bimolecular termination of radicals. However, the propagation rate was also reduced. The layer thickness was a complicated function of catalyst concentration and reaction time. Baker et al.[35] found that there was a specific concentration that yielded a maximum thickness for a given reaction time.

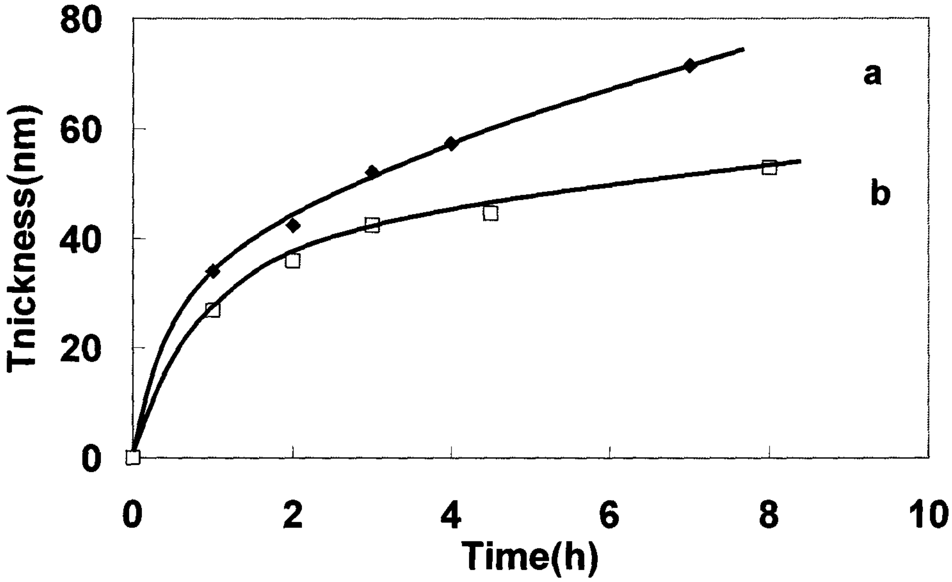

Figure 3.5 PTFEMA thickness versus polymerization time for different [TFEMA]/[CuCl] ratios at [TFEMA] = 2.66M with added excess deactivator. (a) [TFEMA]/[CuCl]/[CuBr$_2$]/[dNnbpy]=173/1/0.1/2.2; (b) [TFEMA]/[CuCl]/[CuBr$_2$]/[dNnbpy] = 50/1/0.1/2.2. Solvent: *α,α,α*-trifluorotoluene.

3.4.5 Preparation of block copolymer brushes

ATRP is advantageous in preparing block copolymers. In this study, PTFEMA chains grafted on silicon wafers with three different thicknesses were used as macroinitiators for an extension of methyl methacrylate (MMA) as second blocks. An increase in the polymer layer thickness was observed by ellipsometry for all the samples. The data are summarized in Table 3.1. The thinner PTFEMA surfaces (shorter chains) increased more in the extended PMMA thickness. It becomes clear that the grafted PTFEMA chains on the surfaces were still "living", but their livingness was lost with an increase in the PTFEMA layer thickness that required a long period of reaction time in preparation and thus suffered significant radical termination.

Table 3.1 Ellipsometric thicknesses of Si/P(1-TFEMA-*b*-MMA).

Thickness(nm) (PTFEMA, 1st block)	Thickness(nm) (PMMA, 2nd block)	Thickness(nm) (Total)
15.4	13.1	28.5
24.6	6.1	30.7
45.3	2.3	47.6

X-ray photoelectron spectroscopy (XPS) was employed to examine the chemical compositions of the surfaces. For Si/PTFEMA., the C_{1s} (285eV), O_{1s} (533eV), and F_{1s} (687eV) peaks corresponding to the PTFEMA layer were clearly seen on the XPS survey spectra. The content of C, O and F were in a good agreement with the theoretical values. For Si/PTFEMA-*b*-MMA, the disappearance of F_{1s} peak at 687eV indicated that

PTFEMA was fully covered by PMMA, which was further supported by the content of elements, as shown in Table 3.2.

Table 3.2 Surface composition of Si/P(1-TFEMA) and Si/P(1-TFEMA-*b*-MMA) surfaces by XPS using 90° take-off angle.

Sample	Element	Experimental Data [c]	Theoretical Composition
Si/P(1-TFEMA)$_{40.0}$[a]	C(%)	54.8	54.6
	O(%)	16.0	18.2
	F(%)	29.2	27.3
Si/P(1-TFEMA$_{15.4}$-*b*-MMA$_{13.1}$)	C(%)	75.1	71.4
	O(%)	23.0	28.6
	F(%)	1.0	0.0

a. Thickness of PTFEMA layer is 40.0nm

b. Data precision is ~±5%

3.4.6 Increase grafting density using difunctional initiator

The grafting density, i.e., the number of chains per unit surface area, is a very important property that determines the surface's performance in various applications. Recently, the grafting densities of 0.1 ~ 0.60chains/nm^2 prepared by surface-initiated ATRP with various monomers were reported.[1,2,36] However, there are still many remaining fundamental questions regarding achievable maximum grafting densities. Take the surface-initiated ATRP of MMA from silicon wafers as an example. The highest grafting density ever reported was only 0.60chains/nm^2.[2] The density of α-bromoester initiator moiety on the surface was ~5/nm^2. The initiator efficiency from surface was very low; every 7 or 8 initiators initiated only one PMMA chain.

Huck et al.[37] found that the layer thickness increased almost linearly with the initiator density at the surface, so that increasing initiator density at the surface may be an effective way to increase the grafting density. We synthesized a novel difunctional surface-attachable initiator, as shown in Scheme 3.1, and functionalized silicon wafers with this initiator. The initiator monolayer was 5.2 ± 0.2nm thick and it was also very uniform (the deviation of the thicknesses at three different points was only 0.2nm). The surface chemical compositions of the functionalized silicon surface were listed in Table 3. The Br_{3d}/Si_{2p} ratios of the difunctional initiator functionalized silicon wafers were much higher than those of the monofunctional initiator surfaces, suggesting that there were more initiator moieties on the surfaces.

Table 3.3 Surface composition of initiator-functionalized silicon surface by XPS using 90° take-off angle.

Elements	Monofunctional initiator	Difunctional initiator
C(%)	34.4	51.3
O(%)	27.4	24.8
Si(%)	37.2	22.4
Br(%)	1.0	1.4

PTFEMA was grafted from the difunctional initiator functionalized silicon wafers with an added amount of free initiator. For comparison, we also grafted PTFEMA from silicon wafers with the monofunctional initiator under the same conditions. Figure 3.6(a) shows that the PTFEMA thicknesses increased linearly with monomer conversion. The PTFEMA layers grafted from the difunctional initiator surfaces were almost twice as thick as those from the monofunctional initiator surfaces. Figure 3.6(b) shows the linear relationship between the thicknesses and the molecular weight of "free" polymer. The grafting densities, estimated from $\Gamma = d\rho/M_n$, were about 0.48chains/nm^2 for the monofunctional initiator surfaces and 0.86chains/nm^2 for the difunctional initiator counterparts. As aforementioned, the actual grafting density was higher than the estimated value. For the difunctional initiator, the initiation on the surface was much slower, so the actual grafting density for the difunctional initiator was much larger than the estimated value, compared with the monofunctional initiator. In this case, we can conclude that the difunctional initiator can effectively help increase the grafting density.

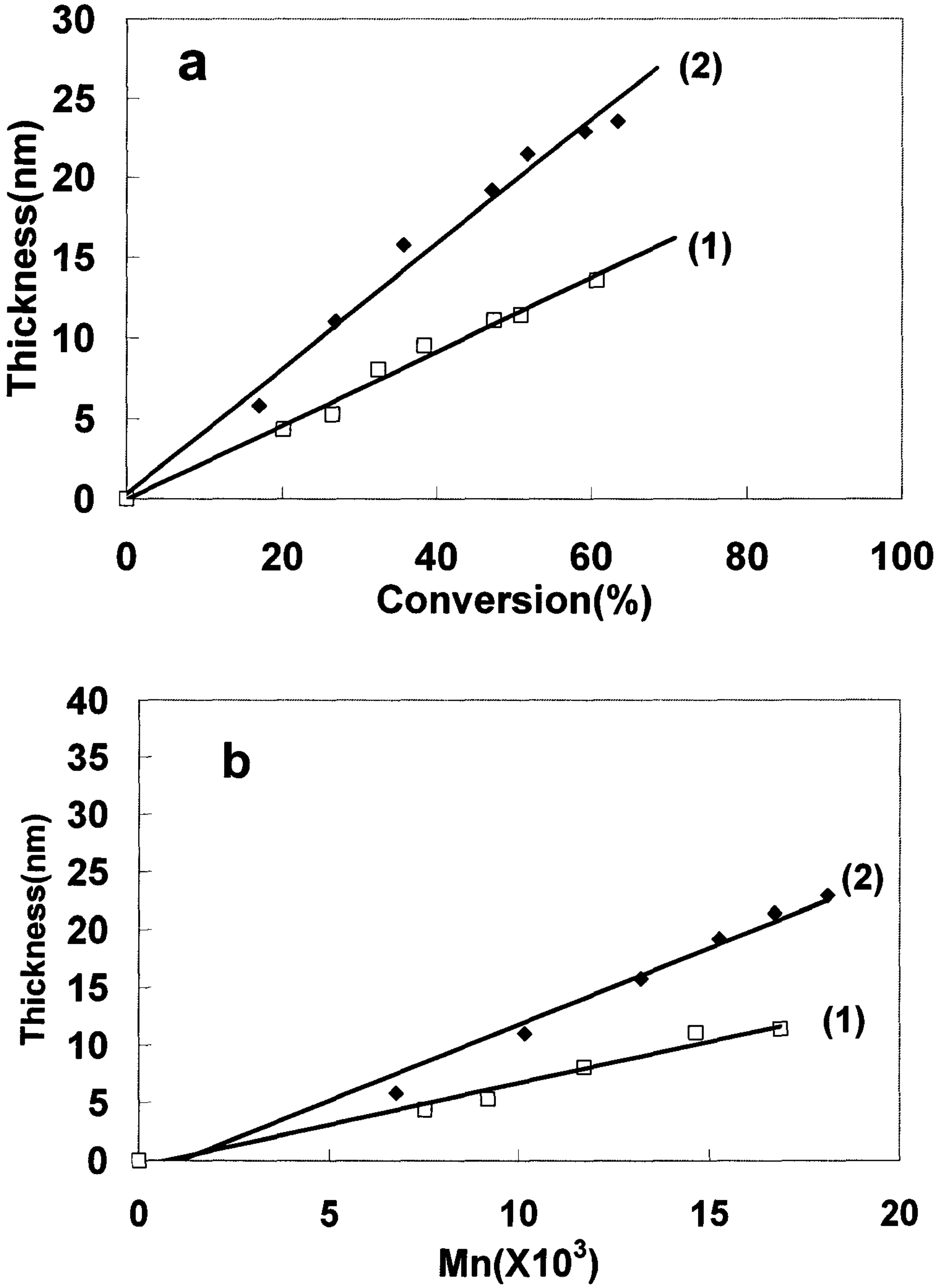

Figure 3.6 Thickness of the PTFEMA layer versus (a) monomer conversion and (b) molecular weight of "free" polymer with added free initiator. (1) Monofunctional initiator and (2) difunctional initiator. [TFEMA]/[CuCl]/[EBiB]/[dNnbpy] = 200/1/1/2, [TFEMA] = 2.66M. Solvent: *α,α,α*-Trifluorotoluene.

3.4.7 Water contact angle characterization of polymer grafted silicon surfaces

Table 3.4 reports the water contact angle data. For Si/P(1-TFEMA) (i.e., PTFEMA-grafted surfaces prepared from the monofunctional initiator), the advancing and receding contact angles were about 93° and 83°, respectively. These values were significantly higher than those of the initiator-functionalized silicon wafers and were independent of the PTFEMA layer thickness. For Si/P(2-TFEMA) (the PTFEMA-grafted prepared from the difunctional initiator), the advancing contact angle of 94° was very close to that of Si/P(1-TFEMA). The receding contact angles increased with the increase of the PTFEMA layer thickness from 72° to 83°. The difference between advancing and receding contact angles reflects the surface roughness. The Si/P(2-TFEMA) surfaces with short polymer chains appeared to be rough because of the bifurcated structure of the initiator. The surface became smooth with an increase in the PTFEMA molecular weight.

The advancing and receding contact angles of the surfaces grafted with the PTFEMA-PMMA di-block copolymer decreased with the increase of PMMA layer thickness. The advancing contact angle of Si/P(1-TFEMA$_{45.3}$-*b*-MMA$_{2.3}$) was 90.1°, indicating that only a small part of the PTFEMA surface was covered by PMMA. For Si/P(1-TFEMA$_{24.6}$-*b*-MMA$_{6.1}$), the advancing contact angle decreased to 67.6°. For Si/P(1-TFEMA$_{15.4}$-*b*- MMA$_{13.1}$), the advancing contact angle was 63.1°, similar to the values of 63°~66° for the pure PMMA surfaces.

Table 3.4 Water contact angle of different silicon surfaces at room temperature. (degree ±SD, *n* = 6)

Sample	θ_{adv} [a]	θ_{rec} [b]
Silicon wafer (after cleaning)	- [c]	- [c]
Si/monofunctional initiator	78.2°	67.4°
Si/difunctional initiator	71.0°	52.1°
Si/P(1-TFEMA)$_{13.7}$ [d]	92.8°	81.0°
Si/P(1-TFEMA)$_{36.0}$ [d]	93.8°	83.4°
Si/P(1-TFEMA)$_{62.3}$ [d]	93.5°	83.5°
Si/P(2-TFEMA)$_{5.8}$ [e]	94.5°	72.4°

Si/P(2-TFEMA)$_{15}$ ^{e}	95.1°	78.4°
Si/P(2-TFEMA)$_{22.9}$ ^{e}	93.8°	83.0°
Si/P(1-TFEMA$_{45.3}$-*b*-MMA$_{2.3}$)	90.1°	73.2°
Si/P(1-TFEMA$_{24.6}$-*b*-MMA$_{6.1}$)	67.6°	58.2°
Si/P(1-TFEMA$_{15.4}$-*b*-MMA$_{13.1}$)	63.1°	56.8°

a . θ_{adv} = advancing contact angle.

b . θ_{rec} = receding contact angle

c. Lower than 10°

d. Polymer film grafted from monofunctional initiator

e. Polymer film grafted from difunctional initiator

3.5 Conclusions

The surface-initiated ATRP of a partially fluorinated monomer, 2,2,2-trifluoroethyl methacrylate, from silicon wafer surfaces functionalized with α-bromoester initiator was carried out with CuCl/4,4'-dinonyl-2,2'-dipyridyl (dNnbpy) complex as a catalyst system. The effects of various experimental conditions on the polymerization kinetics and the development of grafted PTFEMA layer thickness were examined. Based on the experimental results, the following conclusions were reached.

(1) The ATRP grafting process was well controlled using the "adding free initiator" method. The layer thickness increased linearly with the PTFEMA molecular weight. With the "adding excess deactivator" method, PTFEMA films of > 100nm thick were obtained and the layer thickness strongly depended on the experimental conditions, such as $CuBr_2$/CuCl ratio, catalyst and monomer concentrations.

(2) The attached PTFEMA chains acted as macroinitiators for grafting a second block of PMMA. The successful chain extension was confirmed by ellipsometric and X-ray photoelectron spectroscopic studies as well as water contact angle measurement.

(3) A novel surface-attachable difunctional initiator, 11-(2,2-bis(2-bromo-2-methyl propionyloxy methyl)propionyloxy)undecyltrichlorosilane, was synthesized and evaluated for the ATRP grafting of PTFEMA. The initiator was highly effective in increasing grafting density. The grafting densities were almost doubled compared to the monofunctional initiator counterparts, from 0.48chains/nm^2 to 0.86chains/nm^2.

3.6 References

(1) Ejaz, M.; Yamamoto, S.; Ohno, K.; Tsujii, Y.; Fukuda, T. *Macromolecules* **1998**, *31*, 5934.

(2) Husseman, M.; Malmström, E. E.; McNamara, M.; Mate, M.; Mecerreyes, D.; Benoit, D. G.; Hedrick, J. L.; Mansky, P.; Huang, E.; Russell, T. P.; Hawker, C. J. *Macromolecules,* **1999**, *32*, 1424.

(3) Matyjaszewski, K.; Miller, P. J.; Shukla, N.; Immaraporn, B.; Gelman, A.; Luokala, B. B.; Siclovan, T. M.; Kickelbick, G.; Vallant, T.; Hoffmann, H.; Pakula, T. *Macromolecules,* **1999**, *32*, 8716.

(4) Prucker, O.; Rühe, J. *Langmuir*, **1998**, *14*, 6893.

(5) Huang, W. X.; Kim, J.-B. ; Bruening, M. L.; Baker, G. L. *Macromolecules*, **2002**, *35*, 1175

(6) Baum, M.; Brittain, W. J. *Macromolecules* **2002**, *35*, 610

(7) Von Werne, T.; Patten, T. E. *J. Am. Chem. Soc.* **1999**, *121*, 7409.

(8) Ohno, K.; Koh, K.; Tsujii, Y.; Fukuda, T. *Angew. Chem., Int. Ed.* **2003**, *42*, 2751.

(9) Kotal, A.; Mandal, T. K.; Walt, D. R. *J. Polym. Sci. Part A: Polym. Chem.* **2005**, *43*, 3631.

(10) Gravano, S. M.; Dumas, R.; Liu, K.; Patten, T. E. *J. Polym. Sci. Part A: Polym. Chem.* **2005**, *43*, 3675.

(11) Baskaran, D.; Mays, J. W.; Bratcher, M. S. *Angew. Chem., Int. Ed.* **2004**, *43*, 2138.

(12) Yang, J. W.; Li, L.; Wang, C. C. *Macromolecules* **2003**, *36*, 6060.

(13) Dumitriu, S. *Polymeric Biomaterials,* Marcel Dekker, New York, **1994.**

(14) Letant, S. E.; Sailor, M. J. *Adv. Mater.* **2001**, *13*, 335.

(15) Bowden, M. J.; Turner, S. R.; in: *Electronic and Photonic Applications of Polymers, Advances in Chemistry Series, 218,* American Chemical Society, Washington, DC **1988**.

(16) Mansky, P.; Liu, Y.; Huang, E.; Russell, T. P.; Hawker, C. J. *Science* **1997**, *275*, 1458.

(17) Zhao, B.; Brittain, W. J. *Prog. Polym. Sci.* **2000**, *25*, 677.

(18) Prucker, O.; Rühe, J. *Macromolecules*, **1998**, *31*, 592.

(19) Jordan, R.; Ulman, A.; Kang, J. F.; Rafailovich, M. H.; Sokolov, J. *J. Am. Chem. Soc.* **1999**, *121*, 1016.

(20) Matyjaszewski, K.; Xia, J. *Chem. Rev.* **2001**, *101*, 2921.

(21) Feng, W.; Brash, J.; Zhu, S.P. *J. Polym. Sci. Part A: Polym. Chem.* **2004**, *42*, 2931.

(22) Scheirs, J., editor. *Modern fluoropolymers*. Chichester: John Wiley & Sons; **1997**.

(23) Arias, E. M.; Putnam, M. D.; Boss, P. A.; Boss, R. D.; Anderson, A. A.; George, R. D. *ACS Polym. Prepr.* **1997**, *38*, 512.

(24) Benedetti, E.; D'Alessio, A.; Zini, M.F.; Bramanti, E.; Tirelli, N.; Vergamini, P.; Moggi, G. *Polym. Int.* **2000**, *49*, 888.

(25) Brantley, E. L.; Jennings, G. K. *Macromolecules* **2004**, *37*, 1476.

(26) Balachandra, A. M.; Baker, G. L.; Bruening, M. L. *J. Memb. Sci.* **2003**, *227*, 1.

(27) Sun, L.; Baker, G. L.; Bruening, M. L. *Macromolecules* **2005**, *38*, 2307.

(28) Andruzzi, L.; Hexemer, A.; Li, X. F.; Ober, C. K.; Kramer, E. J.; Galli, G.; Chiellini, E.; Fischer, D. A. *Langmuir* **2004**, *20*, 10498.

(29) Granville, A. M.; Boyes, S. G.; Akgun, B.; Foster, M. D.; Brittain, W. J. *Macromolecules* **2004**, *37*, 2790

(30) Roussel, J.; Boutevin, B. *J. Fluorine Chem.* **2001**, *108*, 37.

(31) Angot, S.; Taton, D.; Gnanou, Y. *Macromolecules* **2000**, *33*, 5418.

(32) Vallant, T.; Brunner, H.; Mayer. U.; Hoffmann, H.; Leitner, T.; Resch, R.; Friedbacher, G. *J. Phys. Chem. B* **1998**, *102*, 7190.

(33) Perrier, S.; Jackson, S.G.; Haddleton, D.M. *Macromolecules* **2003**, *36*, 9042.

(34) Rühe, J.; Knoll, W. J. *Macromol. Sci. Polym. C.* **2002**, *C42*, 91.

(35) Kim, J-B.; Huang, W.; Miller, M. D.; Baker, G. L.; Bruening, M. L. *J. Polym. Sci. Part A: Polym. Chem.* **2003**, *41*, 386.

(36) Ejaz, M.; Ohno, K.; Tsujii, Y.; Fukuda, T. *Macromolecules* **2000**, *33*, 2870.

(37) Jones, D. M.; Brown, A. A.; Huck, W. T. S. *Langmuir* **2002**, *18*, 1265.

APPENDIX:

XPS survey scans at a takeoff angle of 90°: (a) self-assembled monofunctional initiator layer on silicon wafer; (b) self-assembled difunctional initiator layer on silicon wafer, (c) a 40.0-nm-thick PTFEMA layer, and (d) a P(1-TFEMA-*b*-MMA) layer with 15.4nm of PTFEMA and 13.1nm of PMMA.

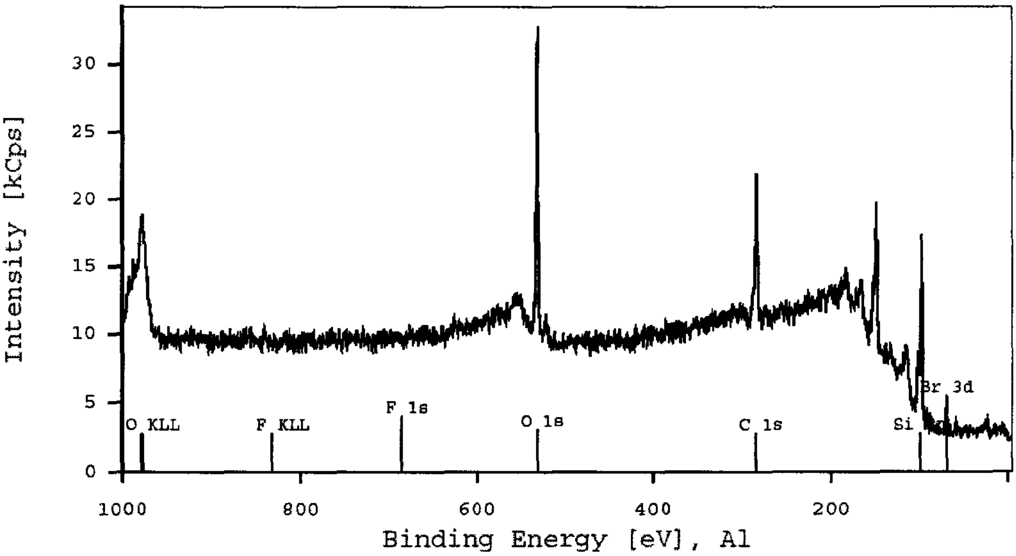
Intensity [kCps]
0
5
10
15
20
25
30
O KLL
F KLL
F 1s
O 1s
C 1s
Si
Br 3d
1000
800
600
400
200
Binding Energy [eV], Al

(a)

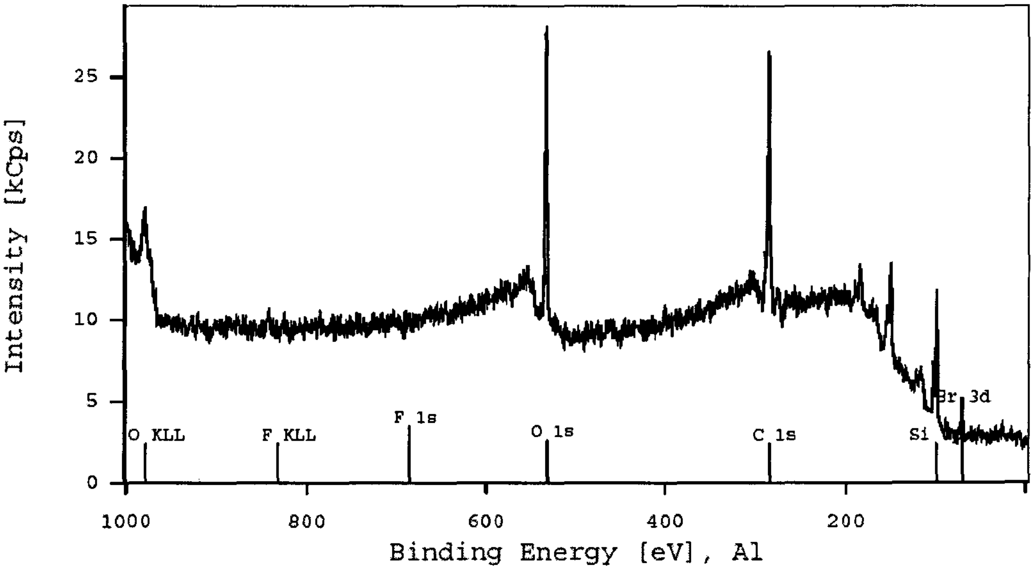
Intensity [kCps]
0
5
10
15
20
25
O KLL
F KLL
F 1s
O 1s
C 1s
Si
Br 3d
1000
800
600
400
200
Binding Energy [eV], Al

(b)

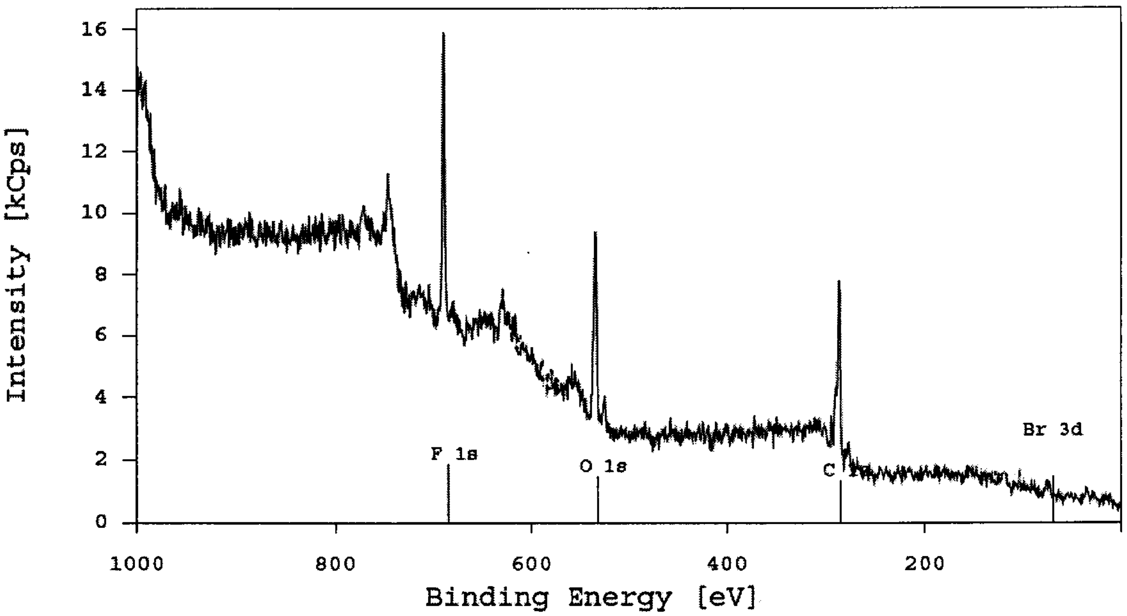
Intensity [kCps]
16
14
12
10
8
6
4
2
0
F 1s
O 1s
C 1s
Br 3d
1000
800
600
400
200
Binding Energy [eV]

(c)

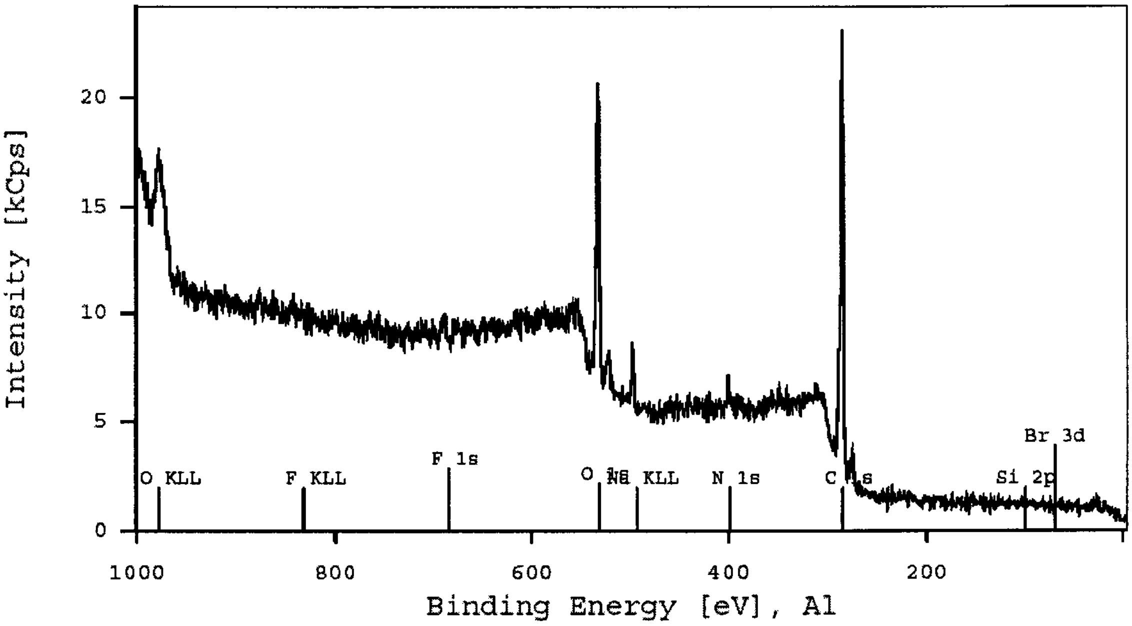
Intensity [kCps]
20
15
10
5
0
O KLL
F KLL
F 1s
O 1s
Na KLL
N 1s
C 1s
Si 2p
Br 3d
1000
800
600
400
200
Binding Energy [eV], Al

(d)

CHAPTER 4

Grafting of Polyhedral Oligomeric Silsesquioxane (POSS)-containing Polymer from Silicon Wafer by Surface-initiated ATRP

This chapter is organized based on the following published article: Chen RX, Feng W, Zhu SP, Botton G, Ong, BS, Wu YL. *Polymer* **2006**, *47*, 1119-1123.

4.1 Abstract

A Polyhedral Oligomeric Silsesquioxane(POSS)-containing methacrylate monomer, 3-(3,5,7,9,11,13,15-heptacyclopentyl-pentacyclo[9.5.1.1.^{3,9}1.^{5,15}1^{7,13}]-octasiloxane-1-yl) propyl methacrylate (POSS-MA), was directly grafted from flat silicon wafers using surface-initiated atom transfer radical polymerization (ATRP). Two methods were chosen to control the polymerization. By "adding free initiator" method, a linear relationship between the thickness of the grafted poly(POSS-MA) layer and monomer conversion was observed, indicating that the polymerization process was well controlled. By "adding deactivator" method, the poly(POSS-MA) thickness increased linearly with polymerization time for the whole stage of polymerization and more than 40nm of Poly(POSS-MA) layer were obtained. The experimental surface chemical

compositions measured by X-ray photoelectron spectroscopy (XPS) agreed well with their theoretical values. Water contact angle measurements revealed that the grafted poly(POSS-MA) was very hydrophobic. The surface morphology of the grafted polymer layer was studied by an atom force microscopy (AFM).

4.2 Introduction

Polyhedral oligomeric silsesquioxane (POSS) is a cage-like silsesquioxane with an inner inorganic silicone $(SiO_{1.5})_x$ framework and external organic substituents. With an average diameter of 1-3nm, POSS particle is considered as the smallest possible particle of silica.[1] POSS particles with different organic substituents have been successfully synthesized.[2-6] These organic substituents can be either total hydrocarbons, or various functional groups. These organic substituents make the particles compatible with organic polymers and biologic systems, which open up a new way to incorporate inorganic silica particles into organic polymer systems.

Recently, POSS monomers that contain polymerizable functional groups have attracted a great attention for their potentials in preparing organic-inorganic hybrid systems. POSS monomers can be either homopolymerized or copolymerized with other monomers to develop a novel class of hybrid polymers. Studies have shown that POSS-containing polymers have excellent material properties, such as extremely high thermal stability, good oxidation resistance, and enhanced mechanical strength.[7-10] A variety of polymerization techniques have been used to prepare different kind of hybrid polymers. In 1995, Lichtenhan et al. synthesized a methacrylate functionalized POSS (POSS-MA) monomer and (co)polymerized the monomer via conventional free radical polymerization.[11] Mather and Haddad prepared a series of random copolymers of norbornyl functionalized POSS with norbornene by ring-opening metathesis polymerization (ROMP).[12] Philips et al. used condensation polymerization to prepare POSS-modified polyimide from POSS-containing dianiline.[13] Pyun and Matyjazewski synthesized POSS-MA polymers of low polydispersities (1.14) by atom transfer radical polymerization (ATRP).[13] They also synthesized linear and star block copolymers of POSS-MA through a “macroinitiator” approach.[14,15]

Although there are many reports on the preparation and properties of POSS-containing polymers, most investigations were focused on “free” polymer systems. To the best of our knowledge, no work has been done to study POSS-containing polymer chains, which are covalently bonded to surfaces. In recent years, surface-initiated ATRP is well recognized as a very convenient method to prepare well-defined polymer brushes from surfaces. A variety of (meth)acrylic and styrenic monomers have been successfully grafted from various surfaces by surface-initiated ATRP, however, most of these monomer have small side groups. There is no work about grafting of monomers with rigid and bulky side groups, such as POSS monomers. In grafting polymer chains from a confined surface via surface-initiated ATRP, the size and rigidity of monomer side group have great effects on the grafting process. For example, the grafting density of tethered polymer chains, a key parameter for surface-initiated ATRP, decreases with increasing the size of monomer side group. Therefore, we made an effort to graft POSS monomers from various surfaces by surface-initiated ATRP and aimed to understand the effect of POSS side group on the grafting.

In this work, we report the polymerization of an *iso*-butyl substituted POSS-MA monomer from self-assembled monolayers (SAM) of ATRP initiators that are covalently immobilized on the flat silicon wafers. The grafted poly(POSS-MA) films are characterized by ellipsometry, X-ray photoelectron spectroscopy (APS), contact angle measurement, and atom force microscopy (AFM).

4.3 Experimental

4.3.1 Materials

3-(3,5,7,9,11,13,15-heptacyclopentyl-pentacyclo[9.5.1.1.^{3,9}1.^{5,15}1^{7,13}]-octasiloxane -1-yl) propyl methacrylate (POSS-MA) was purchased from Hybrid Plastics Company, Fountain Valley, CA. Trichlorosilane (99%), 2-bromoisobutyryl bromide (98%), 10-unden-1-ol (98%), 1,1,4,7,10,10-hexamethyltriethylenetetramine (HMTETA) (97%), ethyl 2-bromoisobutyrate (EBIB) (98%), hydrogen hexachloroplatinate (IV) hydrate (H_2PtCl_6, 99.9%), CuCl (99.999%), $CuBr_2$ (99.999%) were purchased from Aldrich and were used as received. Toluene and tetrahydrofuran (both HPLC grade) were obtained from Caledon Laboratories Ltd. Toluene was distilled twice before use. Double-sided polished silicon wafers (P-doped, (100)-oriented, 10–20Ω·cm resistivity, 0.56mm thickness) were purchased from University Wafer Company (Boston, MA) and cut into 5×5mm pieces using a Micro Ace Series 3 dicer (Loadpoint Ltd., England). Deionized water with a resistivity of 18MΩ·cm was prepared from a Millipore Milli-Q filtration system. Ultra-high-purity-grade argon was used in this study.

4.3.2 Synthesis of initiator

The surface-attachable initiator 11-(2-bromo-2-methyl) propionyloxy undecyltrichlorosilane was synthesized from 10-unden-1-ol according to the published procedure.[16] ^{1}H NMR($CDCl_3$, 200MHz) δ 4.16 (t, 2H, OC*H*$_2$, *J*=8.8Hz), 1.90 (s, 6H, CBr-CH_3), 1.27-1.74(m, 20H, CH_2CH_2).

4.3.3 Preparation of initiator-functionalized silicon wafer

Si(100) wafers were first washed with the "piranha" solution (a mixture of 70vol% concentrated sulphuric acid and 30vol% of hydrogen peroxide) to remove the organic residue. The wafers were rinsed with copious amount of deionized water, dried in argon flow. After that, these wafers were immersed in HF solution to remove the native oxide film and then placed into UV-Ozone cleaner for 30min to grow a uniform oxide film. The clean wafers were placed in a crystallizing dish to that a solution of initiator (15μl) in dry toluene (15ml) was added. 25μl of triethylamine was also added. The dish was covered and left at room temperature for 18h. The wafers was then rinsed with toluene, acetone and methanol and dried in an argon stream.

4.3.4 ATRP of POSS-MA from initiator-functionalized silicon wafer

A representative ATRP grafting run with an added amount of free initiator is as follows: Initiator-functionalized silicon wafers were placed into glass tubes separately. These tubes, capped with rubber septum, were deoxygenated with argon for 10min.

1.415g (1.50mmol) of POSS-MA and 9.9mg (0.10mmol) of CuCl were placed into a 10 ml flask that contains a magnetic stir bar. The flask was fitted with a rubber septum and purged with argon. 3.00ml of toluene, and 55.3μl of HMTETA were added to the flask via syringe (both were bubbled for 1h with argon before use). The mixture was stirred and degassed with argon until a homogeneous brown solution was formed (about 10min). The flask was kept at room temperature and 14.4*μ*l (0.10mmol) of EBIB initiator was added into the mixture via syringe. The reaction mixture was homogenized by intense agitation and quickly transferred into the prepared glass tubes that contain initiator-functionalized silicon wafers via a cannula. These tubes were placed into an oil bath of 50□. After desired periods of time of polymerization, the tubes were sampled and unsealed. The silicon wafers were taken out from solution, rinsed with THF, cleaned ultrasonically for 2 hours in THF, rinsed again with THF and then dried in a nitrogen stream.

For a representative ATRP grafting run with an added excess amount of deactivator, 10mol% of $CuBr_2$ (to CuCl) was added at the beginning of the reaction instead of free initiator EBiB. All the other procedures are the same as those in the added free initiator case.

4.3.5 Ellipsometry

The polymer layer thickness on silicon wafers was determined by an Exacta 2000 ellipsometer (Waterloo Digital Electronics, Waterloo, ON, Canada) equipped with a He-Ne laser (632.8nm) at a 70° incident angle. The optical constants (refractive index, extinction coefficient) of Si (n=3.865, k =0.020) and SiO_2 (n =1.465, k =0) were used to determine the thickness of the SiO_2 layer of the freshly cleaned silicon surfaces. The values of n=1.5000 and k=0 were used to calculate the thickness of the initiator-covered silicon wafers and n=1.4000 and k=0 for the polymer-covered substrates. The data were collected at three spots on each wafer sample.

4.3.6 X-ray photoelectron spectroscopy (XPS)

The surface composition of silicon wafers was determined using a Leybold Max 200 XPS with an aluminum anode non-monochromatic source. Survey scans (0–1000eV) were performed to identify constitutive elements. These scans were measured with a takeoff angle of 90°. Immediately prior to the measurement, the samples were rinsed with 1,1,2-trichloro trifluoroethane to remove contaminants.

4.3.7 Nuclear magnetic resonance (NMR)

The monomer conversion in ATRP grafting in the added free initiator case was measured using a Bruker AC-P200 NMR spectrometer (200MHz) in *d*-chloroform: $x=1-(I_{\delta=6.14\ (C\mathbf{H_2}=CCH_3)}+I_{\delta=5.57\ (C\mathbf{H_2}=CCH_3)})/(I_{\delta=0.74\sim1.22\ (CHC\mathbf{H_3}\text{-isobutyl})}/42)$.

4.3.8 Water contact angle measurement

Water contact angles were measured using a Ramé-Hart NRL goniometer (Mountain Lakes, NJ). Silicon wafers were rinsed in methanol and dried in a nitrogen stream immediately prior to the measurement. Advancing and receding contact angles were measured using the sessile drop method.

4.3.9 Atom force microscopy (AFM)

AFM images were obtained using a NanoScope IIIa Multimode atomic force microscope (Digital Instruments, Inc.). The images were recorded with standard tips in tapping mode at a scan rate of 1.0Hz. The root-mean-square (RMS) surface roughness was calculated from the roughness profiles.

4.4 Results and discussion

The procedure for preparing the poly(POSS-MA) films by surface-initiated ATRP is shown in scheme 4.1. First, ATRP initiators were immobilized on silicon wafers by the reaction of the initiator's trichlorosilane moieties with the surface hydroxy groups. The average thickness of the resulting initiator monolayer was 2.5nm, as measured by ellipsometry at three different points on the surface. Figure 4.1(a) shows the XPS survey spectrum of the initiator-functionalized silicon wafers with a take-off angle at 90°. The successful immobilization of the bromoester initiators on the surface is verified by the appearance of peaks for C_{1s}(285eV), O_{1s}(533eV), Br_{3d}(71eV). The advancing and receding water contact angles of the wafers were 78.2° and 67.4°, respectively. These contact angles were much higher than the value of < 10° for the hydrophilic silicon wafer.

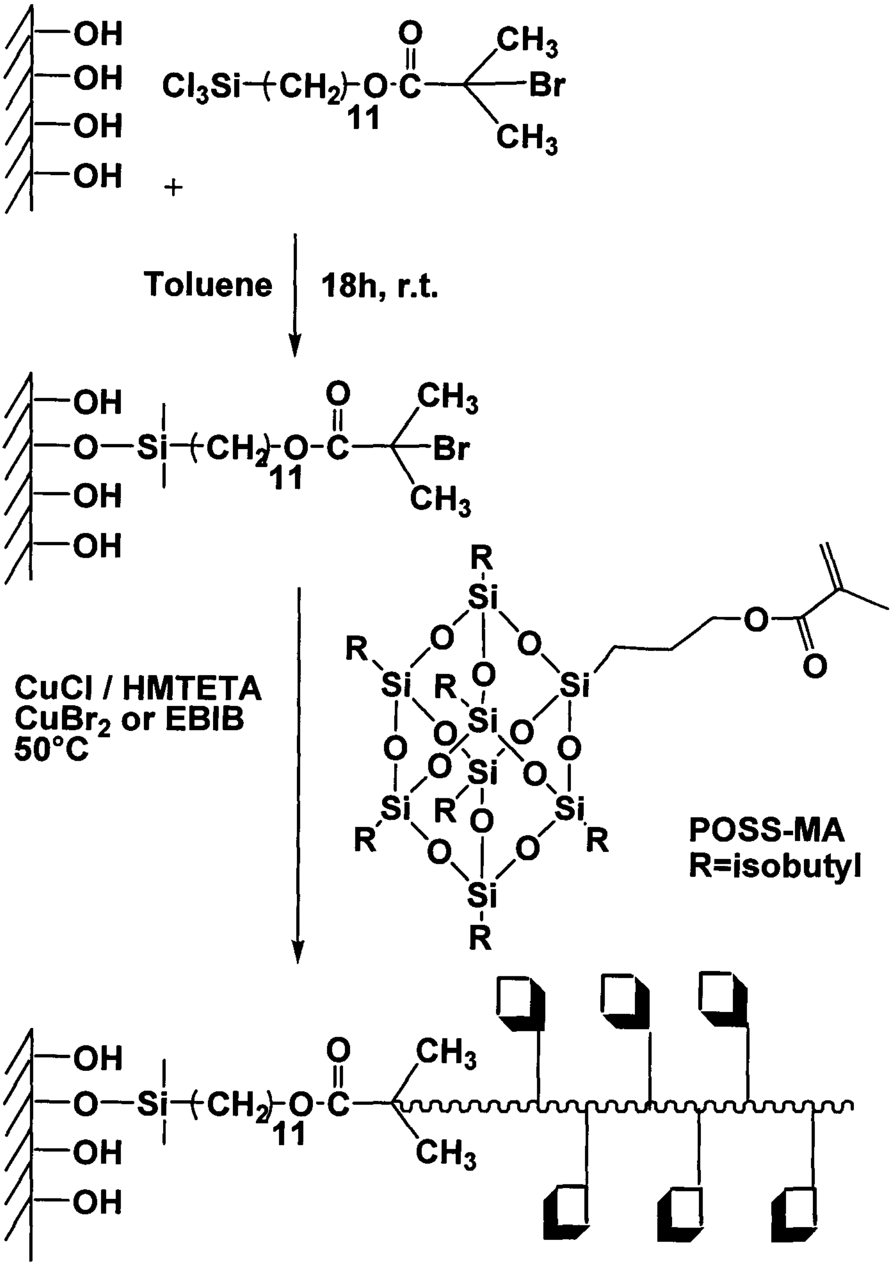

Scheme 4.1 Surface-initiated ATRP of POSS-MA.

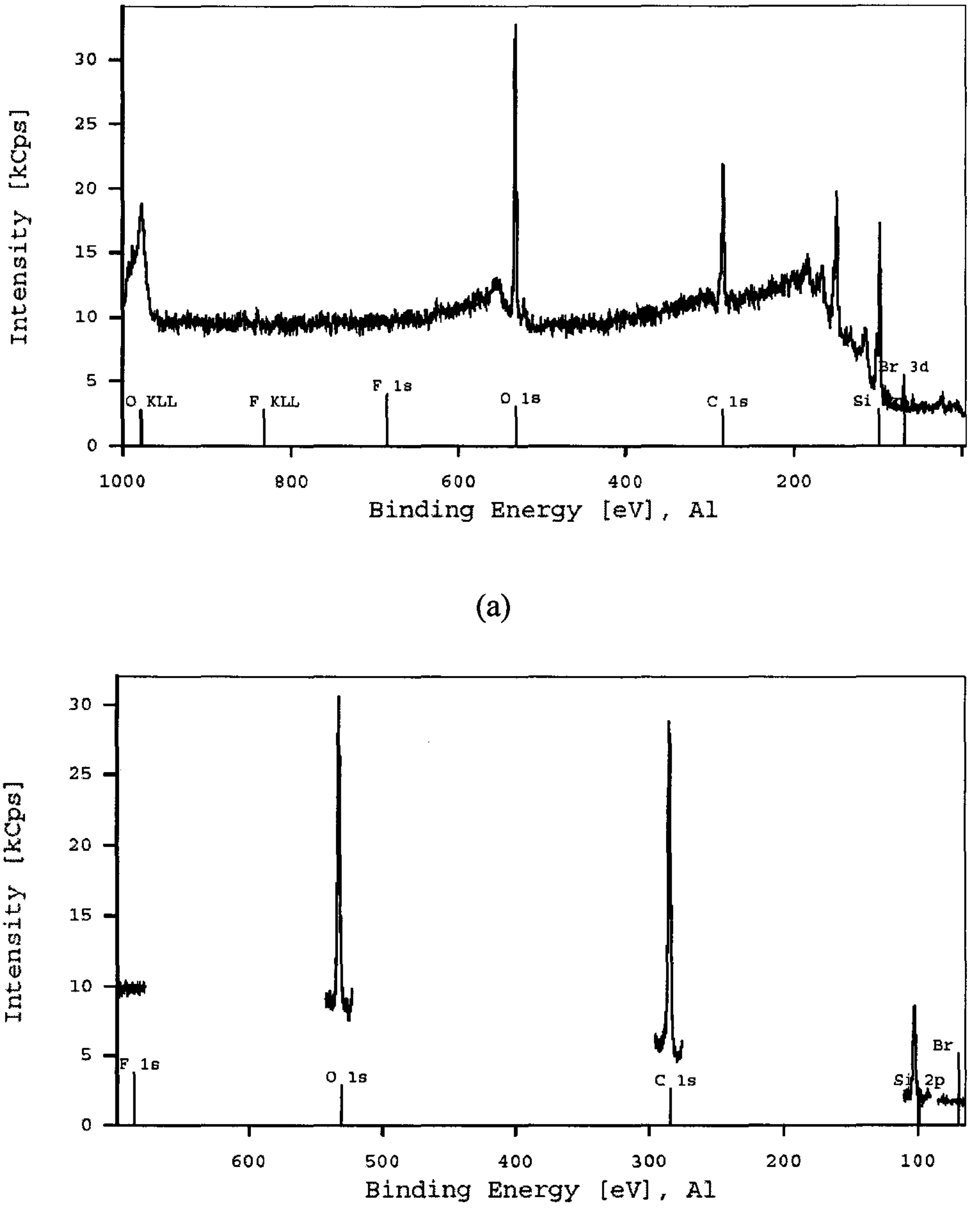

(a)

(b)

Figure 4.1 XPS survey scans at a takeoff angle of 90°: (a) self-assembled initiator layer on silicon wafer; (b) a 33.0-nm-thick Poly(POSS-MA) layer.

4.4.1 ATRP grafting of POSS-MA with added free initiator

For surface-initiated ATRP, the limited amount of initiator moieties on the surface cannot generate enough deactivator species for ATRP system. In order to get better control of surface-initiated ATRP, additional free initiator or deactivator need to be added at the beginning of the reaction to assure the sufficient amount of deactivator species. In this work, we tried both two approaches. In the added free initiator case, we run polymerization at two different targeted degrees of polymerization (DP), one is 15 and the other is 30. The monomer concentration and the molar ratio of [EBIB]/[CuCl]/[HMTETA] remained unchanged while the concentration of EBIB was varied to achieve different DPs. Figure 4.2(a) shows the development of poly(POSS-MA) thickness as a function of reaction time. The thickness kept on increasing with prolonged reaction time for both DPs. At the same reaction time, higher DP gave higher thickness. Figure 4.2(b) shows the grafted poly(POSS-MA) thickness versus monomer conversion. For both DPs, a linear relationship between thickness and monomer conversion was observed, which suggested that the polymerization was well controlled with added free initiator. However, by the adding free initiator method, most of the monomer was consumed by the free initiator in solution, which limited the amount of polymer grafted from the surface. As seen in Figure 2(b), only 5nm of poly(POSS-MA) layer was achieved at monomer conversion of 80% for DP=30. We can use the formula $\Gamma = d\rho/M_n$[17] to estimate the grafting density of poly(POSS-MA). d is the thickness of grafted polymer layer, ρ is the bulk density of poly(POSS-MA) (1.000g/cm^3). M_n is the number average molecular weight of polymer grafted from the surface and molecular weight of "free" polymer in solution was always used instead for the difficulty to get the exact molecular weight of grafted polymer. Accurate molecular weight of poly(POSS-MA) cannot be achieved by SEC for the hydrodynamic differences between poly(POSS-MA) with bulky POSS side groups and linear PS standards, [14] so we used theoretical molecular weight calculated from the monomer conversion as M_n. The grafting density calculated was 0.18chains/nm^2 for DP=15 and 0.15chains/nm^2 for DP=30. The low grafting density should be attributed to the large size of POSS side groups, which exerted a steric hindrance effect on the grafting polymerization.

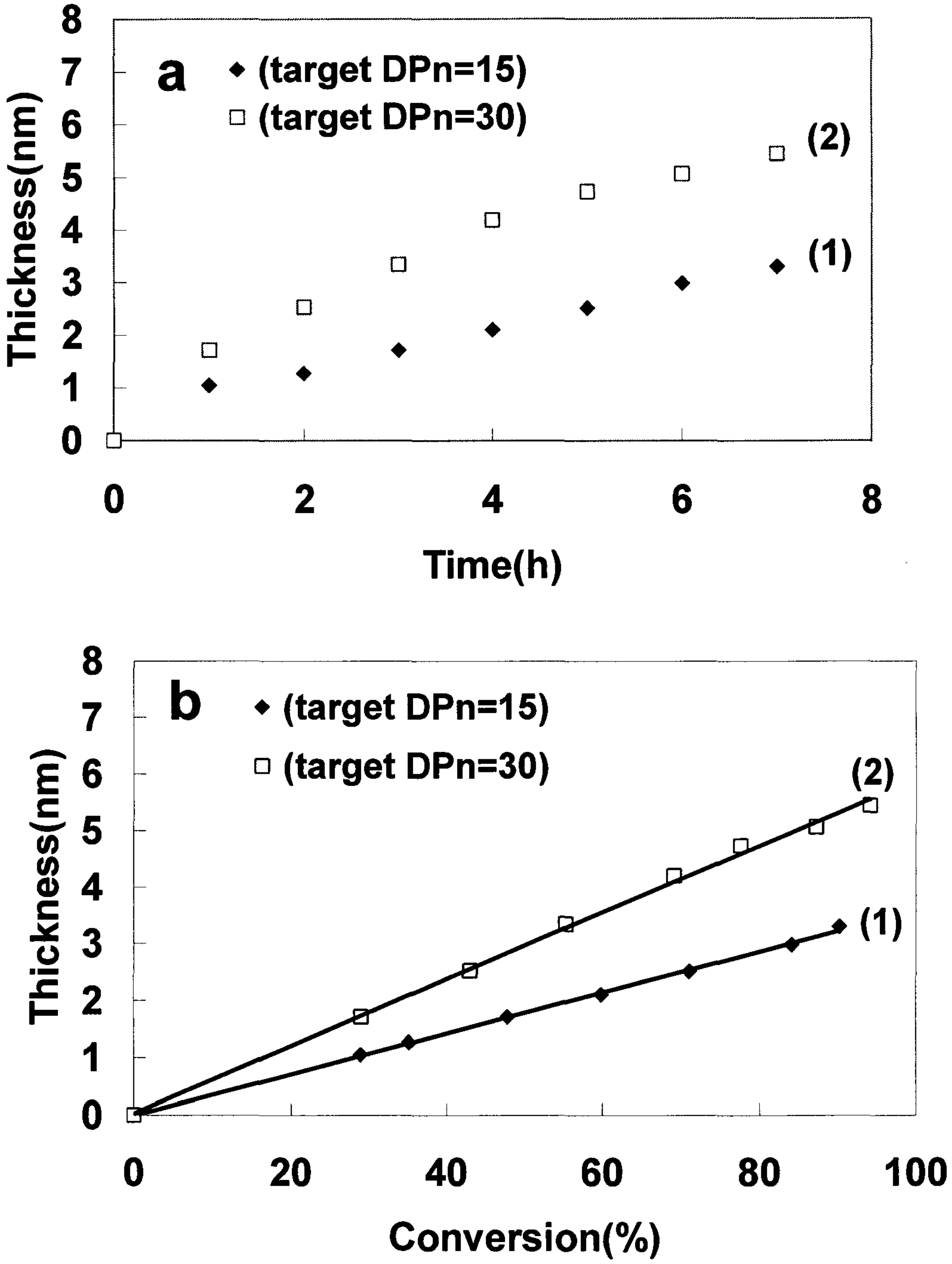

Figure 4.2 Poly(POSS-MA) thickness versus (a) polymerization time and (b) monomer conversion with added free initiator. (1) [POSS-MA]/[CuCl]/[EBIB]/[HMTETA] =

15/1/1/2, (2) [POSS-MA]/[CuCl]/[EBIB]/[HMTETA] = 30/1/1/2. [POSS-MA] = 0.50M. Solvent: Toluene.

4.4.2 ATRP grafting of POSS-MA with added deactivator

As mentioned above, the approach of adding free initiator cannot give thick poly(POSS-MA) films. In order to overcome this drawback, the approach of adding deactivator was used. Figure 4.3 shows the development of the polymer layer thickness at different monomer concentrations. For both monomer concentrations, the thickness of grafted poly(POSS-MA) layer increased linearly with the reaction time, demonstrating good control of the grafting process with added deactivator. For many surface-initiated ATRP cases, the polymer thickness increase rate will be reduced at the later stage due to loss of active chains ends by termination. However, there seems to be almost no termination for the grafting of POSS-MA. There are a lot of POSS side groups on the poly(POSS-MA) chains, and these bulky, rigid POSS side groups can keep the poly(POSS-MA) chains away from each other, which will effectively prevents the occurrence of termination. For a given polymerization time, the poly(POSS-MA) thickness increased with increasing monomer concentration. For [POSS-MA]=1.0M, more than 40nm of poly(POSS-MA) layer was achieved after 7 hours of polymerization, demonstrating the effectiveness of adding deactivator approach in preparing thick poly(POSS-MA) layers.

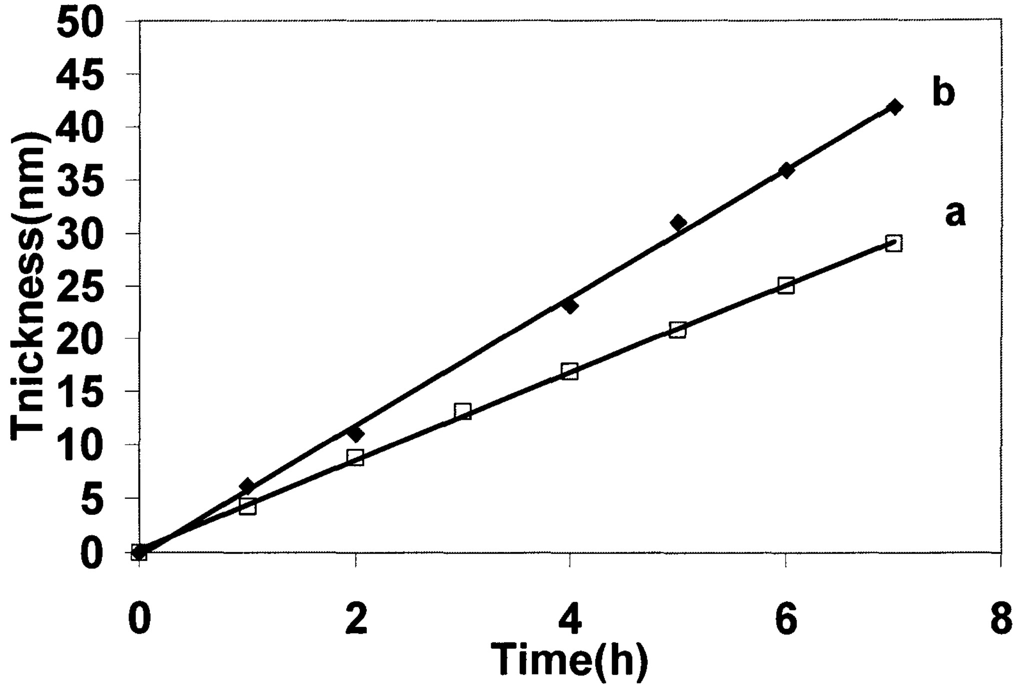

Figure 4.3 Poly(POSS-MA) thickness versus polymerization time for different monomer concentrations with added excess deactivator. (a) [POSS-MA] = 0.50M and (b) [POSS-MA] = 1.0M. [POSS-MA]/[CuCl]/[$CuBr_2$]/[HMTETA] =50/1/0.1/2.2. Solvent: Toluene.

XPS was again used to study the surface chemical composition of the grafted poly(POSS-MA) film. Figure 4.1(b) shows the survey spectrum of silicon wafer with 33nm of poly(POSS-MA) layer. The successful grafting of the poly(POSS-MA) is confirmed by the high intensity of Si_{2p} at BE of 102eV. The ratio of various elemental species is Si/C/O=15.6/62.3/22.1, which is very near the chemical composition of the POSS-MA monomer (Si/C/O=14.0/61.4/24.6). There still remains a small peak of Br_{3d} signal on the spectrum, which is in agreement with the fact that the growth of the poly(POSS-MA) chain from the surface is a surface-initiated polymerization process with a living characteristic. Water contact angles of the sample were also checked. The advancing water contact angle of the polymer is 101.1°, demonstrating the high hydrophobicity of poly(POSS-MA). The receding water contact angle of the polymer is 93.4°, only 7.7 degree lower than the advancing water contact angle, which indicates that the polymer film is pretty smooth.

The surface morphology of the silicon wafers with grafted poly(POSS-MA) was studied by AFM. Figure 4.4 shows the respective AFM image of the silicon wafer with 42nm of poly(POSS-MA), the surface roughness was a little high(~2.10nm). However, compared with the large size of POSS (average diameter of 1-3nm), this roughness is still acceptable.

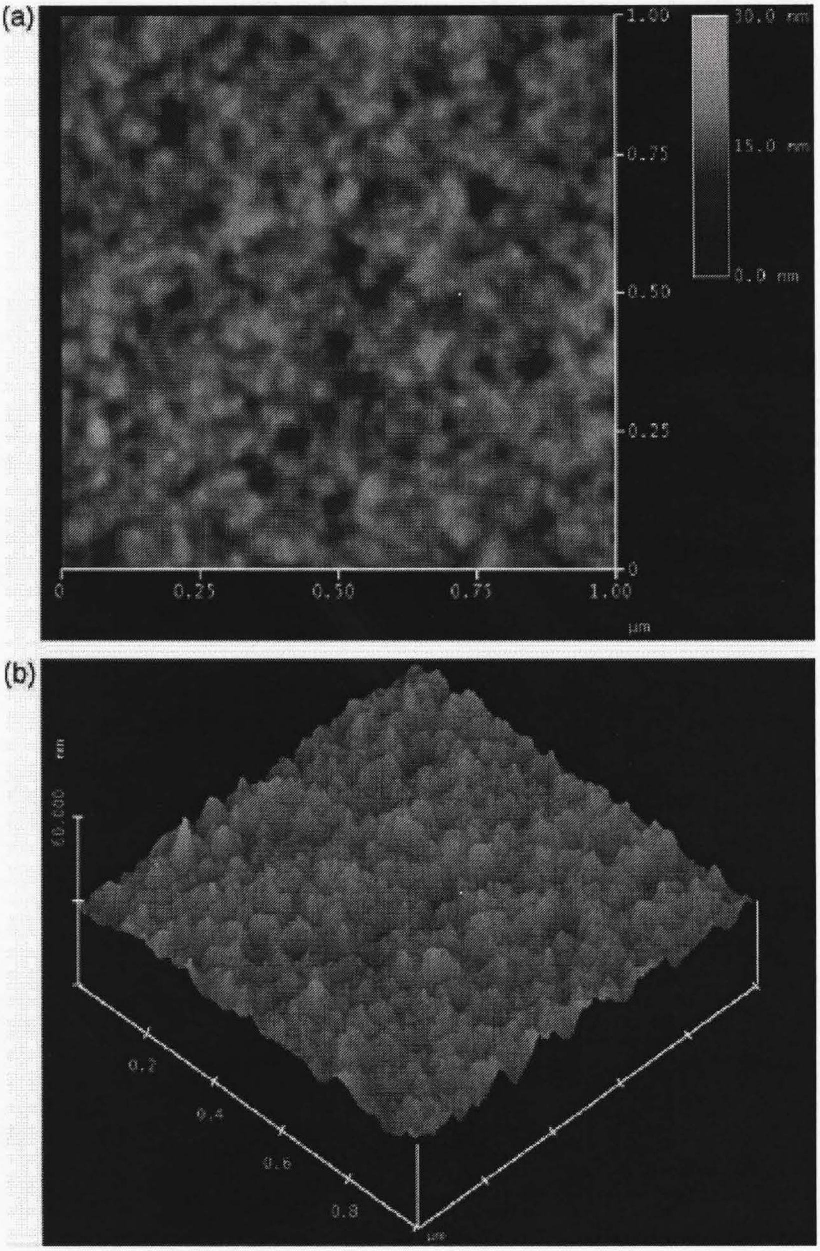

Figure 4.4 AFM image of silicon wafer covered with 42.0nm of poly(POSS-MA).

4.5 Conclusions

In summary, a POSS-containing polymer, poly(POSS-MA) was successfully grafted from flat silicon wafer by surface-initiated ATRP. Two approaches were used and both of them provided well control of the ATRP grafting process. With the approach of adding free initiator, poly(POSS-MA) thickness increased linearly with monomer conversion. With the approach of adding deactivator, poly(POSS-MA) thickness increased linearly with polymerization time and more than 40nm of poly(POSS-MA) was achieved. The surface chemical composition studied by XPS was found to be in great agreement with theoretical values. Both of Water contact angle measurements and AFM studies found that the grafted poly(POSS-MA) film was pretty smooth. Thus, the present study provided a simple and effective approach to prepare well-defined POSS-containing polymer films from flat surfaces.

4.6 References

(1) Li, G. Z.; Wang, L. C.; Ni, H. L.; Pittman, C. U. *J. Inorg. Organomet. Polym.* **2001**, *11*, 123.

(2) Sprung, M. M.; Guenther, F. O. *J. Am. Chem. Soc.* **1955**, *77,* 3990.

(3) Brown, Jr. J. F. *J. Am. Chem. Soc.* **1965**, *87,* 4317.

(4) Frye, C. L. Collins, W. T. *J. Am. Chem. Soc.* **1970**, *92*, 5586.

(5) Gilman, J. W.; Schlitzer, D. S.; Lichtenhan, J. D. *J. Appl. Polym. Sci.* **1996**, *60*, 591.

(6) Lichtenhan, J. D.; Schwab, J. J.; Feher, F. J.; Soulivong, D. U.S. Patent 5942638 **1999**.

(7) Haddad, T. S.; Lichtenhan J. D. *Macromolecules* **1996**, *29*, 7302.

(8) Tsuchida, A.; Bolln, C.; Sernetz, F. G.; Frey, H.; Mulhaupt, R. *Macromolecules* **1997**, *30*, 2818.

(9) Lee, A.; Lichtenhan, J. D. *Macromolecules* **1998**, *31*, 4970.

(10) Jeon, H. G.; Mather, P. T.; Haddad, T. S. *Polym. Int.* **2000**, *49*, 453.

(11) Lichtenhan, J. D.; Feher, F. J.; Gilman, J. W. *Macromolecules* **1995**, *28*, 8435.

(12) Mather, P. T.; Hong, G. J.; Romo-Uribe, J.; Haddad, T. S.; Lichtenhan, J. D.; *Macromolecules* **1999**, *32*, 1194.

(13) Gonzalez, R. I.; Hoflund, G. B.; Phillips, S. H. et al. *Proc International SAMPE Symposium and Exhibition,* **2002**, 7, 1488.

(14) Pyun, J.; Matyjaszewski, K. *Macromolecules* **2000**, *33*, 217.

(15) Pyun, J.; Wu, J.; Matyjaszewski, K. *Polymer* **2003**, *44*, 2739.

(16) Hawker, C. J. et al. *Macromolecules,* **1999**, *32*, 1424.

(17) Rühe, J.; Knoll, W. J. *Macromol. Sci. Polym. C.* **2002**, *C42*, 91.

CHAPTER 5

Grafting Acrylic Polymers from Flat Nickel and Copper Surfaces by Surface-initiated ATRP

This chapter is organized based on the following published article: Chen RX, Maclaughlin S, Zhu SP. *Langmuir* **2008**, *24*, 6889-6896.

5.1 Abstract

Acrylic polymers, including poly(methyl methacrylate) (PMMA), poly(2,2,2-trifluoroethyl methacrylate) (PTFEMA), poly(*N,N'*-dimethyaminoethyl methacrylate) (PDMAEMA) and poly(2-hydroxyethyl methacrylate) (PHEMA) were grafted from flat nickel and copper surfaces through surface-initiated atom transfer radical polymerization (ATRP). For the nickel system, there was a linear relationship between polymer layer thickness and monomer conversion or molecular weight of "free" polymers. The thickness of the polymer brush films was greater than 80nm after 6 hours of reaction time. The grafting density was estimated to be 0.40chains/nm^2. The "living" chain ends of grafted polymers were still active and initiated the growth of a second block of polymer. Block copolymer brushes with different block sequences were

successfully prepared. The experimental surface chemical compositions as measured by X-ray photoelectron spectroscopy (XPS) agreed very well with their theoretical values. Water contact angle measurements further confirmed the successful grafting of polymers from nickel and copper surfaces. The surface morphologies of all samples were studied by atomic force microscopy (AFM).

5.2 Introduction

The past decade has seen tremendous growth in the methods and applications of various controlled radical polymerization (CRP) techniques including nitroxide-mediated radical polymerization (NMP),[1] reversible addition-fragmentation chain transfer polymerization (RAFT),[2] and atom transfer radical polymerization (ATRP).[3] Unlike conventional radical polymerization these techniques can provide excellent control of the molecular weight and molecular weight distribution (MWD). They also allow the preparation of well-defined polymer structures such as block copolymers, star shape polymers and interpenetrating polymer networks.

Among this group of CRP techniques, the transitional metal mediated ATRP has received particular attention because of its compatibility with a range of monomer types, tolerance of various impurities, mild reaction conditions, and possible recycling and/or reduction of used catalyst amount. An important application of ATRP is the grafting of polymer brushes from the surfaces of flat substrates and colloidal particles. Specially designed surface-attachable ATRP initiators, usually silane or thiol derivatives, are first immobilized onto the surface, followed by in-situ ATRP. An important advantage of this "grafting from" method compared to other polymerization grafting methods is the ability to produce polymer brushes with high grafting density, ranging from 0.1 to 0.7chains/nm^2. To date "grafted from" polymers have been prepared with a variety of monomers, including styrene,[4] methyl methacrylate (MMA),[5] and 2-hydroxyethyl methacrylate (HEMA),[6] utilizing substrates with a range of chemical properties and surface dispositions, including silicon wafers,[4,5,] silica and gold particles,[7,8] polymer films,[9] and carbon nanotubes.[10] Despite these successes, the characterization of "grafted from" brush polymers still remains a challenge.

Although there are many different materials that have been successfully used as substrates for surface-initiated ATRP, some of the most common and important materials in our everyday life, metals and alloys, have been largely overlooked by researchers. Unlike other kinds of materials, the surfaces of metals are active in electrochemical and acid/base reactions and this reactivity complicates ATRP reactions. Red-ox deactivation of the ATRP catalyst is a particular risk. Jérôme's group was the first to successfully apply surface-initiated ATRP to metal surfaces in 2003.[11] The inimer 2-chloropropionate ethyl acrylate (cPEA) was electro-grafted to steel surfaces to form a dense layer of ATRP macroinitiators; polystyrene was then grafted from the activated chloride side groups. Copper catalysts, the usual first choice for ATRP reactions, reacted electrochemically to corrode the steel surface, necessitating the use of Grubbs catalyst and a nickel complex catalyst as alternatives. The grafting was successful but these catalysts exhibited poor control over the polymerization and the polystyrene graft was found to have high polydispersity.

Using this "macroinitiator" method, many different monomers were grafted from steel surfaces,[12] including 2-(*tert*-butylamino)-ethyl methacrylate (TBAEMA), monomethyl ether of poly(ethylene oxide) methacrylate (PEOMA) and acrylic acid. More recently,[13] Fan et al. prepared antifouling polymer coatings via ATRP of oligo(ethylene glycol) monomethacrylate (OEGMA) from a novel biomimetic catechol-containing ATRP initiator anchored on titanium and 316L stainless steel surfaces. By combining this technique with molecular assembly patterning by lift-off (MAPL), they also succeeded in preparing micro-patterned polymer coatings on Ti surfaces for potential use as cell arrays.

To date most examples of surface-initiated ATRP on common metals have employed steel, stainless steel and titanium. Other metals in wide use, such as nickel, copper, aluminium and zinc, have not been explored but have chemical and physical properties that make them attractive materials for manufacturing. Nickel has good corrosion resistance to various reducing chemicals, especially to alkalis. For this reason, nickel is widely used in reaction vessels for the processing of foods and manufacture of synthetic fibres. The ability of copper to inhibit the growth of bacteria, virus and fungi motivates its use in the fabrication of water pipes and doorknobs. Both metals have excellent electrical and thermal conductivities. As the most efficient conductor of electricity and heat among non-precious metals, copper might be the most extensively used material in electric and electronic devices. Both nickel and copper are important components of many important alloys such as brass (copper and zinc), cupronickel (copper and nickel) in addition to superalloys. Despite of all these important applications of nickel and copper, no work has been reported on direct grafting of polymers from these two metals.

One of the primary advantages of grafted brush polymers over conventional polymer coatings is in the nature of the interface. Polymer coatings using conventional methods normally adhere to metal surfaces through Van de Waals forces or other weak interactions and are prone to delamination under physical or chemical stresses. In contrast, polymers grafted to a metal by surface-initiated ATRP are covalently bonded to the metal surface and may demonstrate much more stable adhesion. Other than offering stable adhesion, the grafting of brush polymers also provides a simple and effective route for tuning metal surface properties. By grafting polymers with different functionalities, the modified metals become feasible for applications in different areas. For example, by grafting PEG-type or phosphorylcholine-type polymers, the non-specific protein absorptions on metal surfaces can be well prohibited, which is very useful for improving the biocompatibility of metal-made bioimplants. Fluoropolymers have lots of interesting properties, such as high thermal, chemical and photochemical stability, low refractive index and low surface energy. The grafting of fluoropolymers makes metal surfaces become "self-cleaning" due to the polymer's excellent water or oil repellent properties. The high stability of fluoropolymers in all environments can also provide excellent protections to metals from chemical corrosions and photo degradations.

In this work, we report the first examples of surface-initiated ATRP from flat nickel and copper surfaces. The grafting polymerizations were well behaved and readily controlled, and a diverse group of monomers were successfully grafted. The products were characterized by XPS, water contact angle measurements, and AFM.

5.3 Experimental

5.3.1 Materials

3-Aminopropyl triethoxysilane (99%), 2-bromoisobutyryl bromide (98%), ethyl 2-bromoisobutyrate (EBIB) (98%), 4,4'-dinonyl-2,2'-dipyridyl (dNnbpy) (97%), 2,2'-bipyridyl (bpy) (97%), CuCl (99.999%), $CuBr_2$ (99.999%), $FeBr_2$ (98%), $FeBr_3$ (98%), triphenylphosphine (99%), triethylamine (>99%), toluene (anhydrous), *N,N*-dimethylformamide (anhydrous), nickel foil (99.98%, 0.5mm), copper foil (99.98%, 0.5mm) were purchased from Aldrich and were used as received. Methyl methacrylate (MMA) (99%), 2,2,2-trifluoroethyl methacrylate (TFEMA) (98%) *N,N*-dimethylamino-ethyl methacrylate (DMAEMA) (98%), 2-hydroxyethyl methacrylate (HEMA) and α,α,α-trifluorotoluene (anhydrous, +99%) were purchased from Aldrich and distilled over CaH_2 under vacuum, then stored at -15°C before use. Methanol (HPLC), *n*-heptane (HPLC), dichloromethane (Reagent), hexane (Reagent), acetone (Distilled Class), ethyl acetate (Reagent), and tetrahydrofuran (HPLC) were obtained from Caledon Laboratories Ltd. and used as received. Deionized (DI) water with a resistivity of 18MΩ·cm was prepared from a Millipore Milli-Q filtration system. Ultra-high-purity-grade argon was used in this study.

5.3.2 Metal surface pretreatments

Nickel and copper foils were cut into small coupons (8mm × 8mm) and polished on one side using a Strüers RotoPol-31/ RotoForce-4/ Multidoser automatic polisher to give a mirror-like appearance. The polishing sequence for nickel used 320grit silicon carbide paper, 1200grit silicon carbide paper, 9μm diamond suspension, 3μm diamond suspension, and finally 50nm silica powder suspension. The sequence for copper used 320grit silicon carbide paper, 1200grit silicon carbide paper, 1μm diamond suspension, and finally 50nm alumina powder suspension. The polished coupons were immediately placed under distilled acetone for storage until use.

5.3.3 Immobilization of initiators

The surface-attachable initiator was synthesized following the published procedure.[14] One part by volume of initiator was added to ten parts by volume methanol (HPLC grade) and dispersed by stirring for 2min, followed by addition of 89 parts by volume DI water. The mixture was stirred at 40°C until the cloudy solution turned transparent (about one hour). Transparency was equated with hydrolysis to form the water soluble trihydroxy derivative. The transparent solution was then cooled to room temperature. During the hydrolysis process, the polished copper and nickel coupons were prepared by ultrasonic cleaning in *n*-heptane (5min), acetone (5min, twice), ethanol (5min) and methanol (5min). The well-cleaned metal coupons were then immersed into the initiator solution for 2min. The coupons were taken out from the initiator solution and bathed several times ultrasonically in 100ml of methanol (30min, three times), followed by 10min of curing at 75°C in a vacuum oven.

5.3.4 ATRP of polymers from initiator-functionalized metal coupons

ATRP polymerizations were controlled by either "added free initiator" or "added deactivator" approach. The typical procedure for ATRP of MMA from nickel surfaces with the added "free" initiators is as follows: Initiator-functionalized nickel coupons were placed into glass tubes separately. 64.7mg (0.300mmol) of $FeBr_2$ and 236.0mg (0.9000mmol) of triphenylphosphine were placed into a 25ml flask containing a magnetic stir bar. The flask was deoxygenated through several evacuation/backfilling cycles of argon. 9.0g (90mmol) of degassed MMA was then added via syringe. The mixture was stirred and degassed with argon until a homogeneous brown solution formed (about 10min). The flask was kept at room temperature and 43.3μl (0.300mmol) of EBIB initiator was added into the mixture via syringe. The mixture was stirred and degassed with argon for another 5min, and then transferred via a cannula into the glass tubes containing nickel coupons. These glass tubes were placed in an oil bath of 60°C. After the desired reaction time, the tubes were unsealed and sampled. The nickel coupons were ultrasonically rinsed with dichloromethane (30min), THF (30min) and then dried in an argon stream.

A typical ATRP of MMA from nickel surfaces using the "added deactivator" approach is as follows. Initiator-functionalized nickel coupons were placed into glass tubes separately. 64.7mg (0.300mmol) of $FeBr_2$, 8.9mg (0.030mmol) of $FeBr_3$ and 259.6mg (0.9900mmol) of triphenylphosphine were placed into a 25ml flask containing a magnetic stir bar. The flask was deoxygenated through several evacuation/backfilling cycles of argon. 9.0g (90mmol) of degassed MMA were then added via syringe. The mixture was stirred intensively, degassed with argon for another 10min, and then transferred to the glass tubes containing initiator-functionalized nickel coupons via a cannula. The glass tubes were kept in an oil bath of 60°C. Nickel coupons were taken out from the glass tubes after the desired time periods and cleaned by the same procedure as in the added free initiator case (vide supra). Grafting polymerization of TFEMA was performed at 90°C using α,α,α-trifluorotoluene as solvent. Polymerizations of HEMA and DMAEMA were performed at 40°C in DMF.

The same experimental procedure was used for ATRP from copper surfaces. A typical recipe for the grafting of PMMA was as follows: 4.0g (40mmol) of MMA, 4.0 g of toluene, 19.8mg (0.200mmol) of CuCl, 4.9mg (0.020mmol) of $CuBr_2$ and 176.4mg (0.440mmol) of dNnbpy. Grafting polymerization of TFEMA was performed at 90°C using α,α,α-trifluorotoluene as solvent. For HEMA and DMAEMA polymerizations were run at 40°C using bpy as ligand in a solvent mixture of methanol and DI water (1/1 by vol).

5.3.5 Characterization

The surface chemical compositions were determined using a Leybold Max 200 XPS with magnesium or aluminum anode non-monochromatic sources. Survey scans (0–1000eV) were performed to identify constitutive elements. These scans were measured with a takeoff angle of 90°. Immediately prior to the measurement, the samples were rinsed with 1,1,2-trichlorotrifluoroethane to remove contaminants. Water contact angles were measured using a Ramé-Hart Model 200 goniometer with Dropimage standard software (Mountain Lakes, NJ). Metal coupons were rinsed in methanol and dried in a nitrogen stream immediately prior to the measurement. Advancing and receding contact angles were measured using the sessile drop method.

The monomer conversion was measured using a Bruker AC-P200 neutron magnetic resonance (NMR) spectrometer (200MHz) in *d*-chloroform. The molecular weights of PMMA were determined by gel permeation chromatography (GPC). A Waters 710 sample autoinjector, 3 linear columns in series (Waters Styragel HR 5E, 2 Shodex KF-804L), a Waters 600 pump system and a 410 refractive index (RI) detector were used for the assays. The eluent (THF) was pumped through the system at a fixed flow rate of 1ml/min. The columns and detector were heated to 30°C and 35°C, respectively. Narrow polystyrene samples were used as standards to generate the calibration curve. Data were recorded and manipulated using the Waters Millennium software package. The thicknesses of polymer layers on nickel coupons were determined by an Exacta 2000 ellipsometer (Waterloo Digital Electronics, Waterloo, ON, Canada) equipped with a He-Ne laser (632.8nm) at a 70° incident angle. The optical constants (refractive index, extinction coefficient) used were: Ni (n=2.500, k=3.750) NiO (n=1.900, k=0.500), PMMA (n=1.489, k=0), PTFEMA (n=1.437, k=0), PTFEMA (*n*=1.450, *k*=0), PHEMA (*n*=1.512, *k*=0). The data were collected at three separate spots on each sample.

AFM images were obtained using a NanoScope IIIa Multimode atomic force microscope (Digital Instruments, Inc). The images were recorded in tapping mode at ambient conditions using silicon carbide tips. The scan rate is 1.0Hz. The roughness analysis on the two dimensional topography image was based on a calculation of the standard deviation of all height values with the given imaged area (root-mean-square (rms)).

5.4 Results and discussion

5.4.1 Construction of initiator layers on metal surfaces.

Mono- or tri-chlorosilanes, which are commonly used for surface-initiated ATRP because they can be easily attached to hydroxylated surfaces, were not used in this study because of the potential for corrosion of the reactive metal surfaces. Trimethoxysilanes and triethoxysilanes have been widely adopted to prepare corrosion-inhibitive coatings on various kinds of metal surfaces[15,16] and do not present a risk of corrosion damage of reactive metal surfaces. Moreover, trialkoxysilane-containing ATRP initiators have already been proven effective for surface-initiated ATRP from other types of substrates.[17, 18] Inspired by these advantages, we used a triethoxysilane-containing initiator in this work. The accepted sequence of reactions in the attachment of these materials to metal surfaces is as follows. The Si-$(OC_2H_5)_3$ groups were first hydrolyzed to Si-$(OH)_3$ groups in a mixture of methanol and DI water. Immersing metal coupons in the hydrolyzed initiator solution led to the immediate formation of hydrogen bonds between the Si-$(OH)_3$ groups and hydroxyl groups on the metal surface. Curing at 75 °C resulted in condensation to produce very dense initiator layers covalently bonded to the metal surface by direct metal-O-Si bonds. The thickness of the monolayer was 2.8 ± 0.3 nm measured by ellipsometry, which was very close to the reported thickness for OTS (Octadecyltrichlorosilane) monolayers (2.2nm).[19] For each sample, the deviation of the thicknesses at three different spots was not larger than 0.3nm.

XPS was employed to determine the surface chemical compositions [see Figure 5.1 (a), Figure 5.5(a), Table 5.1 and Table 5.2]. The characteristic Br_{3d} peaks were found at BE of ~70eV, indicating the successful immobilization of initiator species on both metal surfaces. Compared to the atomic percentages of the elements in the free silane, the intensities of the Br_{3d}, Si_{2p} and N_{2p} signals were low while those of carbon and oxygen signals much higher than expected. This is consistent with either a very thin layer, a discontinuous layer, or some combination of the two. XPS results on the grafted polymer layers, together with contact angle measurements and estimated graft densities (vide infra) are consistent with the formation of a thin but continuous initiator film.

Water contact angle measurement is also very useful tool to monitor changes in surface properties (see Table 5.4, Table 5.5). As-polished metal surfaces were very hydrophilic, presenting advancing and receding water contact angles of 36.4° and 23.5° for nickel, 44.6° and 31.5° for copper, respectively. After the initiator immobilization, both of advancing and receding angles increased markedly to 70.3° and 41.9° for nickel, 78.7° and 43.1° for copper, respectively, consistent with the presence of a coating of hydrophobic bromoisobutyrate moieties on the surfaces.

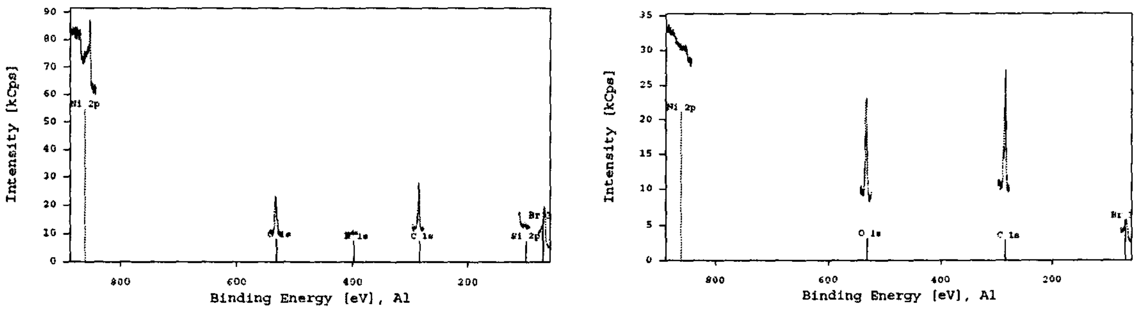

(a)

(b)

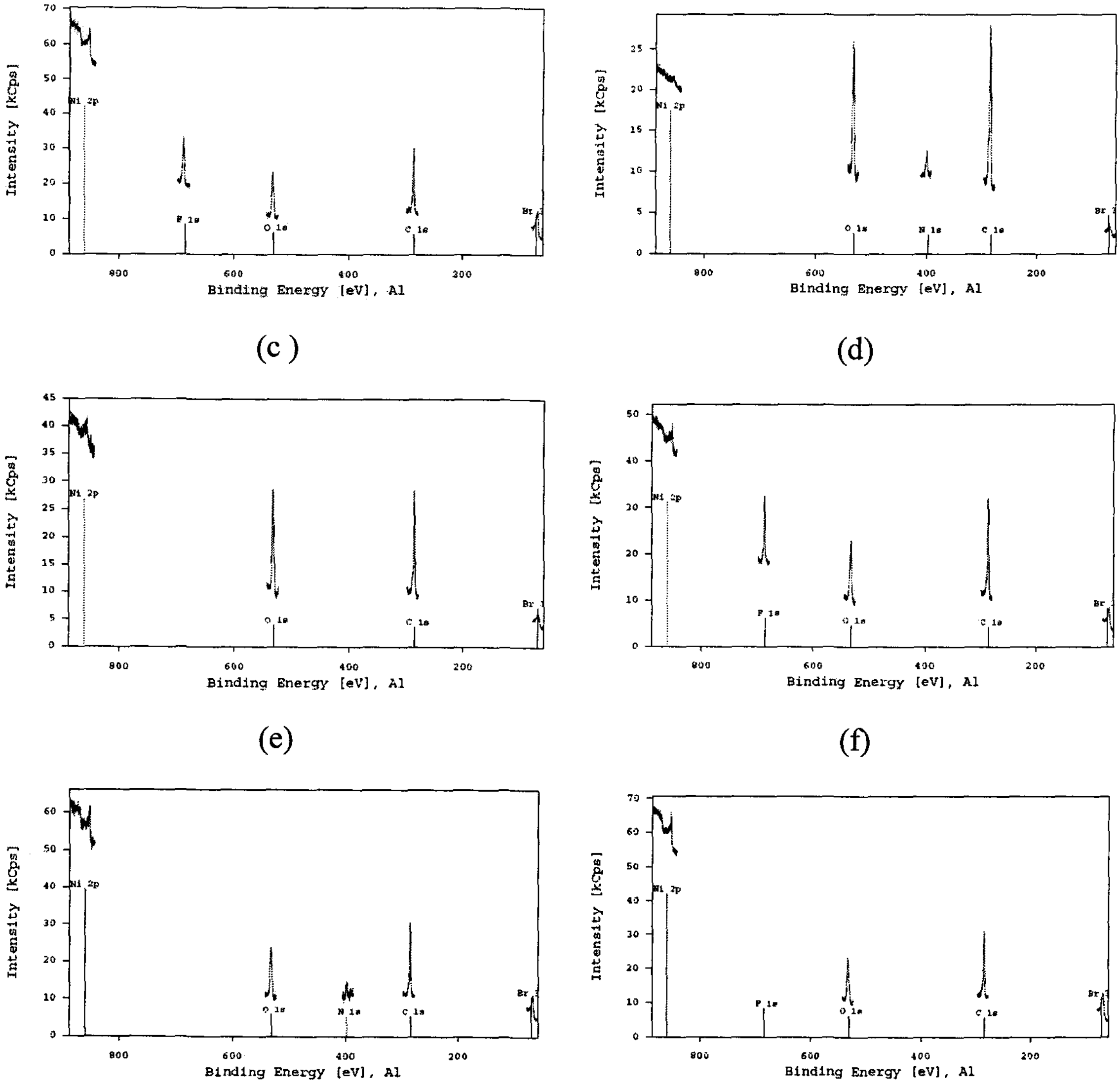

(c) (d)

(e) (f)

(g) (h)

Figure 5.1 XPS survey scans of the nickel surfaces with various organic layers at a takeoff angle of 90°: (a) self-assembled initiator; (b) PMMA; (c) PTFEMA; (d) PDMAEMA; (e) PHEMA; (f) PMMA-*b*-PTFEMA; (g) PMMA-*b*-PDMAEMA; (h) PTFEMA-*b*-PMMA.

5.4.2 Surface-initiated ATRP from Ni surfaces.

It is well known that in ATRP system a sufficient amount of deactivating species (i.e., Cu(II) ligand complex) is indispensable for the control of radical concentration and then the minimization of the undesirable termination reactions. Different from solution ATRP, in which Cu(II) can be generated by the red-ox reaction between Cu(I) and "free" initiators, the small number of initiator moieties on surface in the surface-initiated ATRP are not able to create enough Cu(II) species to offer good control over the grafting polymerization. To solve this problem, additional "free" initiators or deactivators are often added to the surface-initiated ATRP system at the beginning of the reaction. These added "free" initiators or deactivators help to obtain an adequate level of deactivators in the system. The grafting polymerization can then be controlled. In this study, both methods were employed for the ATRP initiated from the flat nickel surfaces.

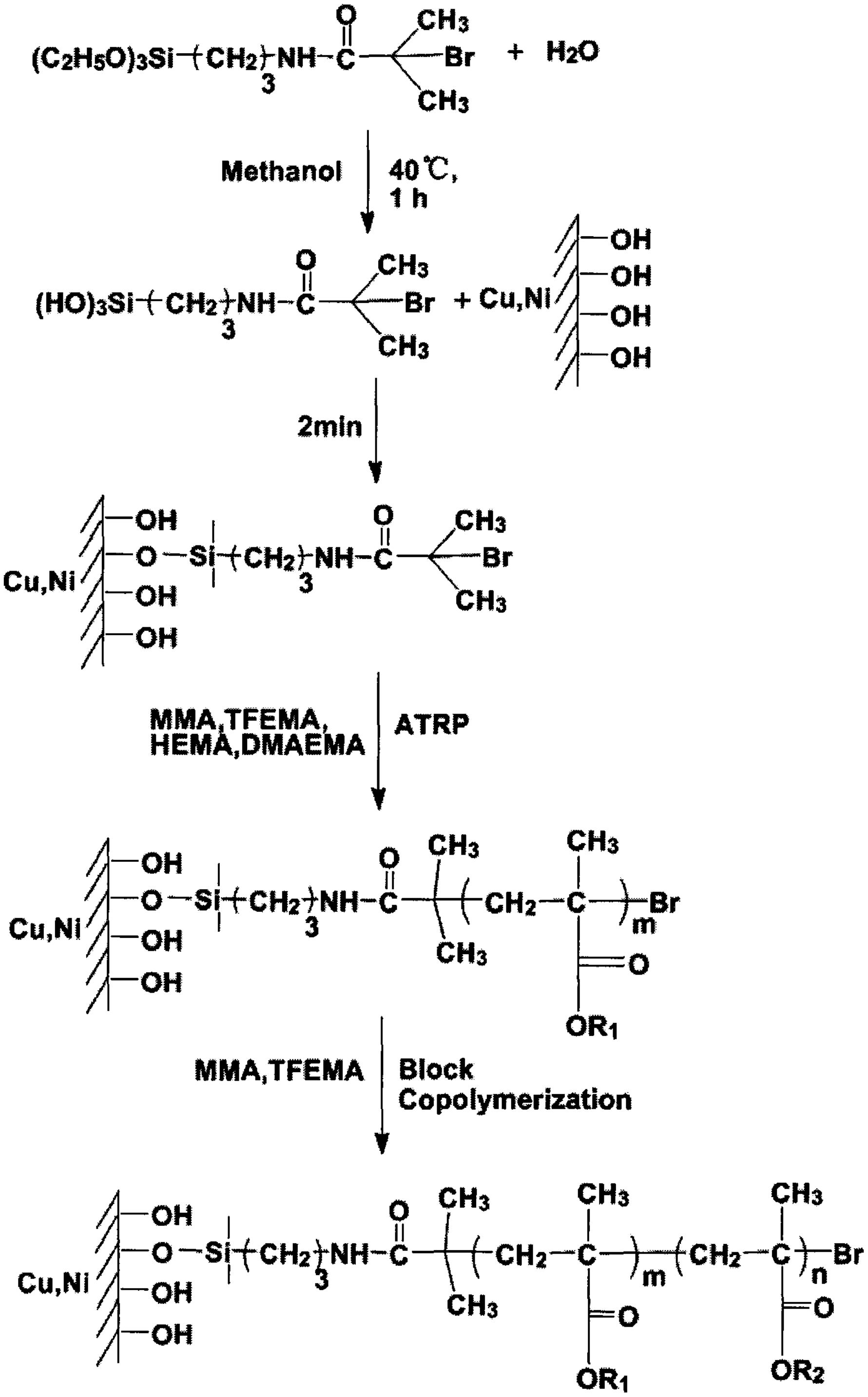

Scheme 5.1 Surface-initiated ATRP of polymers from flat metal surfaces.

Cu(I)/Cu(II) halides are the most widely used catalysts for ATRP; however the Fe(II)/Fe(III) catalyst system was chosen for polymerization on the nickel surfaces because of the potential for electrochemical reactions between the nickel surface and a Cu(II) catalyst. In a preliminary kinetic study, MMA was used as a model monomer and was polymerized from the nickel surface in the presence of added "free" EBIB initiator. The amount of EBIB was varied to control the degree of polymerization (DP). As shown in Figure 2, the thickness of the grafted PMMA films increased linearly with monomer conversion and for both DPs. Also, the molecular weight distribution of "free" polymers in solution was very narrow, with all polydispersities lower than 1.30. These results indicated that ATRP grafting of PMMA from the nickel surface was well behaved and controlled. The grafting densities can be estimated from the equation: $\Gamma = d\rho/M_n$, where d is the thickness of the grafted polymer layer, ρ is the bulk density of the polymer (1.16g/cm^3 used for PMMA), and M_n is the number-average molecular weight of the polymer grafted from the surface. Although the exact molecular weight of the grafted polymer is unknown, we can just use the molecular weight of the polymer formed in solution for estimation. For the targeted DP=300 and DP=600, the grafting densities were 0.42chains/nm^2 and 0.40chains/nm^2, respectively, suggesting that DP did not affect the grafting density. Advancing and receding water contact angles of the modified nickel coupons were 66.4° and 48.3°. The advancing water contact angle is close to the reported value for pure PMMA films.[20]

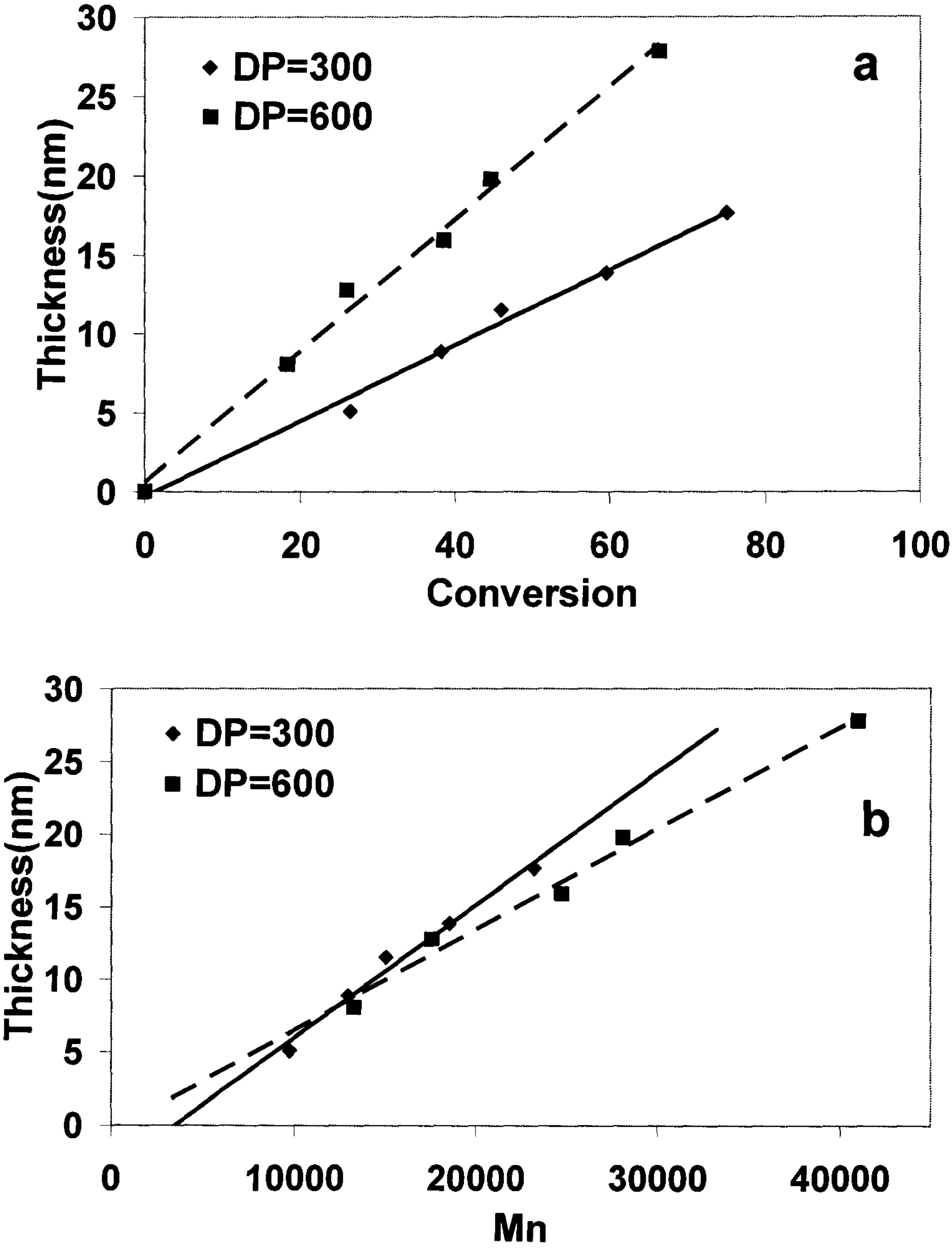

Figure 5.2 Thickness of the PMMA layer versus (a) monomer conversion and (b) molecular weight of "free" polymer with added "free" initiator.

The "added free initiator" approach was not suitable for preparation of thick polymer films because most monomers in a reaction mixture of this type are consumed by the free initiators. However, thick films can be prepared using the "added deactivator" approach, in this case by adding additional $FeBr_3$ (10mol% of $FeBr_2$) at the beginning of the reaction. The [monomer]/[catalyst] ratio was varied by changing the catalyst concentration while holding [MMA] constant. As shown in Figure 5.3, for the same reaction time, increasing [monomer]/[catalyst] ratios (lower catalyst concentration) resulted in thicker PMMA films. According to Baker's kinetic studies of surface-initiated ATRP, [21] the growth rate of polymer chains is determined by the opposing influences of the rates of the propagation and termination reactions. Lowering catalyst concentration decreases the radical concentration, which suppresses in different degrees both the rate of bimolecular radical termination and that of propagation. As a result, the polymer layer thickness is a complicated function of both catalyst concentration and reaction time. For any given reaction time, the thickness reaches a maximum characteristic of the catalyst concentration.

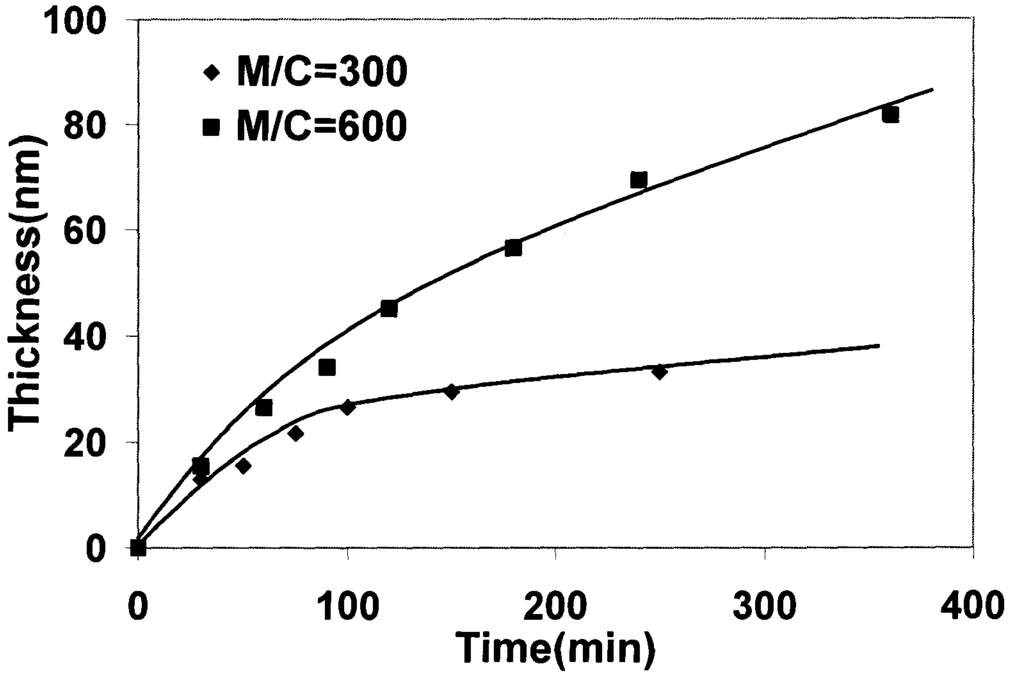

Figure 5.3 PMMA thickness versus polymerization time for different monomer concentrations with added deactivator.

In addition to MMA, we also tried to graft other monomers with different functionalities from the flat nickel surfaces. In a previous paper, we reported the surface-initiated ATRP of the partially fluorinated monomer, TFEMA, from silicon wafers.[22] In this work, the same recipe was used to graft PTFEMA from the flat nickel surfaces. The PTFEMA thickness increased with reaction time as shown in Figure 5.4 although not as rapidly as the PMMA thickness. The advancing and receding water contact angles of the grafted PTFEMA films were 95.3° and 73.9° respectively, which were in consistent with the hydrophobic nature of the PTFEMA polymer. In order to explore the potential of this grafting approach in preparing biocompatible surfaces, two well-known biocompatible polymers, PHEMA and PDMAEMA, were also grafted from the flat nickel surfaces. DMF was selected as the solvent for its good solubility of all experimental components, especially the iron/triphenylphosphine complexes, which helped to provide a homogenous reaction system. For the polymerization of HEMA and DMAEMA, methanol was the most widely used solvent. However, the ligand triphenylphosphine and its complexes with Fe(II) and Fe(III) could not be dissolved very well in methanol. DMF was less polar than methanol; it dissolved the iron/TPP complexes very well and was compatible with HEMA and DMAEMA. As shown in Figure 5.4, both PHEMA and PDMAEMA films had more rapid growth rates than PMMA. After only 4 hours, the PHEMA film had reached 65nm and the PDMAEMA film was 45nm while the thicknesses of PMMA and PTFEMA films after the same time were 30 and 15nm respectively. The advancing and receding water contact angles were 49.8° and 33.9°, respectively, for PHEMA film, and 46.4° and 32.5°, respectively, for PDMAEMA films. These data show that the hydrophilic/hydrophobic nature of the surface could be altered according to the nature of the grafted polymer.

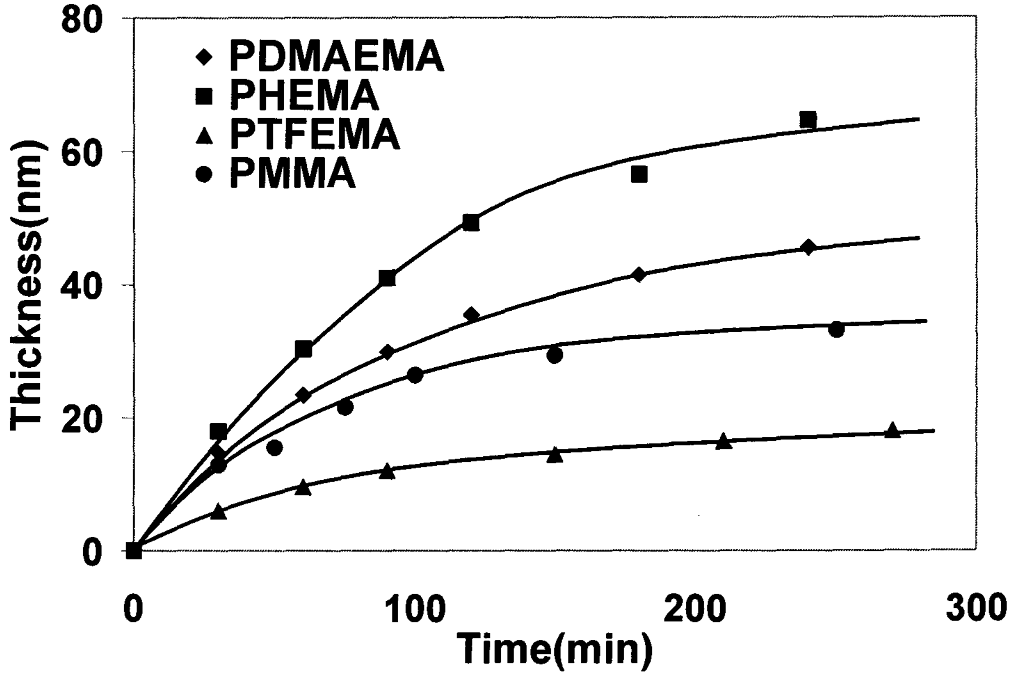

Figure 5.4 Thicknesses versus polymerization time for different polymers with added deactivator.

XPS was employed to study the surface chemical compositions of all the nickel samples (see Figure 5.1 and Table 5.1). The experimental data agreed very well with the theoretical values, which confirmed that all the polymers had been successfully grafted from the nickel surfaces. In particular, we found that the nickel signal decreased to a trace value after the grafting of polymers. That indicated that the nickel surfaces were completely covered by the grafted polymers. The effectiveness of surface-initiated ATRP in preparing high-quality polymer coatings on nickel surfaces was well demonstrated here.

Table 5.1 Surface composition of the nickel samples by XPS using 90° take-off angle.

Sample	C(%)	O(%)	N(%)	Si(%)	Br(%)	F(%)	Ni(%)
Ni-Initiator	61.0	26.9	1.0	0.8	0.8	-	9.5
	(45.2)	(25.8)	(6.5)	(6.5)	(6.5)		
Ni-PMMA	71.3	28.1	-	-	0	-	0.6
	(71.0)	(28.4)					
Ni-PTFEMA	52.0	19.1	-	-	0	25.6	3.3
	(52.7)	(17.6)				(26.4)	
Ni-PDMAEMA	68.9	22.5	8.4	-	0	-	0.3
	(72.5)	(18.1)	(9.1)				
Ni-PHEMA	66.0	31.5	-	-	0	-	2.5
	(65.0)	(32.5)					
Ni-PMMA-*b*-PTFEMA	56.7	18.0	-	-	0	23.8	1.5
	(53.7)	(17.9)				(26.9)	
Ni-PMMA-*b*-PDMAEMA	67.6	21.4	7.9	-	0	-	3.1
	(70.5)	(17.6)	(8.8)				
Ni-PTFEMA-*b*-PMMA	69.4	27.7	-	-	0	0	2.9
	(69.3)	(27.8)				(0)	

a. Data in parenthesis are theoretical values (copper content deducted)

b. Data precision is ~±5%

5.4.3 Surface-initiated ATRP from Cu surfaces.

Working with copper surfaces proved to be more challenging than nickel. During the polishing process, the 50nm alumina nanoparticles were readily embedded inside the relatively soft surface of the copper coupon, resulting in a rougher surface. During ellipsometry measurements, the laser was scattered diffusely from the surface and could not be focused well on the receiver. Consequently, the thicknesses of grafted polymer layers on copper could not be accurately measured by ellipsometry, and the kinetic information relating thickness to monomer conversion, M_n, and reaction time was not accessible. In this situation, the "adding deactivator" method was used to achieve thick polymer films on the copper surfaces, and XPS and contact angle measurements were used to detect the presence of polymers grafted from the copper surfaces.

The same group of monomers were also grafted to the copper surfaces, which were prepared in the same way as the nickel surfaces discussed above. The XPS and contact angle measurements were generally in agreement with those of the corresponding polymers on the nickel surfaces. The single exception was the PMMA-grafted surface, which after 6 hours of polymerization time, gave an anomalously high copper signal in XPS. It was unlikely that the strong copper signal resulted from the penetration of X-ray to the copper surface underlying a thick and continuous PMMA film. The polymer layers grafted by the "adding deactivator" method were thicker than the penetration depth of the XPS X-ray (~10nm). A likely explanation for the strong copper signal in this case could be a discontinuous initiator layer, which in turn resulted in a discontinuous polymer film and exposure of bare copper surface.

The advancing and receding water contact angles of PMMA grafted copper surface were 67.6° and 49.8°, respectively, which are close to the values observed for the PMMA-coated nickel surface. This result confirmed the successful grafting of PMMA. The PTFEMA modified copper surfaces were quite hydrophobic, bearing water contact angles of 101.2° and 78.9°, both were a little higher than their corresponding values for nickel and silicon wafer surfaces. This might be caused by the larger roughness of the copper surfaces. The hydrophilic monomers (HEMA, DMAEMA) were also grafted from the copper surfaces using methanol/water mixture as solvent. Both experiments produced very hydrophilic surfaces. The advancing and receding water contact angles were 54.0° and 36.3° for Cu-PHEMA and 50.2° and30.8° for Cu-PDMAEMA.

Table 5.2 Surface composition of the copper samples by XPS using 90° take-off angle.

Sample	C(%)	O(%)	N(%)	Si(%)	Br(%)	F(%)	Cu(%)
Cu-Initiator	57.6	28.2	0.6	2.1	0.9	-	10.7
	(50.0)	(17.9)	(7.1)	(7.1)	(7.1)		
Cu-PMMA	68.7	25.9	-	-	0.1	-	5.3
	(67.5)	(27.0)					
Cu-PTFEMA	56.3	17.7	-	-	0	24.3	1.7
	(53.6)	(17.9)				(26.8)	
Cu-PDMAEMA	69.8	20.1	7.8	-	0	-	2.3
	(71.0)	(17.8)	(8.9)				
Cu-PMMA-*b*-PTFEMA	55.6	18.4	-	-	0	22.6	3.4
	(52.7)	(17.6)				(26.3)	
Cu-PTFEMA-*b*-PMMA	67.9	27.6	-	-	0	0	4.5
	(68.2)	(27.3)				(0)	

a. Data in parenthesis are theoretical values (copper content deducted)

b. Data precision is ~±5%

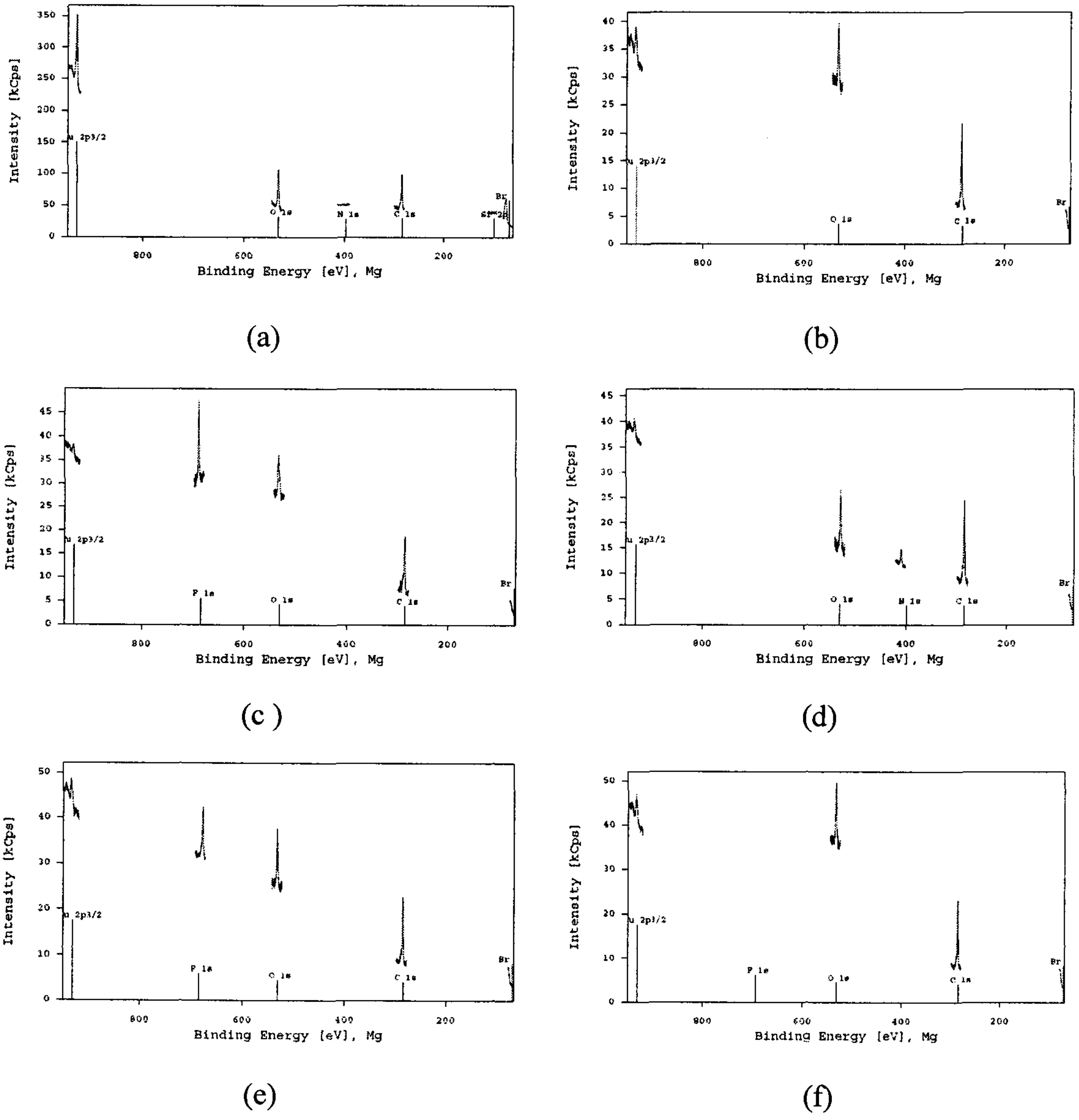

Figure 5.5 XPS survey scans of the copper surfaces with various organic layers at a takeoff angle of 90°: (a) self-assembled initiator; (b) PMMA layer; (c) PTFEMA; (d) PDMAEMA; (e) PMMA-*b*-PTFEMA; (f) PTFEMA-*b*-PMMA.

5.4.4 Block copolymerization from metal surfaces.

The primary advantage of CRP techniques over other polymerization methods is the "living" nature of polymer chain ends. This property can be easily exploited to prepare well designed and structurally coherent block copolymers. Grafting block copolymerization was attempted in this work from both Ni and Cu surfaces.

In one instance, the PMMA brushes grafted from the nickel surfaces were used as macroinitiators and the second block of PTFEMA or PDMAEMA polymer was grafted from the PMMA chain ends. Alternatively, the PTFEMA chain ends were grafted with a second block of PMMA. In order to compare the block grafting efficiency, the thicknesses of the first blocks were very close to each other. Increases of polymer film thicknesses were observed in all the cases (see Table 5.3) and we found that with PMMA as the first block, PDMAEMA grew much faster than PTFEMA. Also, the grafting of PMMA from PTFEMA was a little bit faster than the grafting of PTFEMA from PMMA. All these results were consistent with the homopolymerization kinetics of different monomers from surfaces. The successful chain extension was confirmed by XPS and water contact angle measurements [see Figure 5.1(f), (g), (h), Table 5.1, and Table 5.4].

Table 5.3 Ellipsometric thicknesses of block copolymers on nickel surfaces. (polymerization time for 2nd block is 6 hours)

Substrate	Thickness(nm) (1st block)	Thickness(nm) (2nd block)	Thickness(nm) (Total)
Ni-PMMA	12.91	7.81(PTFEMA)	20.72
Ni-PMMA	13.37	14.18(PDMAEMA)	27.55
Ni-PTFEMA	12.01	9.14(PMMA)	21.15

Table 5.4 Water contact angles of nickel samples at room temperature.

Sample	$\theta_{\text{advancing}}$	θ_{receding}
Ni	36.4°	23.5°
Ni-Initiator	70.3°	41.9°
Ni-PMMA	66.4°	48.3°
Ni-PTFEMA	95.3°	73.9°
Ni-PDMAEMA	46.4°	32.5°
Ni-PHEMA	50.2°	30.8°
Ni-PMMA-*b*-PTFEMA	97.9°	70.1°
Ni-PMMA-*b*-PDMAEMA	48.5°	34.0°
Ni-PTFEMA-*b*-PMMA	69.5°	42.3°

a. The advancing, receding contact angles were an average of six samplings across the sample. The standard deviation of contact angles was less than 2°.

The grafting block copolymerization was also successful with the copper surfaces. As shown in the XPS survey spectra of Cu-PMMA-*b*-PTFEMA [Figure 5.5(e)], the appearance of the F_{1s} peak indicated that PTFEMA had been grafted from the PMMA chain ends. The advancing and receding angles of Cu-PMMA-*b*-PTFEMA (98.6° and 69.4°, respectively) are close to the values of a pure PTFEMA surface. When the block sequence was changed to graft PMMA from Cu-PTFEMA substrates, the PTFEMA layer was completely covered by PMMA. The characteristic F_{1s} peak at 687eV totally disappeared from the XPS survey spectra [Figure 5.5(f)]. In addition, both of the carbon and oxygen contents fitted the theoretical PMMA values very well. The result was further confirmed by the water contact angle measurements, as shown in Table 5.5.

Table 5.5 Water contact angles of the copper samples at room temperature.

Sample	$\theta_{\text{advancing}}$	θ_{receding}
Cu	44.6°	31.5°
Cu-Initiator	78.7°	43.1°
Cu-PMMA	67.6°	49.8°
Cu-PTFEMA	101.2°	78.9°
Cu-PDMAEMA	54.0°	36.3°
Cu-PHEMA	50.2°	30.8°
Cu-PMMA-*b*-PTFEMA	98.6°	69.4°
Cu-PTFEMA-*b*-PMMA	70.1°	40.3°

a . The advancing, receding contact angles were an average of six samplings across the sample. The standard deviation of contact angles was less than 2°.

5.4.5 AFM study

AFM was employed to study the surface morphologies of the bare metal surfaces and the same surfaces coated with grafted polymers. Before all the measurements, the samples were extensively sonicated in corresponding good solvents of the polymers and then dried in a flow of argon gas. Figure 5.6(a) and (b) shows the AFM image of just-polished and initiator-modified nickel surfaces, respectively. The polished nickel surface was very smooth, with an RMS roughness of 0.54nm. The initiator layer on nickel surfaces was also very smooth. The RMS was 0.79nm, which proved that the triethoxysilane groups were very effective in constructing a high quality initiator layer on nickel surface. The AFM images of grafted polymer layers on nickel substrates were shown in Figure 5.6(c), (d) and (e), respectively. The thicknesses of all the polymer layers were: Ni-PMMA(15.51nm), Ni-PTFEMA(16.47nm), Ni-PDMAEMA(14.73nm), all around 15nm. From these images, we found that the surface stayed smooth after the grafting of PMMA and PTFEMA. The RMS roughness was 0.92nm for Ni-PMMA and 0.64nm for Ni-PTFEMA. These findings are strikingly different from those reported by Jérôme's group,[11,12] in which the polymer grafting always resulted in an increase in the surface roughness. One explanation for this difference might be in the different types and immobilization methods of the initiators. Jérôme's group employed a "macroinitiator" approach in their works where single polymer molecules with many initiator moieties were initially grafted to the surface; polymers were then grafted from the initiating side groups of the macroinitiators. The lack of directional control over the grafts grown by this method might account for the resultant rough surface. In the present case, the high quality of the monolayer of initiators attached to the nickel surface promotes the unidirectional growth of polymer brushes from the surface. A second possible cause could be the use of different polymerization catalysts. The Grubbs catalyst and $NiBr_2(PPh_3)_2$ used in Jérôme's work exhibited poor control of the polymerization, resulting in different chain lengths and an uneven polymer brushes with polydispersities 1.5-7.0. Kinetic studies of the iron catalyst used in the present work show that this catalyst mediated the polymerization very well. Linear relationship of $\ln([M]_0/[M])$ with reaction time was found and the polydispersities were lower than 1.30. As a result, the chain lengths of the grafted polymers were much more uniform than in Jérôme's work. In contrast to Ni-PMMA and Ni-PTFEMA, the surface roughness increased after the grafting of PDMAEMA, yielding an RMS roughness of 3.02nm. Although the increase of roughness here may be attributed to the increase in polydispersity with a rapid PDMAEMA growth, a more likely cause is the aggregation of hydrophilic PDMAEMA chains during drying.

Surface morphologies of bare and coated copper samples were also studied by AFM. The AFM image of polished copper surface is shown in Figure 5.6(f). The polished copper surface, with an RMS roughness of 2.87nm, was not as smooth as the polished nickel surface. The higher roughness is attributed to the presence of many small particles on the surface. The diameter of these particles is around 50nm. These findings were consistent with earlier comments that alumina nanoparticles in the polishing agent are easily embedded in the soft surface of the copper coupons. These particles could not even be removed by very intense ultrasonic cleaning. A similar observation was made in a case where cold rolled steel was polished with 800mesh Emery paper.[23,24] Even though the steel is much harder than copper, the results from scanning electron microscopy, quantometer (SEMQ) and Mössbauer spectroscopy revealed the presence of many micrometer-sized particles which had been transferred from the Emery paper and embedded in the surface. Figure 5.6(g) shows the AFM image of the Cu-PDMAEMA surface. After the grafting polymerization, the RMS surface roughness increased from 2.87 to 10.92nm. This increase can be attributed to chain aggregation, as in the case of Ni-PDMAEMA, and to presence of many of small extrusions and some large holes on the surface, which are clearly visible in the AFM image. The small extrusions are believed to result from polymer brushes grafted from alumina nanoparticles, which in turn resulted from attachment of the silane initiator to the alumina nanoparticle surfaces. The holes correspond to areas where polymer grafting did not occur. A likely cause of this is the localized surface contamination that prevented bonding of the initiator to the surface. Regardless of the cause, it is clear that optimization of the polishing process is necessary in order to improve the ability to graft polymers to copper surfaces.

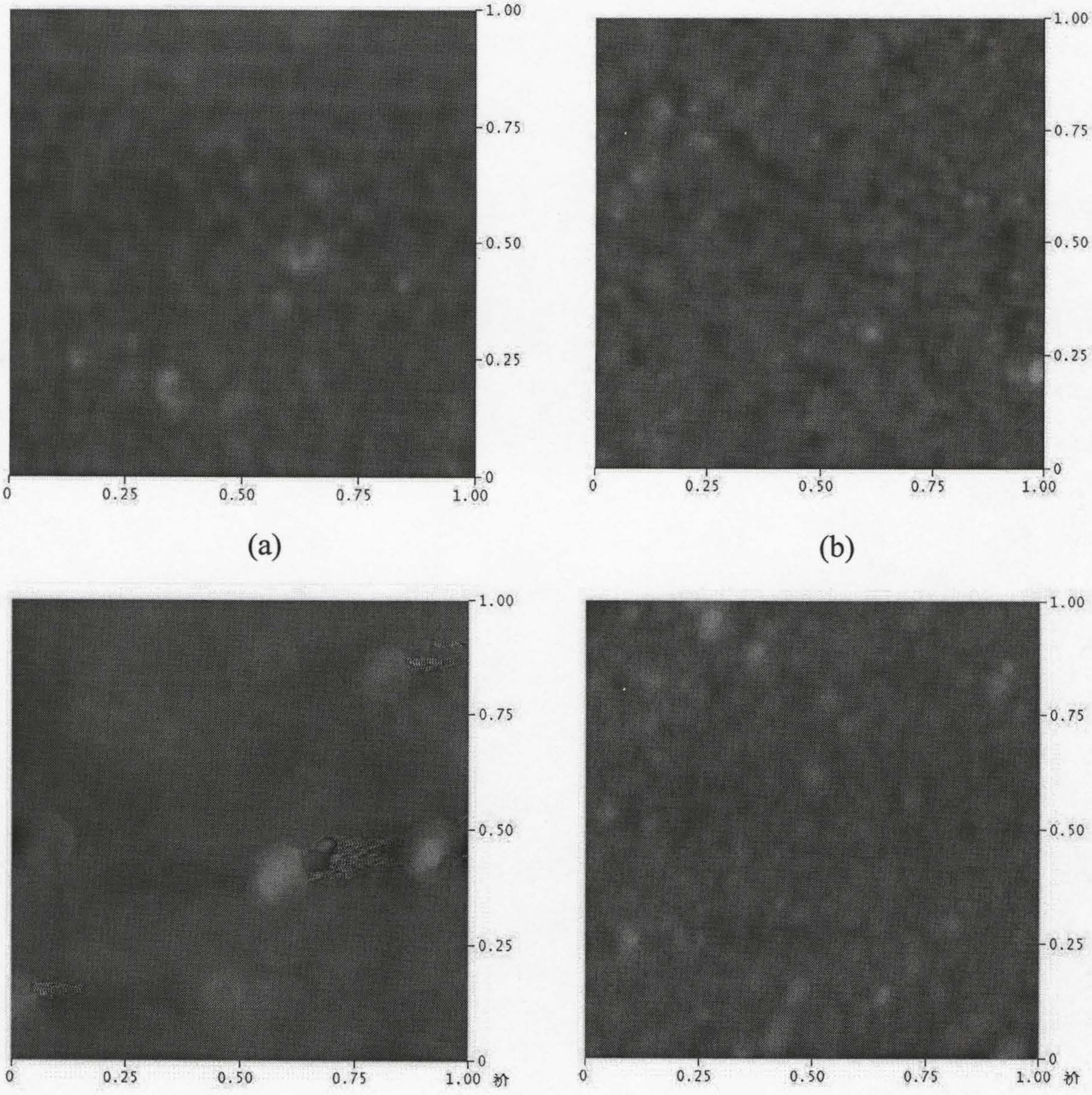

(a) (b)

(c) (d)

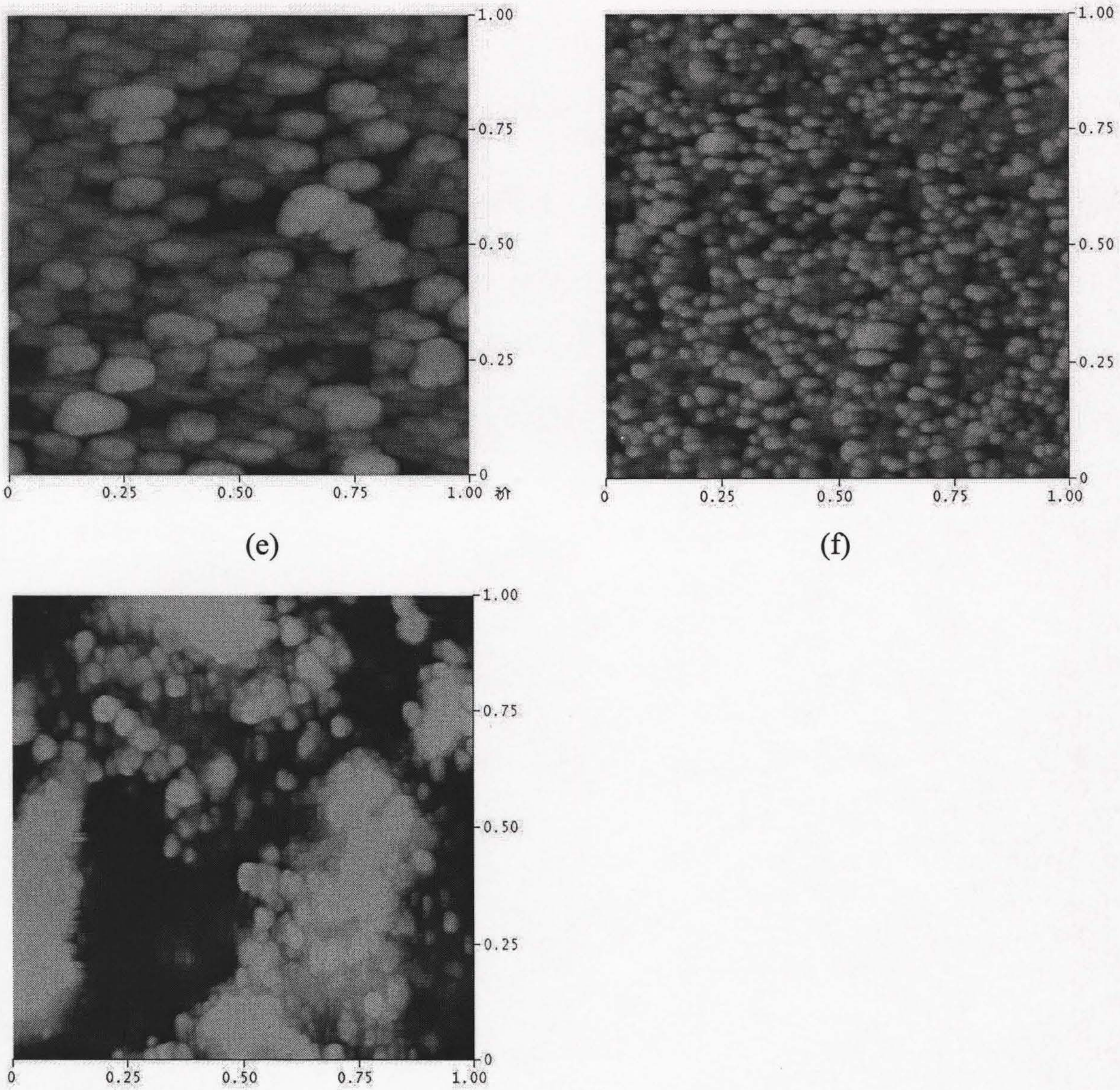

(e)

(f)

(g)

Figure 5.6 AFM images: (a) polished nickel substrate(after sonication in THF); (b) nickel substrate with initiator layer(after sonication in THF); (c) nickel substrate with grafted PMMA layer(after sonication in THF); (d) nickel substrate with grafted PTFEMA layer(after sonication in α,α,α-trifluorotoluene); (e) nickel substrate with grafted PDMAEMA layer(after sonication in methanol); (f) polished copper substrate(after sonication in THF); (g) copper substrate with grafted PDMAEMA layer (after sonication in methanol). Z-scale for all images is 25nm.

5.5 Surface modification of nitinol by surface-initiated ATRP

5.5.1 Introduction of nitinol

Nitinol (NiTi) is a nickel-titanium alloy which was first discovered in 1962.[25] Above its transformation temperature, It is a shape memory alloy and its crystal structure can change between martensite and austenite structures based on the temperature. When the temperature is lower than its transformation temperature (<70°C), nitinol has a martensite structure and it displays the shape memory effect. It will remain in deformed shape until the temperature goes higher than the transformation temperature, at which time it will return to its original shape. At high temperature, nitinol will change to austenite structure. It is able to withstand a small amount of deformation when a load is applied and return to its original shape when the load is removed. This is another very important property of nitinol: superelasticity. Because of the aforementioned unique mechanical properties, nitinol has great potential to be used as artificial body parts. However, 50% of the nitinol surface is covered by the native nickel oxide (NiO), which is very likely to be dissolved in the human body. As a result, an ongoing concern with nitinol is the release of nickel ions into the body through corrosion, which may cause allergic, toxic and carcinogenic effects. In order to solve this problem, several surface treatment techniques were employed to decrease the nickel content on the nitinol surface, such as electropolishing, [26] plasma treatment[26, 27, 28] and chemical etching.[26] Stable and strongly bound self-assembled monolayers (SAMs) of phosphonic acids were also formed on the nitinol surface to prevent the corrosion.[29] In this work, for the first time, we applied the surface-initiated ATRP technique to the modification of nitinol surfaces. Two well-known biocompatible polymers, PDMAEMA and POEGMA were successfully grafted from nitinol surfaces. The reaction kinetics were studied in details and the morphology change was studied by AFM.

5.5.2 Pre-treatment of nitinol

Nitinol foils (austenite phase, 51% nickel/49% titanium; 0.008"thickness, > 99.0% purity) were purchased from Johnson Matthey, Inc. They are cut into 1 × 1cm^2 coupons, polished on one side using a Strüers RotoPol-31/RotoForce-4/Multidoser automatic polisher to give a mirror-like appearance. The polishing sequence was: 220, 320, 400, 800, 1200grits emery paper, and finally 1μm diamond suspension. The polished coupons were rinsed with acetone and methanol and cleaned by ultrasonication in acetone for 1h. They were then rinsed with acetone and stored in the oven at 90°C for 30min. Finally, these coupons were rinsed again and stored in vacuum.

5.5.3 Surface-initiated ATRP from nitinol

For the nitinol surface is composed of nickel oxide (NiO) and titanium oxide (TiO_2), the triethoxysilane-based ATRP initiator used to modify nickel surfaces was also used here. The same procedure was employed to immobilize the initiator onto nitinol surfaces and to graft polymers from the immobilized initiators. Both of "adding free initiator" and "adding deactivator" strategy approaches were to control the polymerization from nitinol surfaces. In the added free initiator case, we run polymerization at two different targeted degrees of polymerization (DP), one is 100 and the other is 200. Figure 5.7(a),(b) showed the thickness growth versus monomer conversion of PDMAEMA and POEGMA, respectively. For both polymers, a linear relationship between thickness and monomer conversion was observed, which suggested that the polymerization was well controlled with added free initiator. We can use the formula $\Gamma=d\rho/M_n$ to estimate the grafting density. For PDMAEMA, the grafting density was calculated to be 0.38chains/nm^2 for DP=100 and 0.41chains/nm^2 for DP=200. For

POEGMA, the grafting density was 0.32chains/nm^2 for DP=100 and 0.31chains/nm^2 for DP=200. The lower grafting density of POEGMA is due to the large size of oligo(ethyl glycol) side groups, which exerted a steric hinderance effect on the grafting polymerization.

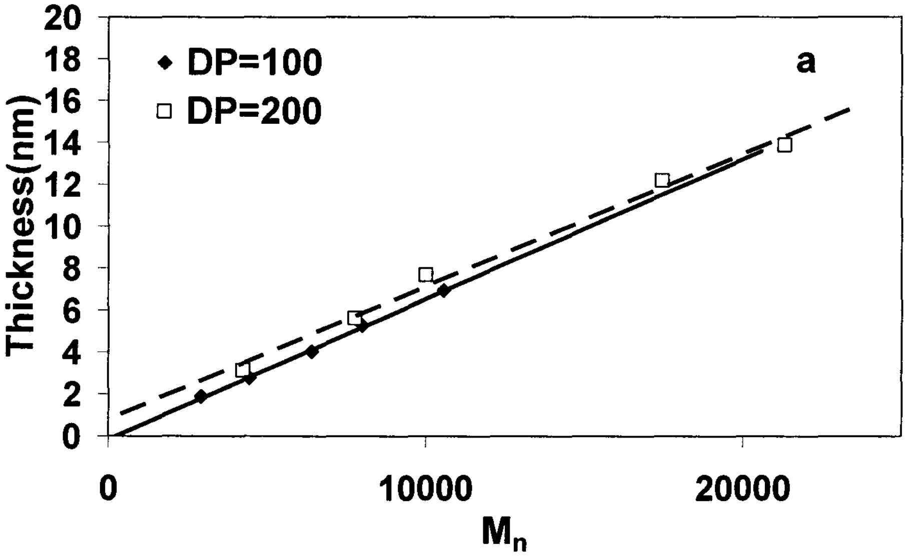

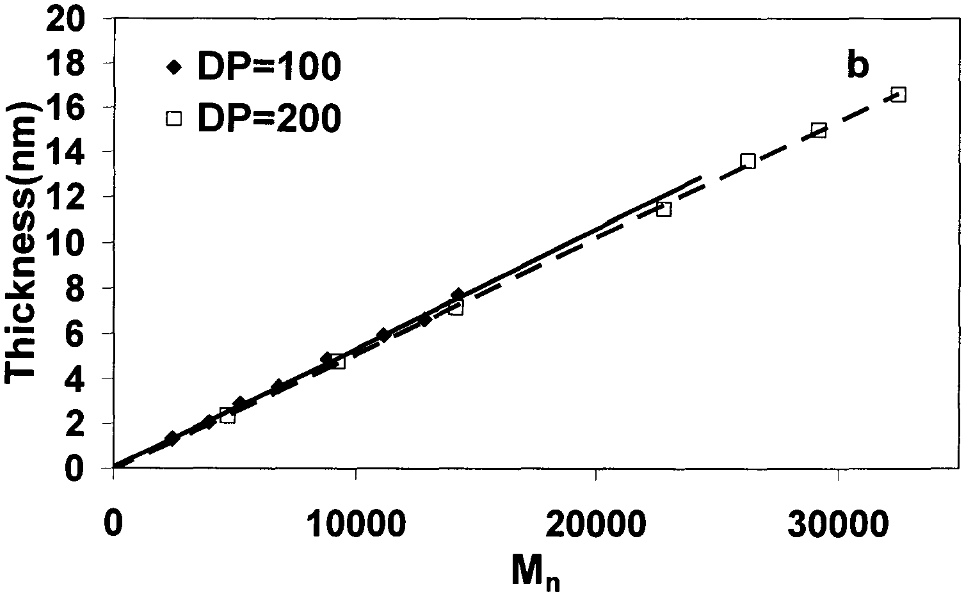

Figure 5.7 Thickness of (a) PDMAEMA, (b) POEGMA layer versus molecular weight of "free" polymer with added "free" initiator.

The "adding free initiator" method can only produce polymer film about 20 nm thick. In order to achieve thicker polymer films, the "added deactivator" approach was also used in this study. Two [monomer]/[catalyst] ratio were used here. One is 100 and the other is 200. As shown in Figure 5.8, for both polymers, at the same reaction time, increasing [monomer]/[catalyst] ratios (lower catalyst concentration) resulted in thicker polymer films. About 80nm thick of PDMAEMA film and more than 80nm thick of POEGMA film were achieved after 6 hours of reaction.

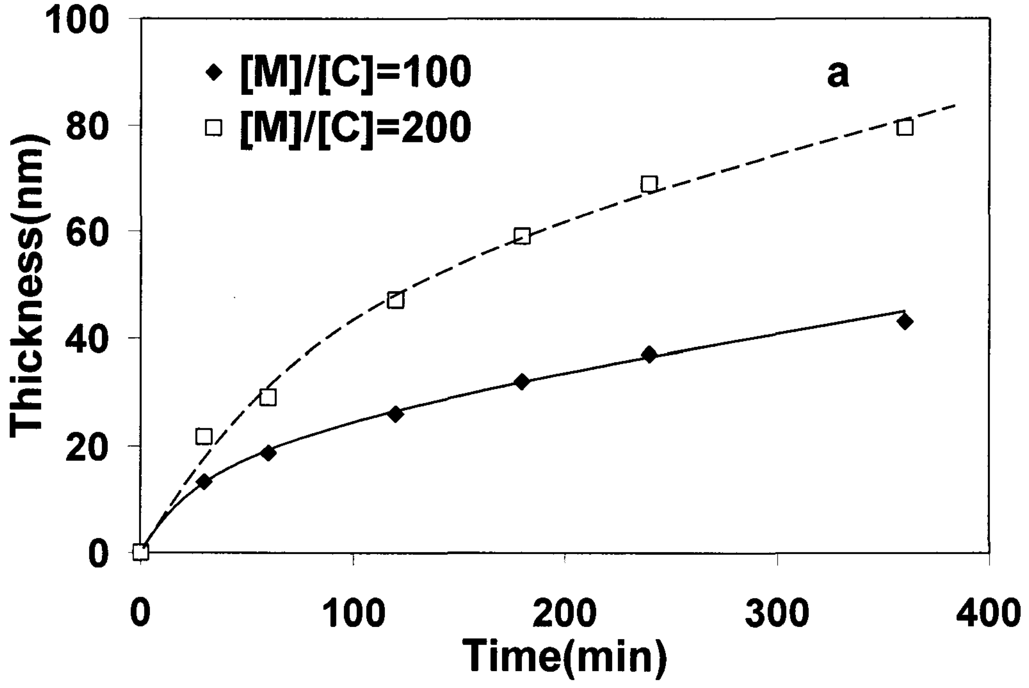

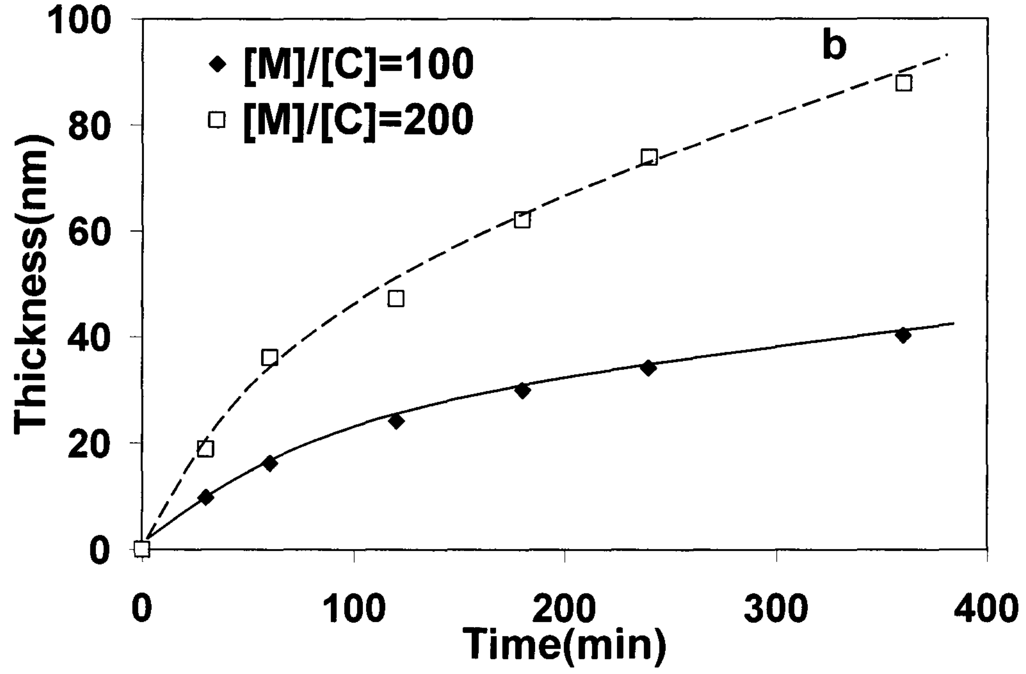

Figure 5.8 Thickness of (a) PDMAEMA, (b) POEGMA layer versus reaction time.

Table 5.6 reports the water contact angle data. The just polished nitinol surface was pretty hydrophilic. The advancing and receding contact angles were about 37.5° and 24.8°, respectively. After the initiator immobilization, the nitinol surface was turned to hydrophobic. The advancing and receding contact angles were about 69.4° and 54.6°, respectively. After the grafting of PDMAEMA and POEGMA, the nitinol surface turned back to be hydrophilic again. For NiTi-PDMAEMA, the advancing and receding contact angles were about 47.9° and 31.5° and for NiTi-POEGMA, the advancing and receding contact angles were about 48.6° and 34.1°. These contact angle values confirmed the successful grafting of polymers from nitinol surface.

Table 5.6 Water contact angles of the nitinol samples at room temperature.

Sample	$\theta_{\text{advancing}}$	θ_{receding}
NiTi	37.5°	24.8°
NiTi-Initiator	69.4°	54.6°
NiTi-PDMAEMA	47.9°	31.5°
NiTi-POEGMA	48.6°	34.1°

a . The advancing, receding contact angles were an average of six samplings across the sample. The standard deviation of contact angles was less than 2°.

5.5.4 AFM study

The surface morphologies were studied by AFM. Before all measurements, the samples were extensively sonicated in appropriate solvents and then dried in a flow of argon gas. Figure 5.9(a) and (b) shows the AFM image of just-polished and initiator-modified nitinol surfaces, respectively. Both of the polished and initiator-modified nitinol surfaces were very smooth, with RMS roughnesses of 0.85nm and 0.92nm, respectively. Figure 5.9(c) and (d) show the AFM images of grafted

PDMAEMA and POEGMA films on nitinol substrates, respectively. The thicknesses of the polymer layers were: PDMAEMA(47.19nm), POEGMA(40.28nm). We found that the nitinol surface roughness increased pretty much after the grafting of PDMAEMA, yielding an RMS roughness of 2.03nm. As discussed before, the increase of roughness is probably caused by the aggregation of hydrophilic PDMAEMA chains during drying. For NiTi-POEGMA, the RMS roughness did not change that much and was 1.09nm. Although POEGMA is also hydrophilic, the larger oligo(ethylene glycol) side chains may construct steric hindrance to prevent the polymer chains from aggregation during drying.

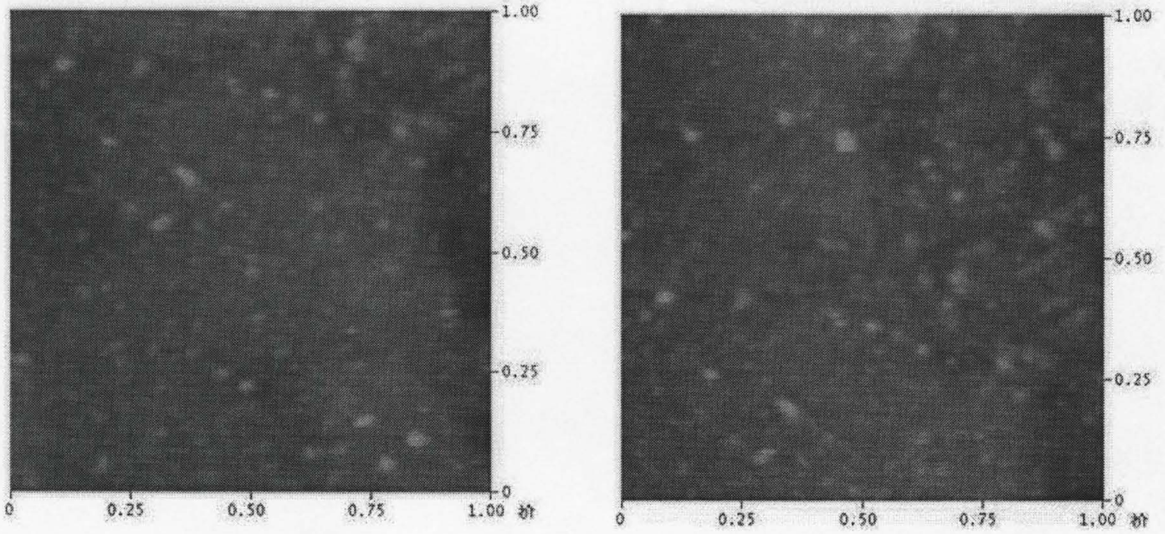

(a) (b)

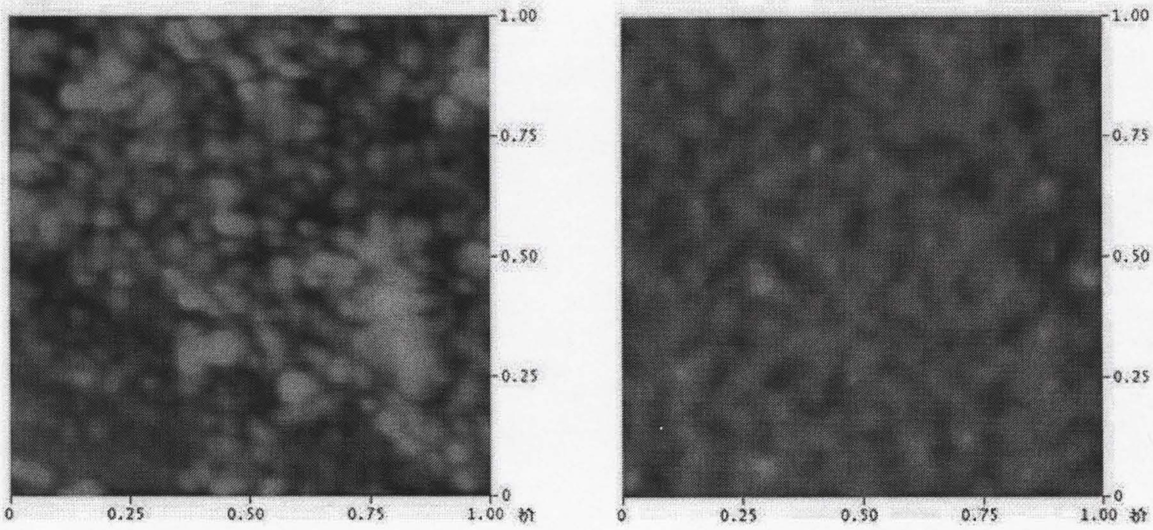

(c)

(d)

Figure 5.9 AFM images: (a) polished nitinol substrate(after sonication in acetone); (b) nitinol substrate with initiator layer(after sonication in acetone); (c) nitinol substrate with grafted PDMAEMA layer(after sonication in methanol); (d) nitinol substrate with grafted POEGMA layer(after sonication in methanol); Z-scale for all images is 25nm.

5.6 Conclusions

Acrylic polymers, including PMMA, hydrophobic PTFEMA, and hydrophilic PDMAEMA and PHEMA were grafted from flat nickel and copper surfaces by surface-initiated ATRP. Kinetic studies showed that the grafting polymerizations from flat nickel surfaces were very well controlled. The grafted polymer chain ends were still "living" and block copolymer brushes with different block sequences were successfully prepared. XPS results revealed that the surface chemical compositions of all grafted polymer layers were in good agreement with theoretical predictions. XPS of coated nickel surfaces confirmed complete coverage by the grafted polymers. Water contact angle measurements were used to monitor changes in surface hydrophobicity characteristic of the different type of grafted polymers. Surface morphology was measured by AFM. Bare polished nickel surfaces were very smooth but RMS roughness decreased after the polymer grafting. Bare polished copper surfaces had a high RMS roughness, presumably due to entrapment of alumina nanoparticles (from the polishing emulsion) in the soft copper surface during the polishing process. This roughness was maintained after the grafting of polymers. This work proved that surface-initiated ATRP was a very simple and effective method to prepare high quality polymer coatings on flat metal substrates. These polymer coatings were covalently bonded to the metal substrate, so that they can offer very strong adhesion. Moreover, the functionalities of polymer coatings can be easily tuned by using different types of monomers. The surface-initiated ATRP technique was successfully extended to the modification of a shape-memory-alloy nitinol (NiTi). Two biocompatible polymers, PDMAEMA and POEGMA were successfully grafted from nitinol surfaces.

5.7 References

(1) Husseman, M.; Malmstrom, E. E.; McNamara, M.; Mate, M.; Mecerreyes, D.; Benoit, D. G.; Hedrick, J. L.; Mansky, P.; Huang, E.; Russell, T. P.; Hawker, C. J. *Macromolecules,* 1999, *32*, 1424.

(2) Baum, M.; Brittain, W. J. *Macromolecules* 2002, *35*, 610.

(3) Matyjaszewski, K.; Xia, J. *Chem. Rev.* 2001, *101*, 2921.

(4) Matyjaszewski, K.; Miller, P. J.; Shukla, N.; Immaraporn, B.; Gelman, A.; Luokala, B. B.; Siclovan, T. M.; Kickelbick, G.; Vallant, T.; Hoffmann, H.; Pakula, T. *Macromolecules* 1999, *32*, 8716.

(5) Ejaz, M.; Yamamoto, S.; Ohno, K.; Tsujii, Y.; Fukuda, T. *Macromolecules* 1998, *31*, 5934.

(6) Huang, W. X.; Kim, J.-B. ; Bruening, M. L.; Baker, G. L. *Macromolecules* 2002, *35*, 1175.

(7) Pyun, J.; Jia, S.; Kowalewski, T.; Patterson, G. D.; Matyjaszewski, K. *Macromolecules* 2003, *36*, 5094.

(8) Ohno, K.; Koh, K.; Tsujii, Y.; Fukuda, T. *Angew. Chem., Int. Ed.* 2003, *42*,2751.

(9) Chen, Y.W.; Liu, D.L.; Deng, Q. L. *J. Polym. Sci. Part A: Polym. Chem.* 2006, *11*, 3434.

(10) Qin, S.; Qin, D.; Ford, W. T.; Resasco, D. E.; Herrera, J. E. *J. Am. Chem. Soc.* 2004,

126, 170.

(11) Claes, M ; Voccia, S.; Detrembleur, C.; Jérôme, C.; Gilbert, B.; Leclère, P.; Geskin, V. M.; Gouttebaron, R.; Hecq, M.; Lazzaroni, R.; Jérôme, R. *Macromolecules* 2003, *36*, 5926.

(12) Ignatova, M ; Voccia, S.; Gilbert, B.; Markova, N.; Cossement, D.; Gouttebaron, R.; Jérôme, R.; Jérôme, C. *Langmuir* 2006, *22*, 255.

(13) Fan, X. W.; Li, L. J.; Dalsin, J. L.; Messersmith, P. B. *J. Am. Chem. Soc.* 2005, *127*, 15843.

(14) Sun, Y. B.; Ding, X. B.; Zheng, Z. H.; Cheng, X.; Hu, X. H.; Peng, Y. X. *Eur. Polym. J.* 2007, *43*, 762.

(15) Zucchi, F.; Grassi, V.; Frigani, A.; Trabanelli, G. *Corros. Sci.* 2004, *46*, 2853.

(16) Flis, J.; Kanoza, M. *Electrochim. Acta* 2006, *51*, 2338.

(17) Kong, X. X.; Kawai, T.; Abe, J.; Iyoda, T. *Macromolecules* 2001, *34*, 1837.

(18) Ohno, K.; Moringa, T.; Koh, K.; Tsujii, Y.; Fukuda, T. *Macromolecules* 2005, *38*, 2137.

(19) Vallant, T.; Brunner, H.; Mayer. U.; Hoffmann, H.; Leitner, T.; Resch, R.; Friedbacher, G. *J. Phys. Chem. B* 1998, *102*, 7190.

(20) Eaton, P. J. ; Graham, P.; Smith, J. R.; Smart, J. D.; Nevell, T. G.; Tsibouklis, J. *Langmuir* 2000, *16*, 7887.

(21) Kim, J-B.; Huang, W.; Miller, M. D.; Baker, G. L.; Bruening, M. L. *J. Polym. Sci. Part A: Polym. Chem.* 2003, *41*, 386.

(22) Chen, R.X; Feng, W.; Zhu, S. P.; Botton, G.; Ong, B.; Wu, Y. L. *J. Polym. Sci. Part A: Polym. Chem.* 2006, *44*, 1252.

(23) Reinhard, G.; *Prog. Org. Coat.* 1987, *15*, 125.

(24) Buser, K.R. *J. Coat. Technol.* 1982, *54*, 29.

(25) "The Alloy That Remembers" *Time* 1968-09-13.

(26) Trigwell, S.; Hayden, R. D.; Nelson, K. F.; Selvaduray, G. *Surf. Interface. Anal.* 1998, *26*, 483.

(27) Cheng, Y.; Zhang, Y. F. *Mater. Lett.* 2006, *60*, 2243.

(28) Shevchenko, N.; Pham, M. T.; Maitz, M. F. *Appl. Surf. Sci.* 2004, *235*, 126.

(29) Quinones, R.; Gawalt, E. S. *Langmuir* 2007, *23*, 10123.

CHAPTER 6

Chapter Preparation of Ni-*g*-Polymer Core-Shell Nanoparticles by Surface-initiated Atom Transfer Radical Polymerization

This chapter is organized based on the article submitted to *Polymer* Chen RX, Maclaughlin, S., Botton, G.A., Zhu, S.P. May 21, 2009

6.1 Abstract

Surface-initiated atom transfer radical polymerization (Si-ATRP) technique was successfully employed to modify Ni nanoparticles with polymer shells. ATRP initiators were covalently bonded onto Ni nanoparticle surfaces by a combination of ligand exchange and condensation reactions. Various kinds of polymers including poly(methyl methacrylate) (PMMA), poly(*n*-isopropylacrylamide) (PNIPAM), polystyrene (PSt) and poly(*N,N'*-dimethylaminoethyl methacrylate) (PDMAEMA) were grafted from the immobilized initiators. The grated polymer shells gave Ni nanoparticles exceptionally good dispersion and stability in solvents. Fourier transform infrared (FT-IR) spectroscopy, thermogravimetric analysis (TGA) and transmission electron spectroscopy

(TEM) were employed to confirm the grafting and to characterize the nanoparticle core-shell structure. Gel permeation chromatography (GPC) studies of cleaved polymer chains revealed that the grafting polymerization was well controlled. The magnetic properties of Ni-*g*-polymer nanoparticles were also studied.

6.2 Introduction

In recent years, because of the unique magnetic properties of nanocrystalline metallic nanoparticles such as Fe, Co and Ni, considerable attention has been devoted to the synthesis of these materials. In particular, Ni nanoparticles have received great interest for their potential applications in many diverse fields, including magnetic recording media, biomedical materials, catalysis, and electro-conductive materials. Numerous different physical and chemical preparative routes have been developed to synthesize Ni nanoparticles, such as pyrolysis,[1] sputtering,[2] microemulsion,[3,4] aqueous[5,6] and nonaqueous[7,8,9] chemical reduction, sonochemical deposition,[10] and polyol methods.[11]

Because of the anisotropic dipolar attraction, Ni nanoparticles have strong tendency to aggregate into large clusters, thus lose their specific magnetic properties associated with the single-domain nanostructures. This greatly limits uses of Ni nanoparticles in various applications. In order to overcome this problem, it is essential to do some modification work on Ni nanoparticle surface to prevent aggregation. In most preparation methods of Ni nanoparticles, capping agents like long chain alkyl acids, amines and phosphates were always applied to control growth of nanoparticles; and at the same time, to prevent them from aggregation.

Compared to small molecular capping agents, polymeric shells have their unique advantages. Because of flexibility in control of polymer composition and functionality, polymer shells are not only able to protect nanoparticles from aggregation, but also readily endow nanoparticles with interesting functionalities. Among many approaches for coating nanoparticles with polymer shells, surface-initiated polymerization techniques have recently become very popular choices, especially surface-initiated atom transfer radical polymerization (si-ATRP). By this method, polymer chains are *in-situ* grafted from initiator molecules previously immobilized onto nanoparticle surfaces. The most significant advantage of this "grafting from" method is its ability to produce dense polymer brushes, with grafting densities ranged from 0.1 to 0.7chains/nm^2. Moreover, ATRP is a well-established controlled radical polymerization technique and can offer good control over polymer molecular weight, and thus polymeric shell thickness, allowing preparation of polymer shells with low polydispersities.

Although Si-ATRP has been employed to graft polymers from various nanoparticles, such as SiO_2,[12,13] Au,[14] $MnFe_2O_4$,[15] etc, no successful experiments have been reported on modification of nanocrystalline metallic nanoparticles. Unlike other types of materials, metal surfaces are highly reactive in electrochemical and acid/base reactions that complicate ATRP reactions. Red-ox deactivation of ATRP catalyst is a particular risk. In our previous study,[16] using triethoxysilane-based initiator and iron catalyst, we succeeded in grafting polymer brushes from flat Ni and Cu surfaces. In this paper, we report the first successful study on surface modification of pristine Ni nanoparticles by Si-ATRP. A combination of ligand exchange and condensation reaction was employed to covalently immobilize triethoxysilane-based ATRP initiators onto Ni nanoparticle surface. Various types of polymers, like poly(methyl methacrylate) (PMMA), poly(*n*-isopropylacrylamide) (PNIPAM), polystyrene (PSt) and poly(*N,N'*-dimethylaminoethyl methacrylate) (PDMAEMA) were grafted *in situ* from the immobilized initiators. After polymer grafting, both dispersion and stability of the Ni nanoparticles in solvents were greatly improved. The grafted polymer shells were very effective to prevent the Ni nanoparticles from aggregation. The improved dispersion and stability, as well as good compatibility with polymer matrices, are of great benefit to preparation of high quality Ni nanoparticle/polymer composite materials.

6.3 Experimental

6.3.1 Materials

nickel acetylacetonate [Ni(acac)$_2$] (95%), hexadecylamine (HDA) (98%), trioctylphosphine oxide (TPPO) (99%), sodium borohydride (99%), *o*-dichlorobenzene (anhydrous, 99%), acetic acid (≥99.7%), 3-aminopropyltriethoxysilane (99%), 2-bromoisobutyryl bromide (98%), triethylamine (>99%), iron(II) bromide (98%), iron(III) bromide(98%), triphenylphosphine (TPP) (99%), toluene (anhydrous,99.8%), *N,N*-dimethylformamide (DMF) (anhydrous, 99.8%), *n*-isopropylacrylamide (NIPAM) (97%) were purchased from Aldrich and were used as received. Methyl methacrylate (MMA) (99%), styrene (St) (≥99%), *N,N*-dimethylaminoethyl methacrylate (DMAEMA) (98%) were purchased from Aldrich and distilled over CaH_2 under vacuum, then stored at -15°C before use. Ethanol (anhydrous), hexane (reagent), chloroform (reagent), dichloromethane (reagent), ethyl acetate (reagent), tetrahydrofuran (THF) (HPLC) and hydrochloric acid solution (37%) were obtained from Caledon Laboratories Ltd. and used as received. Deionized (DI) water with a resistivity of 18MΩ·cm was prepared from a Millipore Milli-Q filtration system. Ultra-high-purity-grade argon was used in this study.

6.3.2 Synthesis of Ni nanoparticles

Ni nanoparticles were synthesized following the published procedure.[17] The synthesis was conducted using a standard airless technology. 0.2g of Ni(acac)$_2$ was dissolved in 5ml *o*-dichlorobenzene at 100°C, and the solution was quickly injected into a mixture containing 40ml dichlorobenzene, 1.5g TOPO, 1.5g HAD, and 0.15g sodium borohydride at 140°C during vigorously stirring. The mixture was quickly heated to 180°C and stirred for 30min under Ar atmosphere. It was then cooled to room temperature. 100ml ethanol was added to precipitate Ni nanoparticles. The nanoparticles were separated by centrifugation (3500rpm, 1h) and dried in vacuum. The dried nanoparticles were re-dispersed into toluene and re-precipitated in ethanol. The cycle was repeated for three times to remove excess ligands. Finally, Ni nanoparticles were dispersed in toluene with a concentration of 10mg/ml.

6.3.3 Immobilization of initiators

The surface-attachable initiator was synthesized following the same procedure as in our previous work.[16] The initiator was immobilized onto Ni nanoparticles as follows:

0.25ml initiator, 50μl acetic acid and 50ml toluene based Ni nanoparticle dispersion were mixed in a 100ml round-bottom flask. The mixture was stirred at room temperature for 72h under argon protection. 100ml *n*-hexane was added into the mixture to precipitate the initiator-modified Ni nanoparticles. The nanoparticles were separated by centrifugation (3500rpm, 1h) and dried in vacuum. The dried nanoparticles were re-dispersed into toluene and re-precipitated by *n*-hexane. The wash cycle was repeated for five times to remove excess initiators. Finally, the initiator-modified Ni nanoparticles were dispersed in toluene with a concentration of 10mg/ml.

6.3.4 Surface-initiated ATRP on Ni nanoparticle

The typical procedure for ATRP of MMA from Ni nanoparticle surface is as follows: 64.7mg (0.300mmol) $FeBr_2$, 8.9mg (0.030mmol) $FeBr_3$ and 259.6mg (0.9900mmol) triphenylphosphine were placed into a 25ml flask containing a magnetic stir bar. The flask was deoxygenated through several evacuation/ backfilling cycles of argon. 6.0g (60mmol) MMA and 6.0g initiator-modified Ni nanoparticle dispersion in toluene were purged with Ar for 1h before added into the flask containing iron catalyst via a double-tipped needle. The mixture was stirred intensively, degassed with argon for another 10min, and put into an oil bath of 60°C. After the desired reaction time was reached, the polymerization solution was taken out from the oil bath, diluted with 50ml THF. The Ni-*g*-PMMA nanoparticles were collected by centrifugation (20000rpm, 1h). The nanoparticles were repeatedly rinsed with large amount of THF to remove residual monomer and free polymer. Finally, the samples were dried in vacuum at 50°C for 6h. The polymerization of NIPAM was performed at 40°C in DMF. After the reaction, the polymerization solution was diluted with methanol at a solution/methanol ratio of 1/4. The Ni-*g*-PNIPAM nanoparticles were also collected by centrifugation (20000rpm, 1h), washed intensively with methanol and then dried in vacuum.

6.3.5 Cleavage of PMMA chains from Ni nanoparticles

Grafted PMMA brushes were cleaved from the Ni nanoparticle surfaces with the method described by Matsuno et al.[18] Hydrochloric acid solution was used to dissolve the Ni nanoparticles. PMMA was extracted with chloroform. The chloroform was then removed under vacuum and PMMA was subjected to GPC measurement.

6.3.6 Characterization

Fourier transform infrared analysis was performed on a Bio-Rad FTS-40 FT-IR spectrometer. All samples were prepared as pellets using spectroscopic grade KBr in a Carver press at 15000psi. The spectra were scanned over the range 4000-400cm^{-1} in the transmission mode, accumulating 16 scans at a resolution of 2cm^{-1}. TEM was carried out on a Philips CM-12 transmission electron microscope. The samples were dispersed in appropriate solvents with ultrasonication for 2min and then dropped onto the copper grid to dry. Magnetic studies were carried out using a Quantum Design MPMS SQUID magnetometer at 5K and 298K.

TGA was performed on using a Thermowage STA409, at a scan rate of 10°C/min, up to 800°C in nitrogen atmosphere. The initiator density on nanoparticle surfaces and the grafting densities of polymer chains were calculated from the TGA results according to the following equation:

$$\text{Density (molecules/nm}^2\text{)} = \frac{W \times r \times N_A \times d_{Ni}}{M(1-W)\times 3\times 10^{21}}$$

where W is the weight loss of sample, r is the radius of Ni nanoparticles, N_A is Avogadro's constant, d_{Ni} is the density of nickel (8.90g/cm^3), and M is the polymer molecular weight.

The molecular weights of PMMA were determined by gel permeation chromatography (GPC). A Waters 710 sample auto injector, 3 linear columns in series

(Waters Styragel HR 5E, 2 Shodex KF-804L), a Waters 600 pump system and a 410 refractive index (RI) detector were used for the assays. The eluent (THF) was pumped through the system at a fixed flow rate of 1ml/min. The columns and detector were heated to 30°C and 35°C, respectively. Narrow polystyrene samples were used as standards to generate the calibration curve. Data were recorded and manipulated using the Waters Millennium software package.

6.4 Result and discussion

6.4.1 Immobilization of initiators on Ni nanoparticles

Ligand exchange reaction is an effective way to modify nanoparticle surface with ATRP initiators. For metal oxide nanoparticles, carboxylic acid-based initiators are often used to replace the ligands on nanoparticle surfaces, followed by *in-situ* polymerization. However, this method has a drawback. The carboxylate bond between polymer chain and nanoparticle surface is not strong enough to achieve a stable linkage. The polymer chains are readily dissociated from the nanoparticle surface through dynamic exchange with other competing ligands. Trialkoxysilane-containing ATRP initiators have already been proven effective for surface-initiated ATRP from many different substrates,[16,19,20] including flat copper and nickel surfaces in our previous studies. The trialkoxysilane-type initiators can be immobilized onto metal surfaces with stable metal-O-Si bonds. The reaction is mild and does not present a risk of corrosion damage of reactive metal surfaces. Inspired by these advantages, we tried the same triethoxysilane-containing initiator in this work. A catalyst, such as acetic acid, was required in the initiator immobilization process. It can react with replaced amine ligand to accelerate the ligand exchange reaction. It could also accelerate the hydrolyzation of Si-$(OC_2H_5)_3$ groups to Si-$(OH)_3$ groups. The Si-$(OH)_3$ groups form hydrogen bonds with hydroxyl groups on metal surfaces, followed by condensation reactions to produce a very dense initiator layer covalently bonded to the metal surface by metal-O-Si bonds.

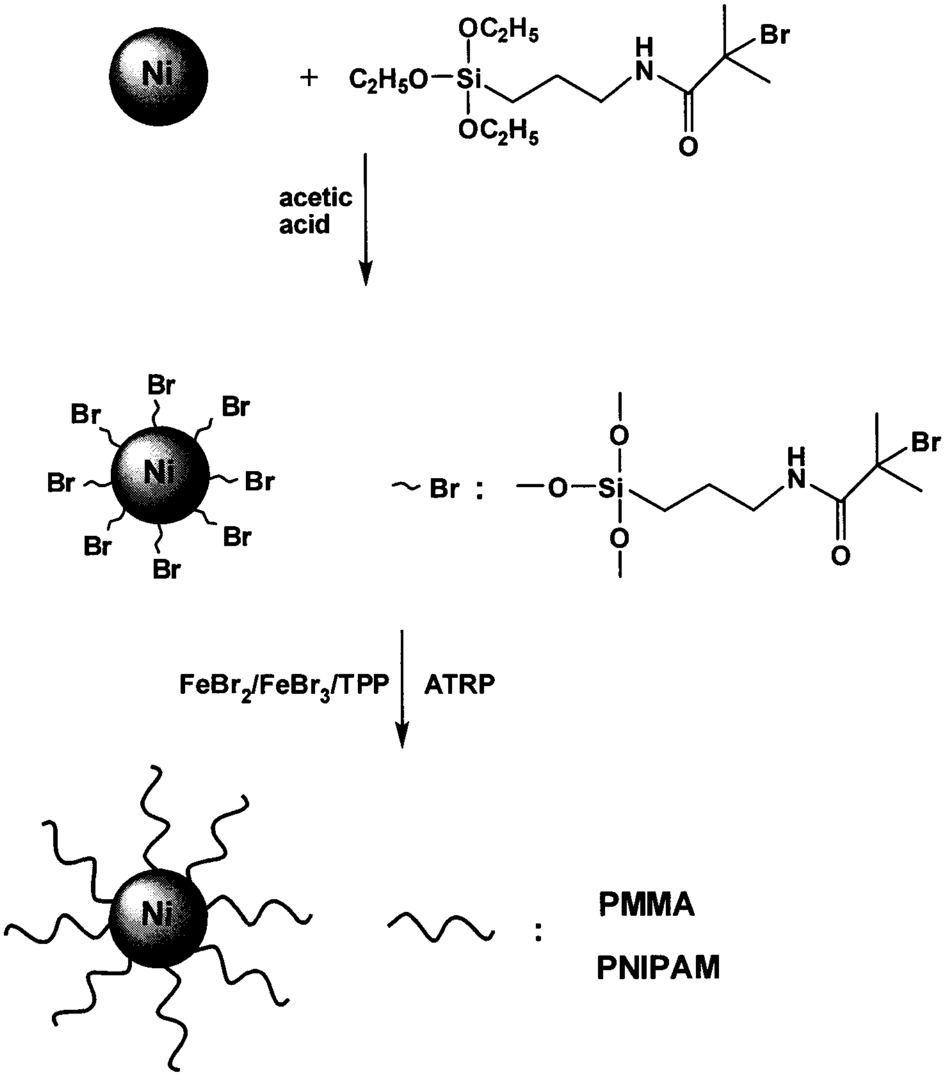

Scheme 6.1 Surface-initiated ATRP of polymers from Ni nanoparticle surface

6.4.2 Surface-initiated ATRP on Ni nanoparticles.

An iron catalyst system was chosen for the polymerization on nickel surface instead of copper catalyst because of the risk of nickel corrosion by Cu(II) catalyst. MMA was first used as a model monomer and was polymerized from Ni nanoparticle surface with added deactivator. In order to study the Si-ATRP kinetics, hydrochloric acid was added to dissolve the nickel cores and "free" PMMA chains were released for GPC characterization. Figure 6.1 shows the conversion profiles. A first-order kinetic plot of monomer conversion versus time was obtained. The grafted polymer chains were cleaved from the nanoparticles by dissolving the Ni core with hydrochloric acid (37wt.-%) followed by the molecular weight measurement. Figure 6.2 shows the molecular weight (M_n) and polydispersity index (M_w/M_n) of the cleaved PMMA polymers. The molecular weight increased linearly with the monomer conversion. For all the polymers, the polydispersity remained lower than 1.40, independent of the polymerization time. These results indicated that the grafting polymerization from Ni nanoparticle surface was well controlled by the ATRP technique.

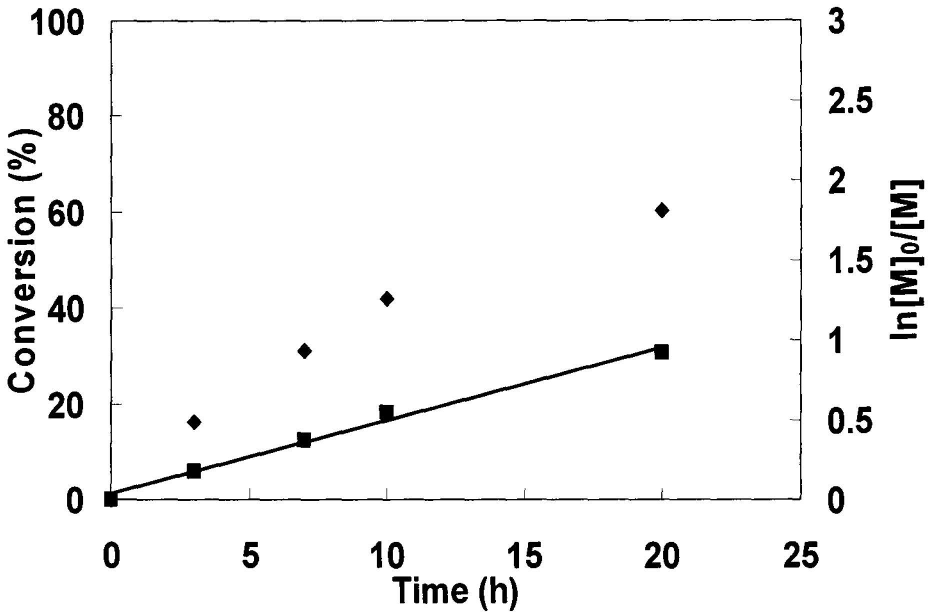

Figure 6.1 Plot of $\ln([M]_0/[M])$ versus reaction time for the solution polymerization of MMA from Ni nanoparticles at 70°C.

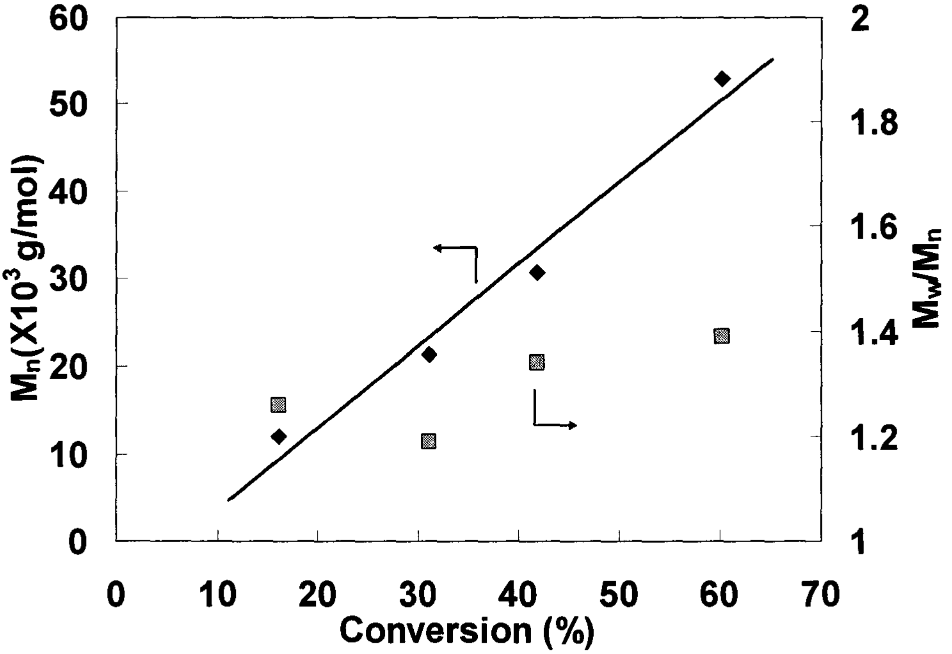

Figure 6.2 Plot of M_n and polydispersity versus monomer conversion for the solution

polymerization of MMA from Ni nanoparticles at 70°C.

Other than MMA, we also grafted other monomers with different functionalities using this ATRP technique. In grafting PNIPAM, more polar DMF, instead of toluene, was selected as the solvent for its good solubility of all the experimental components. FT-IR spectroscopy was employed to study the chemical structure of the core-shell Ni-*g*-polymer particles. Figure 6.3(a) shows the FT-IR spectrum of pristine Ni nanoparticles. The absorption bands characteristic of the functional groups in alkyl chain surfactants, such as 2965 and 2938cm^{-1} of the -CH_3 and -CH_2 groups, 1439cm^{-1} of the alkane, were observed. After the initiator modification, the characteristic peaks of the N-C=O bond at 1643cm^{-1} and 1537cm^{-1} became apparent in Figure 6.3(b). The peak at 1119cm^{-1} and the neighboring peak at 1036cm^{-1} were attributed to the Si-O-Ni and Si-O-Si vibrations, respectively. These results confirmed the formation of an initiator layer around the Ni nanoparticles. The FT-IR spectrum of Ni-*g*-PMMA is shown in Figure 6.3(c). The characteristic peak of the O-C=O group of PMMA was found at 1731cm^{-1}, which was not present in the spectrum of pristine Ni nanoparticles. The successful grafting of PNIPAM was also verified by FT-IR spectroscopy. The absorption bands centered at about 1649cm^{-1} and 1574cm^{-1} in Figure 6.3(d) were attributed to the vibration of amide (N-C=O) groups.

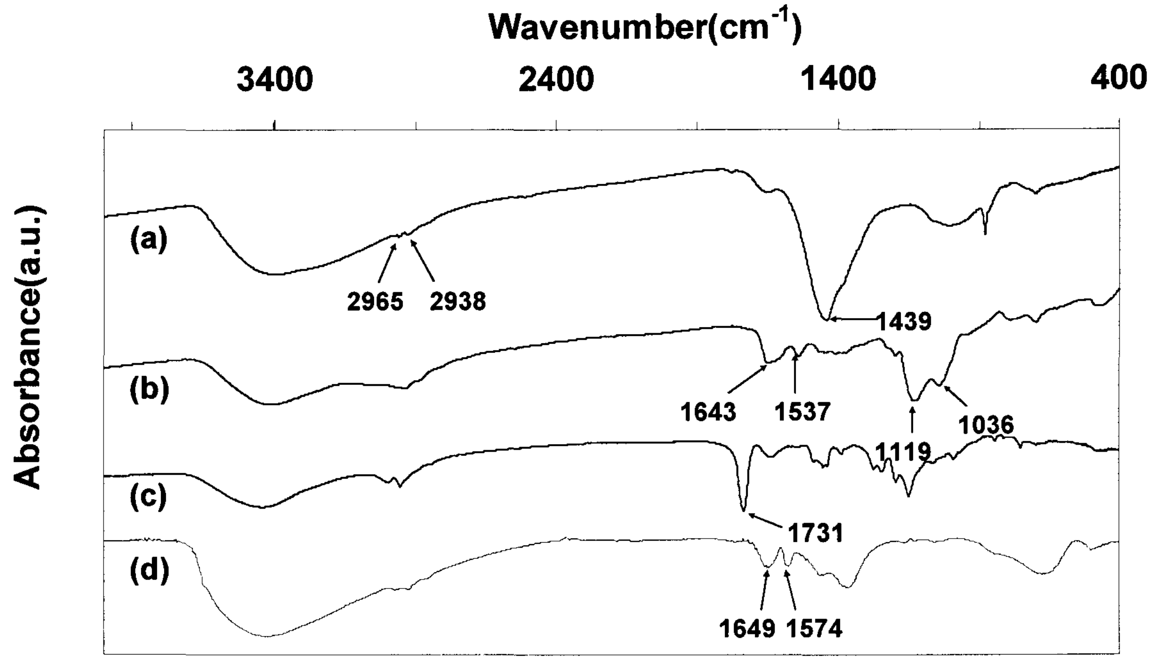

Figure 6.3 FT-IR spectra of (a) pristine Ni nanoparticles; (b) Initiator coated Ni nanoparticles; (c) PMMA coated Ni nanoparticles; (d) PNIPAM coated Ni nanoparticles.

Styrene is another widely used model monomer for surface-initiated polymerization studies. In this work, we also tried to graft polystyrene from Ni nanoparticles. Figure 6.4(a) shows the FT-IR spectrum of Ni nanoparticles modified with PSt. The observed strong peaks at 3030-2800cm^{-1}, 1600cm^{-1}, 1400-1000cm^{-1}, and 700cm^{-1} agreed very well with the PSt standard, indicating that the polymer grafting was successful. Other than PNIPAM, another widely-used biocompatible polymer, PDMAEMA were also grafted from Ni nanoparticle surface. The FT-IR spectrum of

Ni-g-PDMAEMA nanoparticles was shown in Figure 6.4 (b). The bands at 1632 (the carbonyl group), 1475 (CH_2 bending), and 1173cm^{-1} (C-N stretching) are the characteristic absorption bands of PDMAEMA units, which suggests successful grafting.

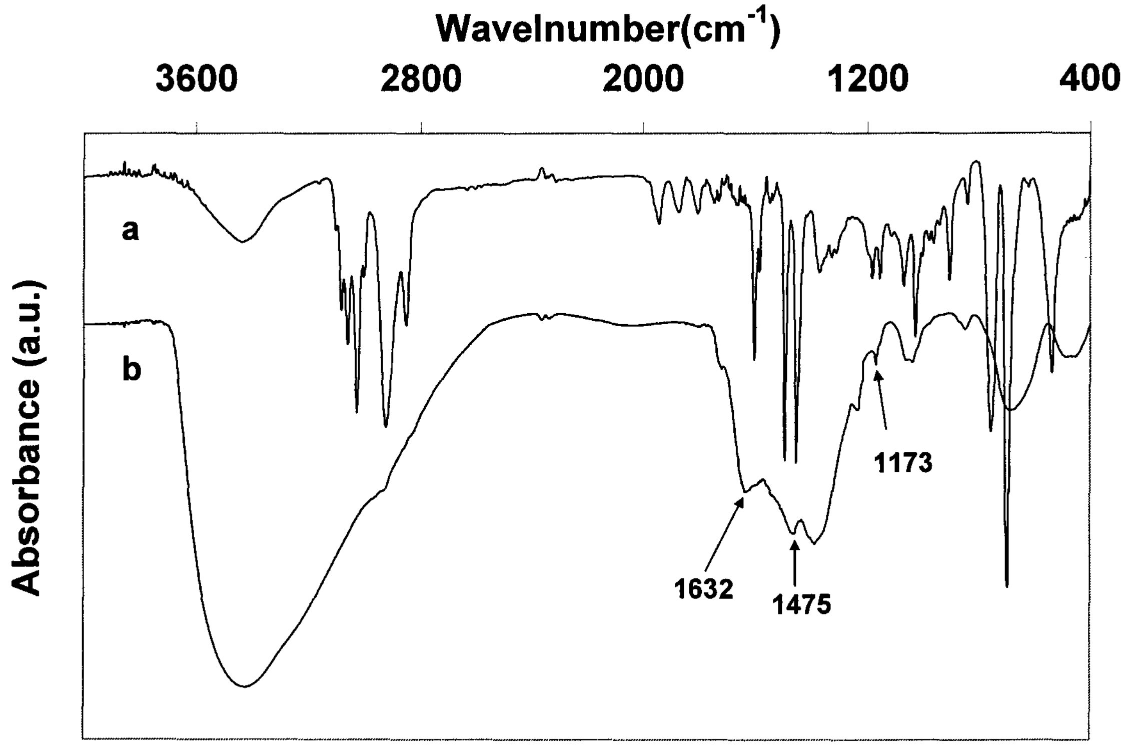

Figure 6.4 FT-IR spectra of (a) PSt coated Ni nanoparticles; (b) PDMAEMA coated Ni nanoparticles.

TGA is an effective method to determine grafting densities of polymer chains anchored to inorganic nanoparticles. Figure 6.5 shows the TGA curves. The weight losses and grafting densities for Ni-g-PMMA are summarized in Table 6.1. As shown in Figure 6.5, the polymer content in the composite increased with the polymerization time.

However, the grafting densities were pretty similar at different stages of the polymerization ranging from 1.13-1.32chains/nm^2. The initiator densities on the nanoparticle surfaces were also estimated from the TGA results. Taking into account the fact that SiO_2 ashes remained in the residue after the burn-off of initiators, we estimated the initiator density to be 26.7molecules/nm^2. This very high level of initiator density indicated that the triethoxysilane-based initiators did not form well-organized monolayers on the nanoparticle surface. Instead, a multilayer structure of initiators was formed due to the self-condensation of triethoxysilanes. Comparing the polymer grafting density to the surface initiator density, we found that the grafting efficiency was very low; about every 20 initiator moieties initiated one polymer chain. Low initiation efficiency is a common problem in surface-initiated ATRP. It is probably due to steric congestion of initiators on the nanoparticle surface, or due to the termination reactions between neighboring free radicals.

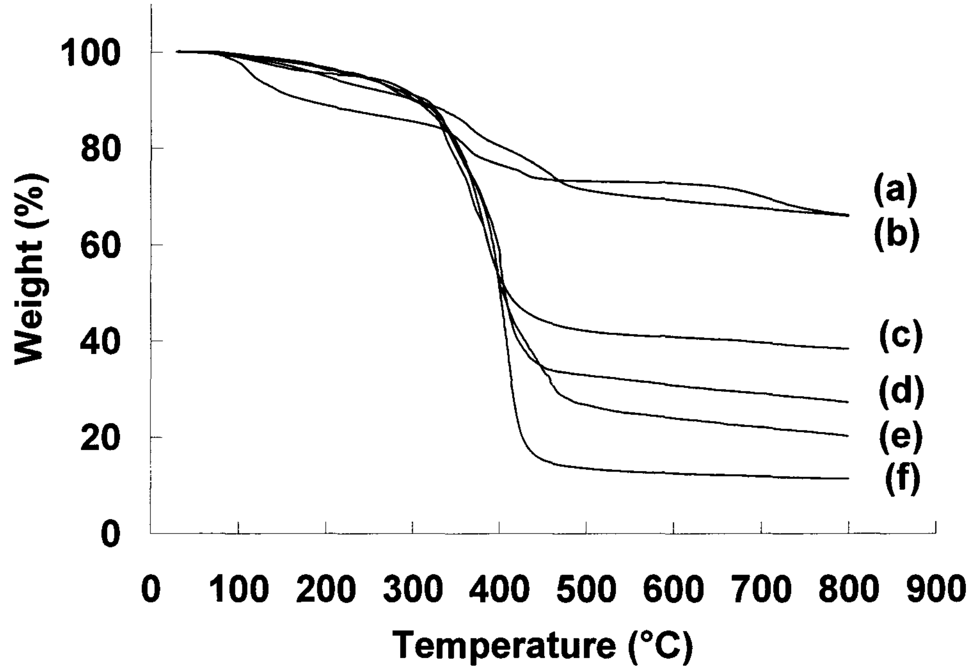

Figure 6.5 TGA curves of (a) pristine Ni nanoparticless; (b) Initiator coated Ni nanoparticles and (c, d, e, f) PMMA coated Ni nanoparticles with polymerization time of 3, 7, 10 and 20h, respectively.

Table 6.1 Weight loss and grafting density data of Ni nanoparticle samples

Sample	Weight loss (%)	Grafting density (chains/nm^2)
Ni NPs	34.03	
Ni-initiator	34.23	26.7
Ni-*g*-PMMA(3h)	61.76	1.20
Ni-*g*-PMMA(7h)	72.76	1.13
Ni-*g*-PMMA(10h)	79.82	1.15
Ni-*g*-PMMA(20h)	88.76	1.32

Figure 6.6 shows the TEM images of pristine Ni, Ni-*g*-PMMA and Ni-*g*-PNIPAM nanoparticles cast from dilute solutions and dried under ambient conditions. The average size of the pristine Ni nanoparticles was roughly 10nm. Some aggregation could be seen in the image of Figure 6.6(a). After the polymer modification, as shown in Figure 6.6(b) and (c), the Ni-*g*-PMMA and Ni-*g*-PNIPAM nanoparticles were well separated without significant aggregation. The aggregation of nanoparticles in Figure 6.6(c) may arise during the solvent evaporation, where the hydrophilic PNIPAM coated nanoparticles aggregated together to reduce their surface energy in the atmosphere. The

TEM data further confirmed that the grafted polymers really helped improve dispersion and stability of Ni nanoparticles in solvents. No appreciable size changes of the Ni nanoparticle before and after grafting were found in the TEM images. This might be because the polymer layers were difficult to be seen under TEM.

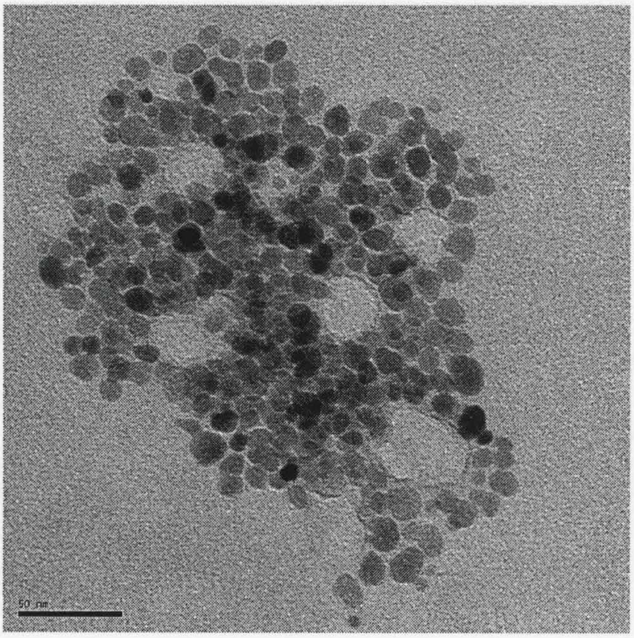

(a)

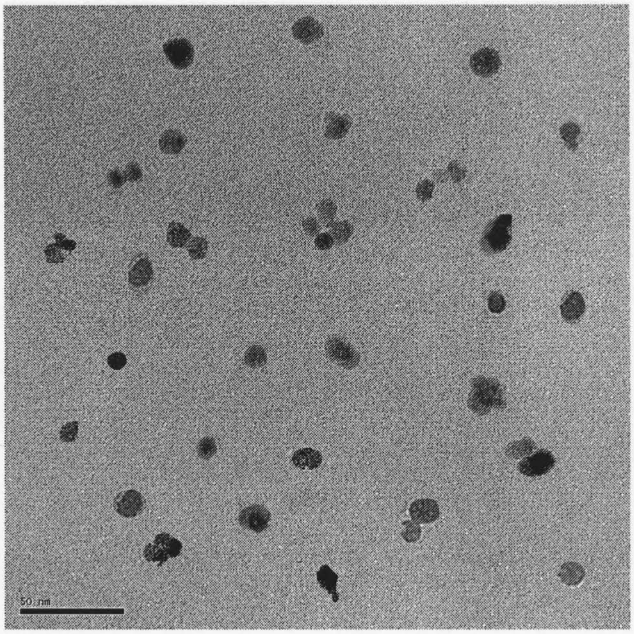

(b)

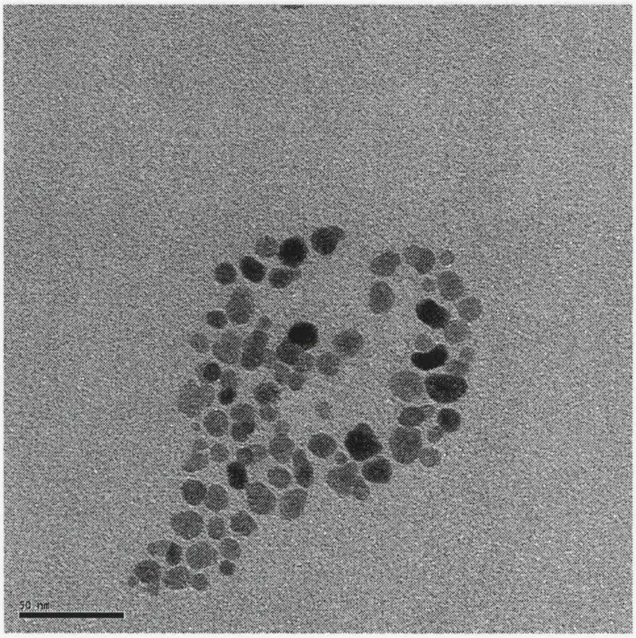

(c)

Figure 6.6 TEM images of (a) Pristine Ni nanoparticles in toluene; (b) PMMA coated Ni nanoparticles in toluene; (c) PNIPAM coated Ni nanoparticles in methanol. Scale bar: 50nm

The dispersibility and dispersion stability of nanoparticles is of great importance for practical applications. Before the polymer modification, the pristine Ni nanoparticle and initiator modified Ni nanoparticle dispersions were not very stable. We can observe that the nanoparticles can slowly precipitate out from organic solvents, such as THF, DMF, methanol etc. On the other hand, after the polymer modification, the stability of Ni nanoparticle dispersions in appropriate solvents was greatly improved. For instance, Ni-*g*-PMMA can be well dispersed in organic solvents like toluene, THF, CH_2Cl_2 etc. Ni-*g*-PNIPAM can be readily dispersed in more polar solvents like methanol, DMF and water. Even after dispersion in solvents for 6 months, no precipitation of the Ni-*g*-polymer nanoparticles was observed. From the huge difference in dispersibility and stability between the pristine Ni nanoparticles and Ni-*g*-Polymer nanoparticles, we can draw the conclusion: The polymer chains were grafted from the nanoparticle surfaces. They can act as a new interface to increase the affinity between the solvent and the nanoparticles, also, they can effectively inhibit aggregation of the nanoparticles.

Nickel nanoparticle is an important type of magnetic materials. To investigate the effect of polymer coating on its magnetic properties, magnetic measurements were performed on pristine Ni nanoparticles, Ni-*g*-PMMA (3h) and Ni-*g*-PMMA (10h) with a superconducting quantum interference device (SQUID). Magnetic hysteresis loops above and below its blocking temperature were measured and the magnetic characteristic datas were listed in Table 6.2. At 5K, below the blocking temperature, all samples were ferromagnetic, and the coercivity was about 400Oe. The saturation magnetization value could be adjusted through control of the polymer shell thickness. For pristine Ni nanopaticle, the saturation magnetization was 32.7emu/g. After 3 and 10h polymerization, the magnetization value was reduced to 12.1 and 6.4emu/g, respectively. The reduction of magnetization was due to an increased content of the non-magnetic polymers. When calibrated against the Ni mass, the saturation magnetization value was quite similar for the pristine and PMMA-grafted Ni nanoparticles, at about 32emu/g. The magnetic hysteresis loops at 298K were also measured. As seen in Figure 6.7, no appreciable hysteresis phenomenon was observed, which indicated that both pristine Ni and Ni-*g*-PMMA nanoparticles exhibited superparamagnetic behavior. The saturation magnetization was 31.1emu/g for the pristine Ni and 11.7, 6.2emu/g for Ni-*g*-PMMA(3h), Ni-*g*-PMMA(10h), respectively, corresponding to ~31emu/g based on the Ni mass. These values are smaller than the saturation magnetization values (50–70emu/g) of the most widely used magnetic nanomaterials, such as Fe_3O_4 or Fe_2O_3 nanoparticles, but are still adequate for many practical applications.

Table 6.2 Magnetic characteristics of pristine Ni and Ni-*g*-PMMA nanoparticles

Sample	Saturation Magnetization at 5K (emu/g)	Saturation Magnetization at 298K (emu/g)	Coercivity at 5K (Oe)	Coercivity at 298K (Oe)
Ni	32.7	31.1	410	0
Ni-*g*-PMMA(3h)	12.1	11.7	382	0
Ni-*g*-PMMA(10h)	6.4	6.2	389	0

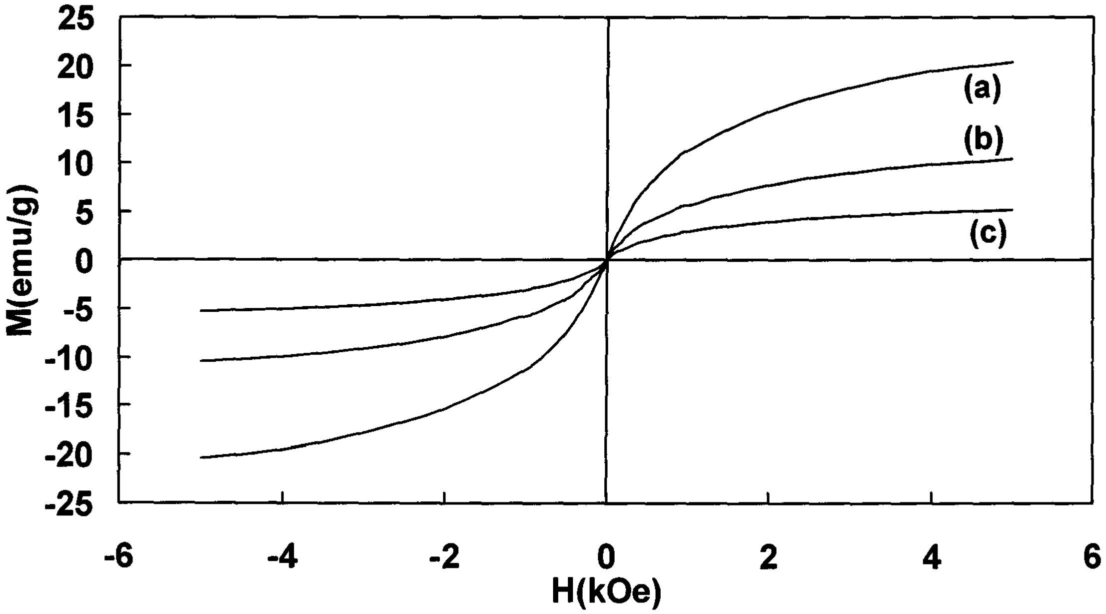

Figure 6.7 Field dependant magnetization at 298K for (a) pristine Ni nanoparticles and (b,c) PMMA coated Ni nanoparticles after polymerization time of 3 and 10h, respectively.

6.5 Conclusions

Ni nanoparticles have been modified with triethoxysilane-containing ATRP initiators without any aggregation through the combination of ligand exchange and condensation reaction. Various types of polymers including PMMA, PNIPAM, PSt and PDMAEMA were successfully grafted from the modified Ni nanoparticles by Si-ATRP technique. The iron catalyst system offered good control over the polymerization and did not impose corrosion threat to the nanoparticles. After grafted with polymers, the Ni nanoparticles possessed greatly improved dispersion and stability appropriate solvents. TEM studies confirmed that the grafted polymer formed a shell structure around the Ni nanoparticle core. The formed core-shell nanoparticles retained their magnetic properties. This work demonstrated an effective and controllable approach to modify reactive metal nanoparticles with stable polymer shells.

6.6 References

(1) He, Y. Q.; Li, X. G.; Swihart, M. T. *Chem. Mater.* 2005, *17,* 1017.

(2) Sedlackova, K.; Czigany, Z.; Ujvari, T.; Bertoti, I.; Grasin, R.; Kovacs, G. J.;

Radnoczi, G. *Nanotechnology* 2007, *18*.

(3) Chen, D. H.; Wu, S. H. *Chem. Mater.* 2000, *12*, 1354.

(4) Chen, D. H.; Hsieh, C. H. *J. Mater. Chem.* 2002, *12*, 2412.

(5) Wu, S. H.; Chen, D. H. *Chem. Let.* 2004, *33*, 406.

(6) Wojcieszak, R.; Zielinski, M.; Monteverdi, S.; Bettahar, M. M. *J. Colloid. Interf. Sci.* 2006, *299*, 238.

(7) Park, J.; Kang, E.; Son, S. U.; Park, H. M.; Lee, M. K.; Kim, J.; Kim, K. W.; Noh, H. J.; Park, J. H.; Bae, C. J.; Park, J. G.; Hyeon, T. *Adv. Mater.* 2005, *17*, 429.

(8) Alonso, F.; Calvino, J. J.; Osante, I.; Yus, M. *Chem. Let.* 2005, *34*, 1262.

(9) Han, M.; Liu, Q.; He, J. H.; Song, Y.; Xu, Z. ; Zhu, J. M. *Adv. Mater.* 2007, *19*, 1096.

(10) Zhong, Z. Y.; Mastai, Y.; Koltypin, Y.; Zhao, Y. M.; Gedanken, A. *Chem. Mater.* 1999, *11*, 2350.

(11) Couto, G. G.; Klein, J. J.; Schreiner, W. H.; Mosca, D. H.; de Oliveira, A. J. A.; Zarbin, A. J. G. *J. Colloid. Interf. Sci.* 2007, *311*, 461.

(12) Zhou, L.; Yuan, W.; Yuan, J.; Hong, X. *Mater. Let.* 2008, *62*, 1372.

(13) Wu, T.; Zhang, Y. F.; Wang, X. F.; Liu, S. Y. *Chem. Mater.* 2008, *20*, 101.

(14) Li, D. X.; Cui, Y.; Wang, K. W.; He, Q.; Yan, X. H.; Li, J. B. *Adv. Func. Mater.* 2007, *17*, 3134.

(15) Vestal, C. R.; Zhang, Z. J. *J. Am. Chem. Soc.* 2002, *124*, 14312.

(16) Chen, R.X; Zhu, S. P.; Maclaughlin, S. *Langmuir* 2008, *24*, 6889.

(17) Hou, Y.; Kondoh, H.; Ohta, T.; Gao, S. *Appl. Surf. Sci.* 2005, *241*, 218.

(18) Matsuno, R.; Yamamoto, K.; Otsuka, H. Takahara, A. *Macromolecules* 2004, *37*, 2203.

(19) Kong, X. X.; Kawai, T.; Abe, J.; Iyoda, T. *Macromolecules* 2001, *34*, 1837.

(20) Ohno, K.; Moringa, T.; Koh, K.; Tsujii, Y.; Fukuda, T. *Macromolecules* 2005, *38*, 2137.

CHAPTER 7

Contributions and Recommendations for Future Work Developments

7.1 Research contributions

As discussed, the biggest obstacle which limits the uses of polymeric materials for surface modification is the lack of proper techniques which can produce uniform, robust and well-defined polymer thin films on different kinds of substrates. The unprecedented development of controlled/living radical polymerization technique, especially atom transfer radical polymerization (ATRP) in the past decade has provided a new key to tackle the challenge. The surface-initiated ATRP technique has been proven to be a very powerful tool for the preparation of polymer thin films from various kinds of substrates, having good control over the structures and functionalities. This thesis work has contributed significantly to the application of the surface-initiated ATRP technique in preparation of polymer brushes with special structures and functionalities. It also investigated the reactive metal surface modification. The major contributions may be summarized as follows.

In Chapter 3, we studied the polymerization of a partially perfluorinated monomer, 2,2,2-trifluoroethyl methacrylate (TFEMA) from silicon wafer surfaces by surface-initiated ATRP. TFEMA-containing homopolymers and copolymer have very interesting properties and this is the first work to directly graft PTFEMA films from surfaces. The polymerization kinetics was studied in details to investigate the effects of experimental conditions, i.e. monomer concentration, monomer/catalyst ratio, Cu(I)/Cu(II) ratio on the growth of PTFEMA brushes. The operational window for this system was optimized based on the kinetic study results. Another very important contribution of this chapter is the design of a novel surface-attachable difunctional initiator, 11-(2,2-bis(2-bromo-2-methylpropionyloxy methyl)propionyloxy) undecyltrichlorosilane, which has the ability to greatly increase the grafting density. Grafting density is a very important character for surface-initiated polymerization; normally high grafting density means very dense and thick polymer films. Currently, the grafting density for surface-initiated ATRP is still very low, lower than 0.6chains/nm^2. This chapter introduced the first effective method to increase the grafting density. For the grafting of PTFEMA brushes, very high grafting densities of 0.86chains/nm^2 was achieved by using this difunctional initiator, while the monofunctional initiator can only offer grafting densities of 0.48chains/nm^2.

Chapter 4 investigated the surface-initiated ATRP of a polyhedral oligomeric silsesquioxane (POSS)-containing hybrid polymer, poly(POSS-MA) from flat silicon wafers. POSS-cotaining polymers have very high thermal stability, good oxidation resistance and excellent mechanical strength. Also, this chapter is the first surface-initiated ATRP work using a monomer with rigid and bulky side groups. The kinetics of POSS-MA grafting was well studied and the rigid, bulky POSS side groups were found to effectively prevent the termination reaction.

In Chapter 5, acrylic polymers, including PMMA, PTFEMA, PDMAEMA and PHEMA were grafted from flat nickel and copper surfaces through surface-initiated ATRP. This is the first work to apply the surface-initiated ATRP technique to surface modification of these two important metals. The purpose of this work is to prepare polymer coatings covalently bonded to the metal surfaces, which can offer highly stable adhesion between the polymer coatings and the metal surfaces. Detailed kinetic studies of the grafting polymerization were provided to find the optimal operation window for this system. The same strategy was then extended to the modification of alloy surfaces. NiTi, a shape-memory-alloy with lots of interesting properties was chosen as the substrate. PDMAEMA and POEGMA brushes were successfully grafted from its surface.

In Chapter 6, the substrate was changed from flat metal surface to metal nanoparticles. For the first time, the surface-initiated ATRP technique was successfully employed to modify nickel nanoparticles with polymer shells. Various kinds of polymers including PMMA, PSt, PDMAEMA and PNIPAM were grafted from initiator-functionalized nickel nanoparticles. After the modification, the dispersibility and dispersion stability of the nickel nanoparticles in appropriate solvents was greatly improved.

7.2 Recommendations for the Future Work

7.2.1 Surface-initiated ATRP from alloy nanoparticles

Due to their superior magnetic properties, in the recent years, superparamagnetic particles have been widely used in biomedical diagnosis and therapy applications, including labeling and magnetic separation of biological materials, directed drug delivery, magnetic resonance imaging (MRI) contrast enhancement, and hyperthermia treatment. In all these applications, materials having high magnetic moments are required. In the cases of magnetic separation and directed drug delivery, a magnetic field gradient is used to apply force to the particles. Because the force is directly proportional to the magnetic moments of the particle, the advantage of high magnetization becomes obvious. In MRI scans and hyperthermia treatments, strong magnetic fields are used and superparamagnetic particles would be expected to have their magnetization saturated. Materials of high magnetic moments offer better contrast for MRI and high peak heating values for hyperthermia treatments. Today, the most commonly used superparamagnetic materials are iron oxide nanoparticles, however, their magnetic moments are low (~300-400 emu cc^{-1}), which greatly limits their performance in biomedical applications. In order to overcome the limitation, materials with high magnetic moments are in great demand. Zero-valent metal nanoparticles such as Fe and Co have very high magnetic moments (Fe, ~1700 emu cc^{-1}, Co, ~1400 emu cc^{-1}). However, they are not stable under biological conditions. Coating dense inorganic or organic shells may prevent the oxidation; however, their magnetic moments decrease after the coating. In 2000, monodispersed FePt nanoparticles were first synthesized by Sun and his colleagues in IBM.[1] FePt nanoparticles containing a nearly equal atomic percentage of Fe and Pt are an important class of magnetic nanomaterials. Their magnetic moment reaches ~1000 emu cc^{-1}, comparable to zero-valent metal nanoparticles and more than twice larger than iron oxide. Moreover, FePt nanoparticles are much more chemically stable than metal nanoparticles and previous investigations have revealed that thiol and dopamine terminated molecules can easily form self-assembly monolayers (SAM) on their surface.

Taking these advantages, we believe FePt nanoparticles are excellent candidates for biomagnetic applications.

For *in vivo* applications, the FePt nanoparticles must be coated with a biocompatible polymer to prevent the formation of large aggregates, changes from the original structure and biodegradation when exposed to the biological system. For we have successfully used the surface-initiated ATRP technique to graft polymers from Ni nanoparticles; here we can also apply this technique to modify FePt nanoparticles surfaces with polymers having different biofunctionalities. Thiol and dopamine-containing ATRP initiators are synthesized according to literatures. Through ligand exchange reaction, the carboxylate or amine surfactants on FePt nanoparticle surface can be easily replaced by thiol or dopamine-containing ATRP initiators. Because thiol bonds with Pt atom and dopamine bonds with Fe atom, the two initiators are used together to ensure the most complete surface coverage. Two well-known biocompatible monomers, oligo(ethylene glycol) monomethacrylate (OEGMA) and 2-methacryloyl oxyethyl phosphorylcholine (MPC) can be polymerized from the initiator-functionalized FePt nanoparticles.

A magnetometer can be used to study the magnetic properties of the modified

FePt nanoparticles, including the saturation magnetization, blocking temperature and coercivity. The biocompatibility of the nanoparticles can be checked by *in vitro* cell uptake experiments using a macrophage cell line, and inductively coupled plasma–mass spectroscopy (ICP-MS) be used to determine the iron concentration in microphage cells. The application of these nanoparticles as contrast agents for *in vivo* MRI can also be studied to assess their performance. Finally, the effects of material structure, such as particle size, polymer shell thickness, polymer functionalities, on the magnetic and biological properties, are elucidated, and the preparation process is optimized to further improve the performance.

Except for bioscience, the FePt nanoparticles may find applications in some other areas. Thermo-responsive polymers such as poly(*n*-isopropylacrylamide) (PNIPAM) receive much attention in the recent years for their applications in controlled drug release. Surface-initiated ATRP has been successfully used to graft PNIPAM from various kinds of surfaces. PNIPAM can be grafted from FePt nanoparticle surface. The PNIPAAM modified FePt nanoparticles can be incorporated into PNIPAM-based hydrogels. Due to relaxation process, the superparamagnetic FePt nanoparticles are capable of transforming electromagnetic energy from an external high frequency field to heat. The hyperthermia treatment is based in this property. In this case, the prepared hydrogels can be used as drug carriers. As soon as an external electromagnetic field is applied, the FePt nanoparticles will release heat, once the temperature is higher than the lower critical solution temperature (LCST) of the hydrogel, the hydrogel shrinks to release drugs. This idea proposes a special "remote control" non-contact method to control the drug release; moreover, the magnetic nanoparticles can also control the movement of drug container inside the body.

7.2.2 Biomedical applications of polymer-modified nitinol alloys

As we discussed in Chapter 5, the nitinol alloy has very desirable mechanical properties such as superelasticity and shape memory effect for biomedical applications. However, the bright future of nitinol biomaterials faces a great challenge. The nickel oxide layer on nitinol surface may be corroded in human body to release harmful nickel ions. Surface-initiated ATRP technique has been successfully applied to the modification of nitinol surfaces. Two widely-used biocompatible polymers, PDMAEMA and POEGMA were grafted from the nitinol surfaces. However, the effects of these grafted polymers in preventing nitinol from corrosion were not studied in details. The reduction-oxidation reaction at the surface can be measured and compared with the bare surface by cyclic voltammetry (CV) and electrochemical impedance spectroscopy (EIS). Other properties of the NiTi-*g*-polymer hybrid materials can also be studied. For example, quaternized PDMAEMA is well known to have the ability to kill bacteria. The antibacterial properties of NiTi-*g*-PDMAEMA materials should be of great interest. POEGMA is a good candidate to prevent nonspecific protein absorption on the surface. The study of the potential of NiTi-*g*-POEGMA as non-biofouling materials should be very useful for future *in vivo* applications.

7.3 References

(1) Sun, S. H.; Murray, C. B.; Weller, D.; Folks, L.; Moser, A. *Science* 2000, *287,* 1989.